VLÁKNA a TEXTIL

2

Ročník 10.
2003

ISSN 1335-0617

Indexed in:

Chemical Abstracts,

World Textile Abstracts

EMBASE

Elsevier Biobase

Elsevier GeoAbstracts

Vlákna a textil (2) 2003
Fibres and textiles (2) 2003

CONTENTS

OBSAH

Toto číslo je venované 5. medzinárodnej konferencii TEXSCI 2003
This issue is devoted to the 5th international conference TEXSCI 2003

DYEING CHARACTERISTICS OF MODIFIED PET FIBERS

Militký, J.

Textile Faculty, Technical University of Liberec 461 17 Liberec, Czech Republic
e-mail: jiri.militky@vslib.cz

The main aim of this contribution is description of the influence of the modifying component content on the dyeing characteristics of modified polyester (PET) fibers.

The especially prepared copolyester fibers containing isophtalic acid (denoted by KI), adipic acid (denoted by KA), salt of 5-sulphoisophtalic acid (denoted by KS) and polyethylene glycole having molecular mass 3000 (denoted by PG) have been prepared under comparable technological conditions. The dyeability has been characterized by means of dye concentration C_{90} after a dyeing of fibers for a period of 300 min at 90 °C and parameters of non-isothermal dyeing curve (rate constant, equilibrium concentration). The applicability of these parameters for description of dyeing differences caused by the presence of modifying components is discussed.
KEYWORDS: PET fibers modification, dyeing ability, structure characterization, kinetic models

1. INTRODUCTION

One of the disadvantages of polyethyleneterephthalate fibers (PET) is their poor dyeability. Improvement may be achieved by using various modifying components (diols or dicarboxylic acids) in polycondensation [1]. A great number of different comonomers for the improvement of dyeability have been used [4]. Although the modified polyester fiber have been produced for many years, only the fragmentary information are known as for an influence of modifying components on their structure and dyeability.

The main problem is, that comonomers have influence not only on dyeability but affect also on formation and process ability of fibers. Comonomers influence especially molecular weight of the melt, degree of degradation during spinning and the rate of crystallization. Therefore it is very important to prepare copolyester fibers under comparative conditions [3, 5].

In this work the especially prepared copolyester fibers containing isophtalic acid (denoted by KI), adipic acid (denoted by KA), salt of 5-sulphoisophtalic acid (denoted by KS) and polyethylene glycole having molecular mass 3000 (denoted by PG) are used.

The dyeability is characterized by means of dye concentration C_{90} after a dyeing of fibers for a period of 300 min at 90 °C and parameters of non-isothermal dyeing curve (rate constant, equilibrium concentration).

The influence of type and content of individual modifying component on the dyeability characteristics are discussed.

2. FIBER MODIFICATION

In spite of the great number of existing modification methods no consistent classification is available at yet. From the general viewpoint, however, it would appear advisable to classify the modification methods by the production steps at which they are applied. The following classification scheme results [2]:

1. *Modification in course of polymer preparation*
   - preparation of copolymers,
   - using additives,
   - reducing the molecular mass.
2. *Modification in course of fiber preparation*
   - drawing and setting conditions readjusting,
   - speed of spinning changing,
   - texturing,
   - cross section geometry changing,
   - fineness changing,
   - bicomponent and multicompoment fibers production.
3. *Modification applied to commercial fibers*
   - grafting,
   - plasma etching,
   - controlled surface destruction.
4. *Combined modification*
   (e.g. hollow microporous copolyester fibers containing additives)

Details about these modifications are summarized in the book [2].

3. PET FIBERS MODIFICATION

It is well known that polyester (PET) fibers have some negative properties, which reduce their applicability. Main negative properties are low water absorption, high pilling, static electrification and difficult dyeability

Suppressing of these properties needs generally the chemical modification. The non-modified polyester fibers are composed from terephtailic acid and ethylene glycole. Chemical modification is realized by the replacement of part of acid or glycole by another substances(comonemers). For PET fibers the main types of potential commoners are:

adipic acid – concentration range 6–8 mol. %

isophtalic acid – concentration range 10–15 mol. %
5-sulfoisophtalic acid – concentration range 1–3 mol. %
buthyleneglycole – concentration range 8–10 mol. %
polyethyleneglycole (80–150 units) – concentration range 5–8 weight. %
pentaerythrytol – concentration range less than 1 mol. %

The description of effect of modification on fiber properties is complicated by the fact that modification affects not only fiber structure and fiber properties but also conditions of fiber preparation. The main problems can be summarized to the following points:

- It is difficult to measure structural parameters directly influencing given property (tie chain)
- The properties are distinctly dependent on chemical composition of fibers (chain flexibility)
- Structural parameters are measured in static state whereas properties are usually determined in a dynamic state
- Structure is changed during the measurement of some properties

Influence of commoner on fiber properties can be divided to the following categories:

A. Commoner has no effect
B. Commoner has indirect effect
C. Only the commoner amount matters (equilibrium melting point)
D. It is the type of commoner that matters (T_g, dyeability)
E. Commoner type and concentration have effect simultaneously

Modification generally affects on the other technologically important characteristics as technology of fiber preparation, molecular mass of melt, degree of melt degradation and rate of crystallization. It is therefore difficult to separate effect of chemical modification from modification of technological parameters.

4. MOLAR CONTRIBUTIONS METHOD

In the book [7] three main groups of polymeric materials characteristics are defined:

1. Colligative characteristics having the same values (per mole of polymers) independently of chemical composition.

2. Additive characteristics having the value (per mole of polymer), which represents the sum of contributions of individual atoms, bonds or typical groups of atoms.

3. Constitutive characteristics having values, which are dependent on composition of whole chains.

A list of additive characteristics is presented in [1]. The value of additive characteristics Q_M (per one mole of polymer) can be simply computed by using of relation

$$Q_M = \sum_{i=1}^{m} Q_{Mi} \times n_i$$

where Q_{Mi} is molar contribution of the i-th group (or atom or bond) and n_i is number of i-th groups per one mole polymer.

The molar contribution method is very simple and can be used for prediction of some properties of polymers and copolymers. Molar contributions Q_{Mi} for additive physical, optical, thermal and mechanical characteristics are presented in the book [4]. The ideal density of amorphous phase ρ_a and the ideal density of crystalline phase ρ_c of individual copolyesters (see tab.1) were calculated by means of the modified molar contribution method

Let us use molar contribution method for prediction of amorphous density of copolyester fiber containing 10 mol % of adipic acid. Amorphous density of this fiber ρ_a can be computed from simple relation

$$\rho_a = \frac{0.9 \times M_P + 0.1 \times M_A}{0.9 \times V_P + 0.1 \times V_A}$$

Here M_A (M_P) are the molar weights of individual copolymers and V_A (V_P) are their molar volumes. The molar weights can be simply determined from chemical composition of chains. For pure polyethyleneterephtalate (PET) chains is M_P=192.2 and for pure polyethyleneadipate (PEA) chains is M_A = 172.7. The values of molar volumes should be calculated by molar contributions method. Additive characteristic are here V_A and V_P.

The molar contributions to molar volume for PET:

Group	n_i	V_i	n_iV_i
—COO—	2	23.00	46.0
—CH_2—	2	15.85	31.7
benzene ring	1	65.50	65.5

Molar volume of pure PET is $V_P = \sum V_i \times n_i$ i.e. V_P = 143.6 $cm^3\ mol^{-1}$.

The molar contributions to molar volume for PEA:

Group	n_i	V_i	n_iV_i
—COO—	2	23	46.0
—CH_2—	6	15.85	95.1

Molar volume of pure PEA is then V_A = 141.1 $cm^3\ mol^{-1}$.

Molar contributions V_i for typical polymeric groups are given in [7]. In the book [4] are presented only contributions used for copolyesters.

After substitution to equation for ρ_a computation the resulted amorphous density of modified polyester fiber is ρ_a = 1327.13 kg m^{-3}.

The amorphous densities ρ_a for other types of modified PET fibers were computed by the same way. By using of this method the amorphous densities for pure copolymers can be computed as well. For PET ρ_a = 1330.74 kg m^{-3} and for PEA we obtained ρ_a = 1191.49 kg m^{-3} was resulted.

5. EXPERIMENTAL PART

5.1. COPOLYESTER FIBERS

The following four basic modifying components were used:

isophtalic acid (KI),
adipic acid (KA),
sodium salt of 5-sulphoisophtalic acid (KSI)
poly(ethylene glycole) (PG).

The copolyester with different contents of KI, KA, KS and PG were synthesized. For each comonomer three level of concentration were chosen so that overall technological concentration range has been covered (see Table I). From copolymers the fibers were prepared on a laboratory scale. The constant dynamic viscosity of the polyester melt was kept with the melt spinning and fiber forming as well as the constant spinning speed and the comparable conditions of a drawing process and an annealing one [1]. The dosing of melt was as high as 0.16 g s^{-1} with the take-up speed 5 m s^{-1}. Then a drawing process in 2 steps in water baths took place having the total drawing ratio L = 4.4. The following annealing in the free state was made at 130 °C (in hot air) for 30 minutes.

5.2 STRUCTURAL PARAMETERS

The density of single fibers was measured using a gradient density column at 30° C. For estimation of the volume fraction of the crystallinity x, the ideal density of amorphous phase r_a and the ideal density of crystalline phase r_c were calculated by means of the modified molar contribution method [4]. The calculations were made for particular fiber types differing both by the content and by the type of the respective comonomer. Orientation factor of a crystalline phase f_c were derived from WAXD (wide-angle-X ray diffraction) by means of the Hermans relation. The birefringence Δn was measured by the compensatory method by using of the microscope NV (Carl Zeiss, Jena) at the wavelength 551 nm. In order to establish an orientation factor of amorphous phase f_{am}, the well-known relation for two-phase model was used

$$\Delta n = x f_C \Delta n_{co} + (1 - x) f_{am} \Delta n_{ao} \qquad (1)$$

The intrinsic birefringence of crystalline region was chosen to be $\Delta n_{co} = -0.2$. The intrinsic birefringence of amorphous region Δn_{ao} was calculated by using the idealized assumption, that [4]

$$\Delta n_{ao}/\Delta n_{co} \approx r_a/r_c$$

To characterize the orientation of an amorphous region, the average orientation of the amorphous phase was calculated

$$f_m = (1 - x) f_{am} \qquad (2)$$

The values of mean orientation factor f_m are given in the Table 1.

5.3. ISOTHERMAL DYEING

To characterize maximum dyeability the isothermal dyeing at temperature 90 °C for 300 min was realized. The dye used was Palanilblau 3RE (2% o.w.f.). Dyeing process and spectrophotometric evaluation of mean concentration C_{90} are described elsewhere [6]. Resulting concentrations C_{90} are given in Table 1.

5.4. NON-ISOTHERMAL DYEING

For estimation of kinetic and equilibrium parameters of dyeing the nonisothermal sorption curves of Palanilblau 3 RE (2% o.w.f.) were measured. Dyeing started at the temperature $T_1 = 52$ °C. In the first phase the constant rate of heating Q = 0.75 K min^{-1} was used. This phase was finished at $T_2 = 97$ °C (after time period $t_1 = 60$ min). In the second phase up to time t = 400 min the temperature was constant (i.e. Q = 0). In selected times t_i the mean concentrations C_{ti} were determined spectrophotometrically.

6. TREATMENT OF NON-ISOTHERMAL SORPTION CURVES

Kinetic parameters of dyeing can be generally obtained from both isothermal and nonisothermal dyeing experiments.

The macroscopic dyeing processes for selected fiber – dye systems can be described by isothermal *uptake curve,* i.e. dependence of mean dye concentration in fiber c_t on time t at constant temperature T. From isothermal uptake curves at various temperatures is possible to estimate the activation parameters of dyeing and dyeing mechanisms.

Practical dyeing experiments are often realized under nonisothermal conditions and then the *nonisothermal uptake curves* are obtained. Nonisothermal uptake curve is dependence of c_t on t for known time-temperature profile T(t).

Nonisothermal kinetics of dyeing may be described either by the diffusion or the rate type models. Both models are based on the assumption that temperature dependent is the rate constant only. In this simplest case the rate of dyeing can be expressed in the form

$$dc/dt = K(T) f(c_t, c_\infty) \qquad (3)$$

In this equation the K(T) is the temperature dependent rate constant and $f(c_t, c_\infty)$ is the kinetic term. Dyeing experiments are usually realized by using of the piecewise time-temperature profile in the form

$$T(t) = T_1 + \Theta t \qquad \text{for } t < t_1 \qquad (4)$$

and

$$T(t) = T_2 \qquad \text{for } t > t_1 \qquad (5)$$

where Θ is the rate of heating. By the formal integration of the eqn. (3) the following relation results

$$\int_0^{c_t} f^{-1}(c_t, c_\infty)dc_t = \int_0^t K[T(\vartheta)]d\vartheta = F(t) \qquad (6)$$

The form of kinetic term $f(c_t, c_\infty)$ is based on the selected diffusion type or overall dyeing type kinetic model. For dyeing of polyester and copolyester fibers by disperse dyes the Cegarra Puente rate model is suitable. This model leads to the final integral form

$$c_t^2 = c_\infty^2[1 - \exp(-F(t)] \qquad (7)$$

For the piecewise time–temperature profile (see eqn. (4) and (5)) and Arrhenius type model describing the temperature dependence of the rate constant

$$K(T) = K_0 \exp[-E/(R\ T)] \qquad (8)$$

is integral F(t) in the form

$$F(t) = G(T) - G(T_1) \quad \text{for } T<T_2 \qquad (9)$$

and

$$F(t) = K_0\exp(-E/RT_2)(t - t_1) + G(T_2) - G(T_1) \quad \text{for } T<T_2 \qquad (10)$$

Here E is activation energy of dyeing, K_0 is preexponential factor, R is universal gas constant and symbol G(x) denotes the integral

$$G(x) = \left(\frac{K_0}{\Theta}\right)\int_0^x \exp(-E/Rx)dx \qquad (11)$$

Very precisely the Gorbatschev relation can approximate this integral

$$G(x) = \{K_0Rx^2/[\Theta(E + 2Rx)]\}\exp(-E/Rx) \qquad (12)$$

The error of this approximation (in the range $100 <= E <= 250$) is under the 0.1%.

This nonlinear kinetic model has three adjustable parameters (c_∞, K_0, E). These parameters have been estimated from experimental non-isothermal sorption curves (i.e. dependence of dye concentration in fibre c_{ti} on time t_i and corresponding temperature T_i) by the nonlinear least squares. Due to high correlation of estimated K_0 and E the rate constants K_{90} for temperature T = 90 °C were computed

$$K_{90} = K_0\exp[-E/(R \times 363.15)] \qquad (13)$$

Estimated equilibrium concentration C_∞ and computed rate constant K_{90} are given in Table 1.

Table 1 Selected structural and dyeing characteristics of modified polyester fibers

Comonomer	Concent. [mol %]	f_m [–]	C_{90} [mg g^{-1}]	K_{90} 10^3 [min^{-1}]	C_∞ [mg g^{-1}]
PET	0	0.567	0.52	2.79	0.772
KI	4	0.498	0.43	1.001	0.918
KI	8	0.464	0.52	2.919	1.443
KI	12	0.385	1.07	3.727	3.282
KA	2	0.579	0.65	6.902	1.468
KA	4	0.548	0.77	3.170	1.579
KA	6	0.522	1.30	11.560	2.830
KS	1	0.556	0.47	2.589	1.027
KS	1.5	0.647	0.74	5.968	1.33
KS	2	0.589	0.66	1.951	2.452
PG*	3	0.483	1.46	2.780	3.059
PG	6	0.558	2.48	1.244	5.237
PG	9	0.488	10.37	1.658	16.483

* mass %

7. DISCUSSION

It is evident from Table 1 that dyeing-rate constant K_{90} does not vary much and does not properly reflect the changes of dyeability. On the other hand the concentrations C_{90} and C_∞ can express the changes in dyeability of copolyester fibers rather well. For comparison of the dyeability characteristics and structural characteristics of fibers the correlation map has been created. Comonomer type is variable 1 (PET has code 0; KI has code 1; KA has code 2; KS has code 3 and PG has code 4); comonomer concentration is variable 2; f_m is variable 3; C_{90} is variable 4; K_{90} is variable 5 and C_∞ is variable 6. The correlation map on the fig.1 shows that there are very slight correlations between dyeability characteristics and structural parameter. According to the assumption the practically linear relation between concentrations C_{90} and C_∞ exist. The rate constant describes another aspects of dyeing process and therefore do not correlate with concentrations well. The comomomer concentration correlates well with mean orientation of amorphous phase. The correlations between comonomer type and content on the one side and concentrations of dye concentrations C_{90} and C_∞ are moderate. The rate constant does not practically correlate with characteristics of fibers

For deeper investigation of the relation between comonomer type and content, mean orientation of amorphous phase and dyeability characterized by sim-

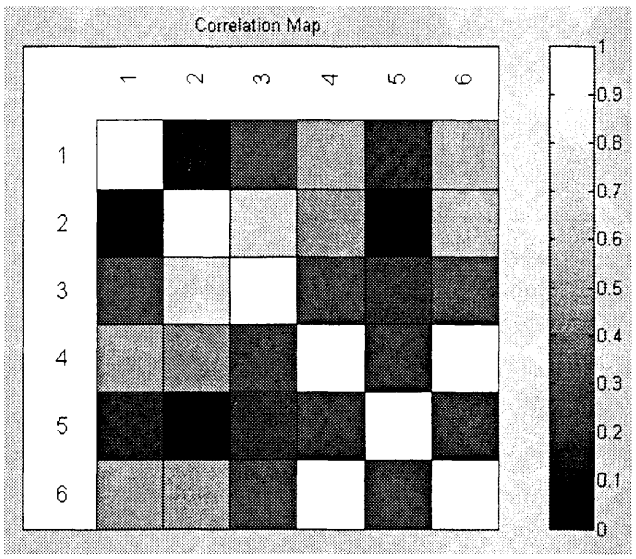

Fig. 1 Correlation map for comonomer type, and concentration, structural parameter and dyeability characteristics

ple parameter C_{90} the partial dependencies between these parameters has been created. The so-called partial regression plots were created. This plot uses the residuals from the regression of y on the predictor x_j, graphed against the residuals from the regression of x_j on the other predictors [8]. To discuss the properties of this type plot let we assume the regression model in the matrix notation

$$\mathbf{y} = \mathbf{X}_{(j)}\beta^* + \mathbf{x}_j c + \varepsilon \qquad (14)$$

where $\mathbf{X}_{(j)}$ is matrix formed by leaving out the j-th column $\mathbf{x}_j$ from matrix $\mathbf{X}$, β^* is (n –1)x1 parameter vector and c is regression parameter corresponding the j-th variable $\mathbf{x}_j$.

For investigation of partial linearity between y and j-th variable $\mathbf{x}_j$ the projection into space L orthogonal to space defined by columns of matrix $\mathbf{X}_{(j)}$ is used. Corresponding projection matrix into space L has the form

$$\mathbf{P}_{(j)} = \mathbf{E} - \mathbf{X}_{(j)}(\mathbf{X}_{(j)}^{\mathrm{T}}\mathbf{X}_{(j)})^{-1}\mathbf{X}_{(j)}^{\mathrm{T}} \qquad (15)$$

By using the projection $\mathbf{P}_{(j)}$ onto both sides of eqn.(14) the following relation results

$$\mathbf{P}_{(j)}\mathbf{y} = \mathbf{P}_{(j)}\mathbf{x}_j c + \mathbf{P}_{(j)}\varepsilon \qquad (16)$$

The product $\mathbf{P}_{(j)}\mathbf{X}_{(j)}\beta^*$ is equal to zero because the space spanned by $\mathbf{X}_{(j)}$ is orthogonal to residuals space.

From eqn. (16) it follows that:

- The term $\mathbf{v}_j = \mathbf{P}_{(j)}\mathbf{x}_j$ is the residual vector of regression of variable $\mathbf{x}_j$ on the other variables which form columns of the matrix $\mathbf{X}_{(j)}$
- The term $\mathbf{u}_j = \mathbf{P}_{(j)}\mathbf{y}$ is the residual vector of regression of variable $\mathbf{y}$ on the other variables which form columns of the matrix $\mathbf{X}_{(j)}$

Partial regression plot is then dependence of vector $\mathbf{u}_j$ on the vector $\mathbf{v}_j$. If the term $\mathbf{x}_j$ is correctly specified the partial regression graph forms straight line. Systematic nonlinearity is indication of incorrect specification of $\mathbf{x}_j$ and random pattern shows unimportance of $\mathbf{x}_j$ for explaining the variability of $\mathbf{y}$. The partial regression plot (PRP) has the following properties:

1. The slope c in PRP is identical with estimate b_j in a full model and intercept is equal to zero.
2. The correlation coefficient in PRP is equal to the partial correlation coefficient R_{yxj}.
3. Residuals corresponding to straight line in PRP are identical with residuals for a full model.
4 The influential points, nonlinearities and violations of least squares assumptions are markedly visualized.

The PRP for comonomer content is shown on the fig. 2

Partial correlation between C_{90} and comonomer content is relatively high but mainly influenced by the presence of high content of highly dyeable PEG modification (point no. 13).

The PRP for comonomer type is shown on the fig. 3

Partial correlation between C_{90} and comonomer type is slightly lower but mainly influenced by the presence

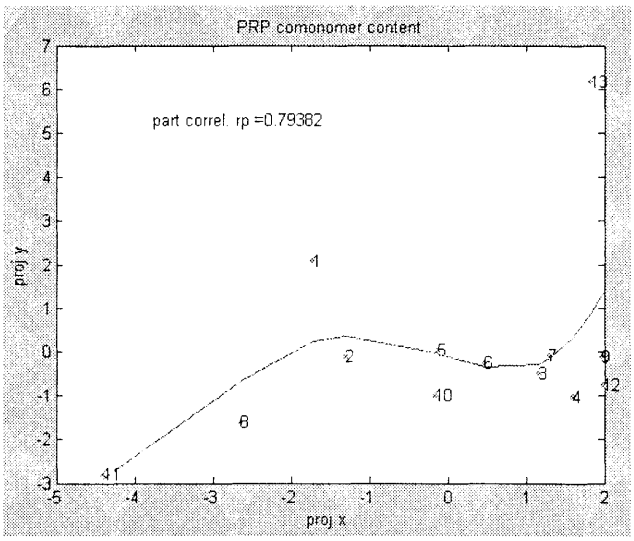

Fig. 2 Partial regression plot for C_{90} and comonomer content

of all highly dyeable PE G modification (points no. 11–13). Partial correlation between C_{90} and mean amorphous phase orientation is very low (partial correlation coefficient is only 0.21).

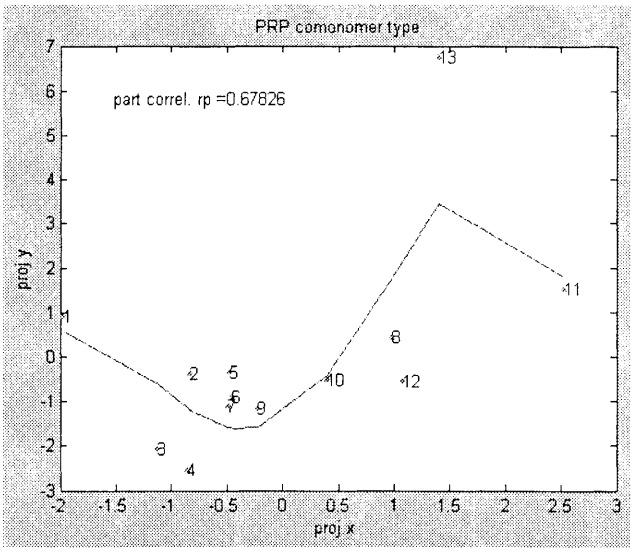

Fig. 3 Partial regression plot for C_{90} and comonomer content

8. CONCLUSION

The dyeablity is very complex phenomena connected not only with comonomer type and content. The above-presented results can be explained by simple idea that dyeing process is primarily affected by overall free accessible volume in fibers. This quantity is characterized by maximum number of dye molecules penetrating into fibers up to near equilibrium (i.e. C_{90} and C_∞). From all modification investigated only the one with PG is suit-

able for preparing of the fibers dyeable at boiling point without carriers.

ACKNOWLEDGEMENTS: the Czech Ministry of Education Grant LN B090 supported this work

9. REFERENCES

[1] Szegö L.: Advances in Polym. Sci. **16**, 90 (1979)
[2] Militký J. et al.: J. Appl. Polym. Sci. **25**,1195(1982)
[3] Militký J., Čáp J.: Proc. 12th IFATCC Congress, Budapest, 1981
[4] Militký J., et al.: Modified Polyester Fibers, Elsevier, Amsterdam, 1991
[5] Militký J., Čáp J., Vaníček J.: Proc. Int. Symp. on Fibre Science, Elsevier, Amsterdam 1986
[6] Militký J.: PhD Thesis, TU Liberec, 1982
[7] Krevelen D.W., Hoftyzer P.J.: Properties of Polymer, Correlation with Chemical Structure, Elsevier Amsterdam, 1972
[8] Meloun M. Militký J. and Forina M. Chemometrics in Analytical Chemistry vol. II, Interactive Model Building and Testing on IBM PC, Ellis Horwood, Chichester (1994)

CHARAKTERIZACE BARVITELNOSTI MODIFIKOVANÝCH PET VLÁKEN

Translation of Abstract:
Dyeing characteristics of modified PET fibers

Cílem práce je popis vlivu modifikační složky na charakteristiky barvitelnosti modifikovaných polyesterových vláken. Byla použita speciálně připravená vlákna s obsahem kyseliny isoftálové(KI), adipové (KA), 5-sulfoisoftálové (KSI) a polyetylénglykolu (PEG). Barvitelnost byla charakterizována koncentrací barviva ve vlákně C_{90} po barvení po dobu *300 min* při *90° C* a parametry neizotermního barvení (rychlostní konstanta, rovnovážná koncentrace).Jsou diskutovány vlivy struktury a chemického složení vláken na tyto charakteristiky barvitelnosti.

COTTONIZATION DEGREE OF PRETREATED FLAX FIBERS

Křemenáková D., Militký J., Antonov V.*

Textile Faculty, Technical University of Liberec 461 17 Liberec, Czech Republic, e-mail: dana.kremenakova@vslib.cz

**Inotex L td. Dvůr Králové n./L., Czech Republic*

The main aim of this contribution is a description of an influence of enzymatic and chemical pretreatment on the separation tendency of flax fibrous bundles. For characterization of bundling tendency the distribution of bundles has been created. The number of ultimate fibers in bundles and number of bundles has been estimated form digital cross section images by using of image analysis system Lucia. The frequency of bundles exceeding some limit sizes is computed.
KEYWORDS: flax bundles separation, enzymatic pretreatment, bundles size distribution

1. INTRODUCTION

The great potential of bast fibers is until now not fully utilized. Hemp and flax fibers are often used for non-textile applications and its process ability for fibrous assemblies is still very difficult. Due to presence of bundles of elemental fibers and non-fibrous substances there are serious limits for creation and utilization of these fibers.

These problems are the challenge for using new technologies and chemical or biochemical procedures to reach better process ability. New technologies, widely used in medicine and food industry, are mainly in utilization of microbes or only their enzymes for production or decomposition of different substrates.

There are several possibilities for chemical and biochemical treatment of bast fibers. The first is usually wet biochemical processing of bast fibers in the stage of scutching or hackling tow and noils. Using good processing method it is possible to reach practically full separation of fibers or to obtain fibrous bundles having few ultimate fibers. These materials or blends with cotton can be spun by classical rotor technology.

This contribution is devoted to description of number of bundles changes of ultimate flax fibers caused by the enzymatic, chemical and combined pretreatment of technical fibers. Combing on the fibro-blender device has simulated the final mechanical treatment. The distribution of fibrous bundles is created and probability of occurrence of bundles having prescribed number of ultimate fibers is computed.

2. BAST FIBERS

Main representatives of the bast fibers are **flax** and **hemp**. These fibers are derived from the stem of the plant. Flax and hemp, although botanically unrelated, have many characteristics in common. Without microscopic or chemical examination, their fibers can only be distinguished by the direction in which they twist upon wetting: hemp will rotate counterclockwise, flax clockwise.

Flax is a dual usage crop, with linen varieties grown for their stem fiber, and other varieties for the oil in their seed. This fact also applies to hemp. Both plants produce very similar drying oils in their seed, oils with a high percentage of linolenic acid, used until mid-century in paints. The oils are also valued for nutritional and even medicinal qualities.

Cellulose is the major constituent of these fibers and the minor constituents are noncellulosic polysaccharides, such as pectin and hemicelluloses, lignin, lipids, and ash. Although most of the noncellulosic components present in the fiber are removed during retting and scutching (mechanical separation of the fiber), poor quality fiber can contain as much as 20–25% of the hemicelluloses, pectin, and lignin. Typical chemical composition of these fibers is shown in the Table 1 [1].

Unlike cotton, these fibers are not single cells but rather an aggregate of the ultimate cell. The ultimate cells are fibrilar and the fibrils are helically disposed with no structural reversals. The sense of the helix is a characteristic one for this fiber group. It is also evident from x-ray diffraction that the cellulose has a higher degree of order or crystallinity in these fibers than in cotton. Some morphological structure factors are given in the Table 2 [1].

Flax, of which there are many varieties, is commercially grown for fiber principally in the states of former Soviet Union, Ireland, Belgium, Holland, the United States, Australia, and Canada. Unlike other vegetable fiber crops, the flax plant is pulled from the earth rather than cut. Having been dried, the plant is subjected to

Table 1 Comparative Chemical Composition

Fiber	CELLULOSE	HEMI-CELLULOSE	LIGNIN
FLAX	78.5	9.2	8.5
HEMP	68.1	15.1	10.6

Table 2 Morphological Structure of Bast Ultimate Fibers

Parameter	Flax	Hemp
mean length, mm	32	20
mean diameter, mm	0.023	0.022
spirality	S	Z
spiral angle	5–10°	5–10°
Length/ diameter	1391	909

retting, which is a chemical or microbial treatment of the stem to permit an isolation of the fibers. Retting is a highly complex operation involving many reactions designed to remove interfiber cementing material. Final removal of fiber from the stem is achieved by a physical process known as scutching. Flax fiber varies in its natural color and in length from about 70 to 92 cm. The mean length of the ultimate fiber cell is about 30 mm, with a mean equivalent diameter (fibers are noncircular) of 0.023 mm. The cellulose fibrils are deposited in a helical configuration with an „S" disposition of the helix. Yarns and fabrics made from flax fiber are referred to as linen.

Hemp fiber is longer than a flax fiber but it is less flexible and coarser. It does not bleach well and as it lacks elasticity and flexibility it is not used for fine textiles. The ultimate fiber cells vary in length from 5 to 55 mm, and have an average length of about 20 mm, their equivalent diameter varies between 0–016 and 0–050 mm, with a mean of 0´022 mm. The thickness of the cell wall varies much more than it does in flax, increasing towards the end of the fiber so that the lumen is narrower there. When viewed under the microscope fiber cells are seen to be irregular in shape, being flattened at some points along their length but cylindrical at others. There are striations on the surface of the fiber but no nodes like those found in flax. The ultimate fibers have forked ends, and these serve to distinguish them from the flax. Hemp has a ´Z´ twist, and this is one way how to distinguish it from flax. Hemp can be used for ropes, twines, cables, nets, sailcloth, canvas, tarpaulins, etc., but its main use is as a substitute for flax in the manufacture of yarns and twines.

Processing of high quality bast fibers is as much an art as a science. Since antiquity, bast fibers have been obtained by „retting" and „breaking" the stem. Retting (rotting) is the decomposition of the pectines, which bind the fibers to the woody inner core of the plant stem. After retting, a fiber is separated from the woody inner core (hurds or shives) by „breaking". The hurds are cleaned from the fiber by „scutching" and the fiber is further refined by „hackling" before being spun into twine and rope.

The main characteristic of technical flax fibers is that they are in the form of bundles of elementary fibers („ultimates"). The ultimate fibers are glued in the bundle by the pectinuos gums composed mainly from pectines of the inner lamellae. This pectinuos substance permeates through the fiber walls and joints the bundles with surrounding cortex or bark. The pectines of the inner lamellae are encrusted with lignin, which makes it even more difficult to split a bundle into fibers. The structure of unretted flax is on the fig. 1A.

For some applications there is interesting to extract ultimate fibers because their length characteristics are similar to the cotton fibers. Such a process is called cottonisation. For cottonization the mechanical, chemical and microbiological attack can be used separately or in combination. Sub surface of enzymatically retted flax stem is shown on fig. 1B. The significant separation of bundles from epidermis cemented by pectins and polysaccharides is clearly visible [4].

3. MATERIAL AND METHODS

Czech flax row Kotex 4C was processed by using of different chemical and enzymatic pretreatment. At first

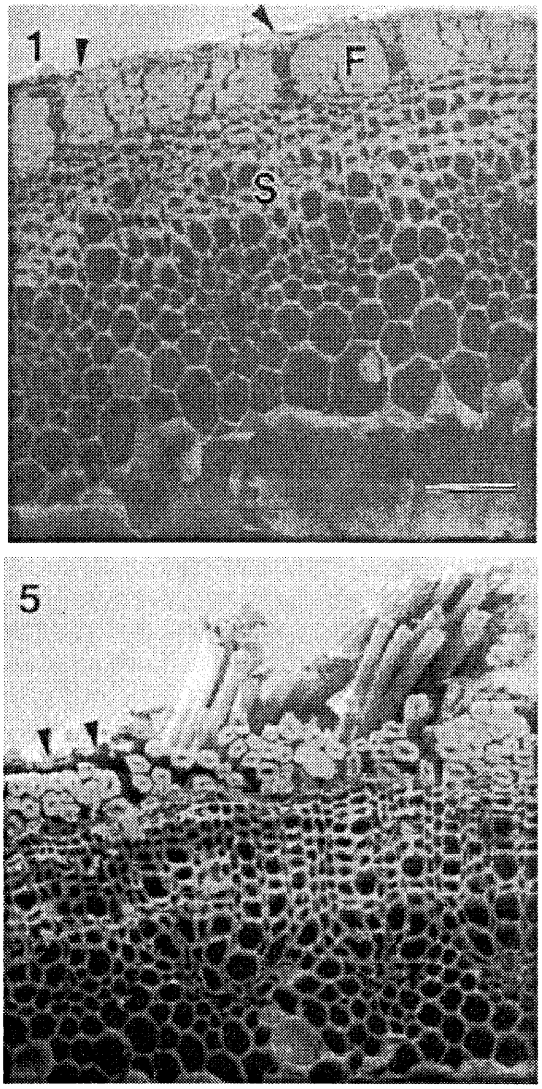

Fig. 1 A: Sub surface of unretted flax (F..fiber bundles, S Shives – Xylan,1 Parenchyne); B: Sub surface of retted flax

Table 3 Flax samples

1 (KP)	Original tow
2 (E)	Enzymatic treatment
3 (AE)	Alkaline scouring + Enzymatic treatment
4 (EB)	Enzymatic treatment + Peroxide bleaching
5 (K)	Enzymatic treatment + Alkaline scouring + Peroxide bleaching

enzymatic treatment of tow with Texazym DLG and other enzymatic agents made in Inotex Ltd was done. Additionally combinations of enzymatic treatment with alkaline scouring, peroxide bleaching or both were carried out. For estimation of these procedures influence on the changes of bundles distribution the samples with various combination of pretreatment procedures were prepared. The samples are described in the table 3.

The part of all flax samples was mechanically separated by using of Fibro blender device. These samples abbreviated as M were used for comparison of bundle size distribution only. Details about technology of these procedures are described in the work [3].

For estimation of the number of fibers in fibrous bundles and number of fibrous bundles the image analysis system LUCIA has been used. From individual samples the parallel knot of fibers has been created by manual drafting. The knots are glued and cut by microtome for a preparation of cross sections samples. By the analysis of these images (the image analysis system LUCIA has been used) the individual fibers and multiple fiber bundles were identified. The differences between flax ultimate fibers and fibrous bundles were often clearly visible but in some cases there was difficult to decide about size of bundle (see fig. 2).

4. RESULTS AND DISCUSSION

The main aim of analysis is to characterize the distribution of fibrous bundles. Let the x_i is number of bundles having number of fibers equal to i, where i = 1,2,3,...,n, and whole number of bundles is

$$Nb = \sum_{1}^{n} x_i$$

The relative frequency of i-th bundle is

$$f_j = x_j / Nb$$

and cumulative frequency is equal to

$$F_j = \sum_{j=1}^{j} f_j$$

The cumulative frequency is rough estimator of bundles size distribution function. Total number of fibers is equal to

$$N = \sum_{1}^{n} i \times x_i$$

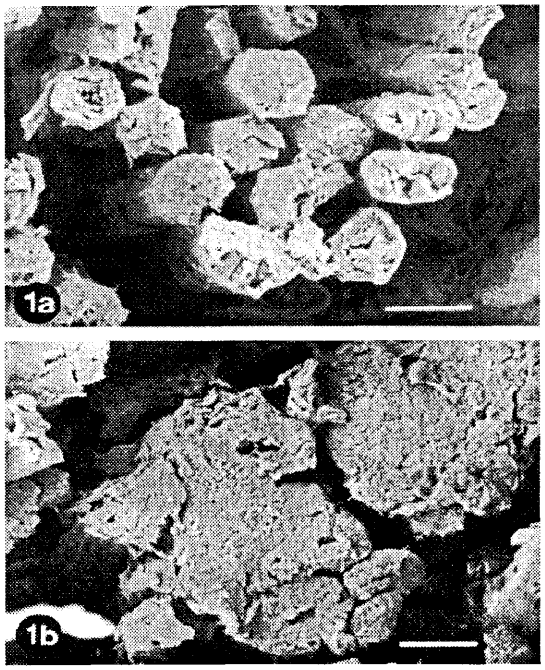

Fig. 2 Differences between ultimate fibers and fibrous bundles

By careful inspection of relative and cumulative frequencies it was recognized that:

- The number of single fibers characterizes not only the separation tendency but include the severity of treatments leading to the tow formation. For characterization of this behavior the frequency f_1 of single fiber occurrence has been used. Values f_1 are given in the table 4.
- The frequency of fibrous bundles exceeding 10 is very small and in some cases no fibrous bundles having higher number of fibers has been found. For characterizing of occurrence of bigger fibrous bundles the relative portion F10 of fibrous bundles having number of fibers exceeding 10 has been computed from relation $R10 = 100(1 - F_{10})$. These values are given in the table 4.
- In the range $2 \leq i \leq 10$ is behavior of fibrous bundles distribution similar (see fig 3), monotonically decreasing function. The aim is to describe this behavior by suitable theoretical distribution.

Because the number of bundles is discrete random variable the frequency ratio is useful for identification of suitable distribution in the range [2]. It is well known that for a lot of discrete distribution the following relation is valid

$$\frac{i \times f_i}{f_{i-1}} = C_0 + C_1 \times i$$

where C_0 and C_1 are parameters characterizing type of discrete distribution. The typical frequency ratio plot for the pretreatment K (combined action) is given on the fig. 4.

The correlation exceeding 0.78 were obtained in all cases. Positive slope in this graph indicates negative

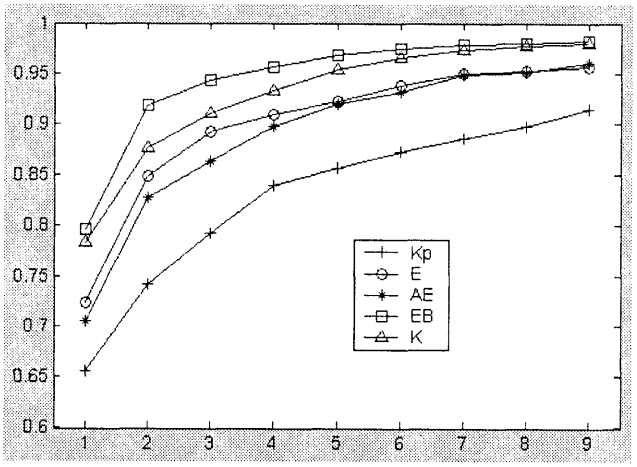

Fig. 3 Distribution function of fibrous bundles having *i* fibers in the range $2 \leq i \leq 10$

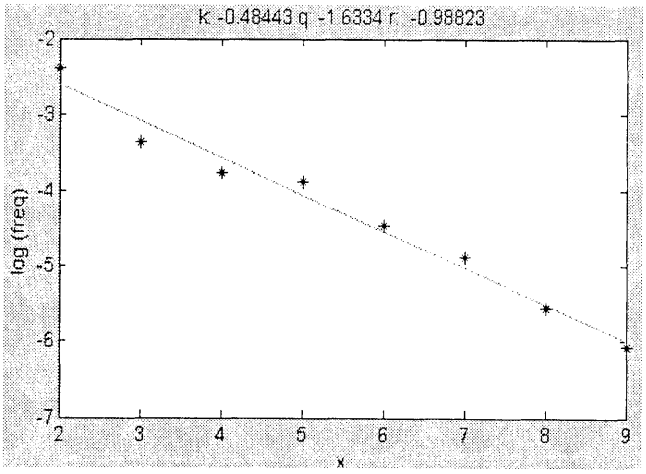

Fig. 5 Logarithmic plot for geometric distribution checking

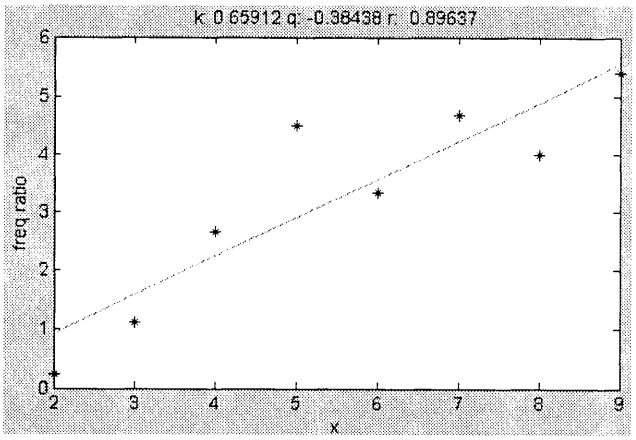

Fig. 4 Frequency ratio plot for pretreatment K

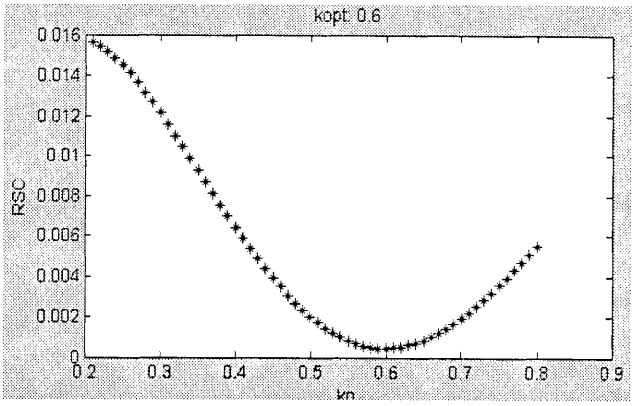

Fig. 6 Dependence of RSC on p for pretreatment K.

binomial or geometric distribution [2]. Due to simplicity the geometric distribution has been selected. Probability function of this distribution

$$f_i = p(1-p)^i$$

has the one adjustable parameter p only. For checking of this distribution the logarithmic transformation can be adopted i.e.

$$\ln(f_i) = q + ik$$

where $q = \ln(p)$ and $k = \ln(1-p)$. The dependence of $ln(f_i)$ on i should be therefore linear. This dependence for the pretreatment K is given on the fig. 5.

The correlation exceeding 0.9 were obtained in all cases. From the slope in these graphs the rough estimator $pa = 1 - \exp(k)$ of parameter p was computed. Results are given in the table 2. For more precise estimation of geometric distribution parameter the direct minimization of sum of squared distances between model frequencies and experimental frequencies *RSC* has been used.

$$RSC = \sum_i \left[f_i - p \times (1-p)^i \right]^2$$

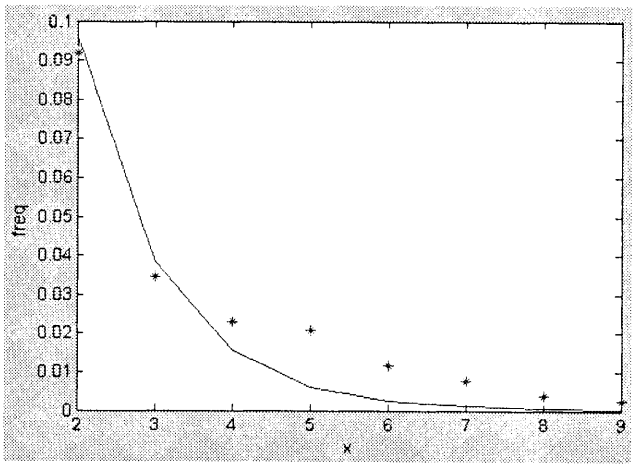

Fig. 7 Relation between experimental frequencies (stars) and frequencies from geometric distribution (line) for the pretreatment type K.

The dependence of *RSC* on p for the pretreatment type K is shown on fig. 6.

Similar graphs were obtained for another types of pretreatment as well. The optimal parameter *po* obtained

Table 4 Parameters characterizing bundles size distribution

Sample	pa	po	f_1	R10
KP	0,237	0,56	0,655	7,987
E	0,386	0,53	0,724	4,011
AE	0,332	0,53	0,706	3,143
EB	0,399	0,57	0,797	1,71
K	0,384	0,60	0,784	1,68

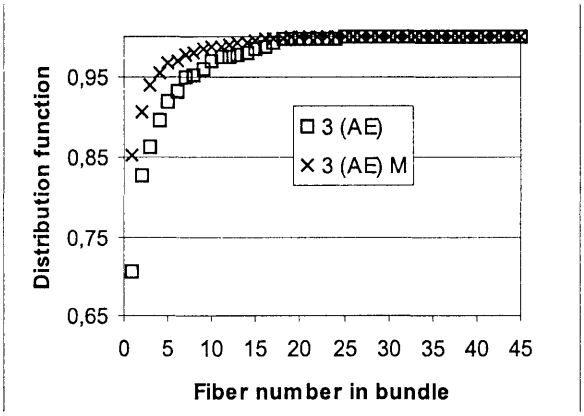

Fig. 8 Comparison of bundle size distribution for sample (AE) and (AE)M after mechanical separation

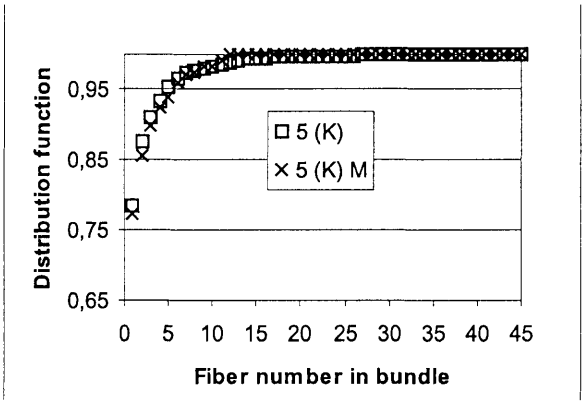

Fig. 9 Comparison of bundle size distribution for sample (K) and K(M) after mechanical separation

by this way are given in the table 4. For the pretreatment type K is relation between experimental frequencies (stars) and frequencies from geometric distribution (line) given on the fig. 7.

Due to one estimable parameter is degree of fit only moderate. Similar results were obtained for another types of pretreatment.

The selection of parameters for separation tendency description is dependent on the practical needs and simplicity of computations. From these points of view are the *R10* and f_1 preferred.

The influence of mechanical separation on bundles size distribution for sample AE is shown on the fig. 8 and for sample K on fig 9.

The graphs for other samples excluding original tow KP (similar to fig. 8) are similar to fig. 9.

It is clear that mechanical separation leads to increasing the portion of bundles with small number of element fibers only for pretreatment AE. The difference in distribution for sample K is practically negligible. (see. fig. 9). The same conclusions are valid for samples E and EB as well.

5. CONCLUSIONS

From the inspection of table 2 is clear that parameter R10 is very useful for characterization of bundles separation tendency. Parameter f_1 reflect the portion of ultimate fibers and is suitable as well. Fibrous bundles distribution can be approximated by geometric distribution with one parameter *p*. There are large differences between estimates obtained from linearization and nonlinear estimation. The parameter of geometric distribution is similar for all pretreatments excluding KP. Higher value of parameter *p* leads to the higher rate of frequency drop (quicker tendency to bundles separation)

ACKNOWLEDGEMENTS:

This work was supported by the research project LN00B090 of Czech Ministry of Education

6. REFERENCES

[1] Koch A. Fasertafels, Reutlingen 1994
[2] Meloun M., Militký J.,Forina M.: Chemometrics for Analytic Chemistry I, Ellis Horwood, 1992
[3] Internal Rep., INOTEX, Dvůr Králové, 2002
[4] Militký J. et all: Proc. Int. Conf. TEXTSCI 2000, Liberec July 2000

STUPEŇ KOTONIZACE PŘEDZPRACOVANÉHO LNU

Translation of Abstract:

Cottonization degree of pretreated flax fibers

Cílem této práce je popis vlivu enzymatického a chemického předzpracování na oddělitelnost vlákenných svazků. Pro charakterizaci této oddělitelnosti bylo stanoveno rozdělení vlákenných svazků. Bylo využito obrazové analýzy příčných řezů . Je určena četnost svazků překračujících zadanou mez.

A NOVEL METHOD OF TEXTILE MELANGE COLOR PREDICTION

Wiener, J., Kryštůfek, J., Prášil, M.

Department of textile finishing, Technical University of Liberec, Hálkova 6, 461 17 Liberec 1, Czech Republic, jakub.wiener@vslib.cz

The classic Kubelka-Munk function cannot be used for prediction of color of melanges. For the color of melanges the additive functions are used. The most frequent citations are Friele's and Stearns's functions, which are in this study applied on the blend viscose/viscose and viscose/polyester. Both of models are useable for description of color of tested samples.

At the mixture of viscose/polyester also was studied the influence of fineness of non-colored polyester components on the color of melange and on the values of Friele's and Stearns's parameters.

In this study is proposed a novel method for elimination of differences of fiber fineness by description of melange composition in a surface ratio.

1. INTRODUCTION

Colored staple fibers, namely black, dark brown and dark blue etc. are sometimes intimately blended (in loose material or in sliver) with the colorless or only lightly colored fibers to achieve the specific and aesthetic very interesting effect: *"melange"*, which is demanded mainly for the wool-working articles.

The textile producers are often surprised how much the dyes consumption can be cut down by the alternation of e.g. black/white *melange* to *uni*-grey assortment (usually piece dyeing – it is more operational too). And on the contrary: the differences in dyes consumption could be much greater than 50 % (sometimes even than 100 %) by the optically approx. same grey hue in melange-form.

By other words: the same dye-concentration gives much lower optical effect by the greater incoherent dislocation of dyes molecule (or greater dyes particles) in the fiber textile system.

Indication of the equal phenomenon becomes evident on a smaller canvas but perhaps even more often by all sorts of deviations from uniform dyeings (the typical examples are the tippy dyed wool and the insufficiently dyed unnatured fibres in cotton).

The full curve in figure 1 demonstrates from us observed real dependance of the Kubelka-Munk constants K/S on the approximate concentration of dyes (C_B) in the blend. The concentration is proportional to the block-mass dyed-viscose staple fibers, which are mixed with colorless fibres (in both cases: 1.4 dtex, 40 mm). The „ideal" dashed direct line in figure 1 responses this relation by the ideal validity of Kubelka-Munk equation:

$$\frac{K}{S} = \frac{(1-R)^2}{2R} = \text{const. } C_B \qquad (1)$$

where R is the reflectance of the textile.

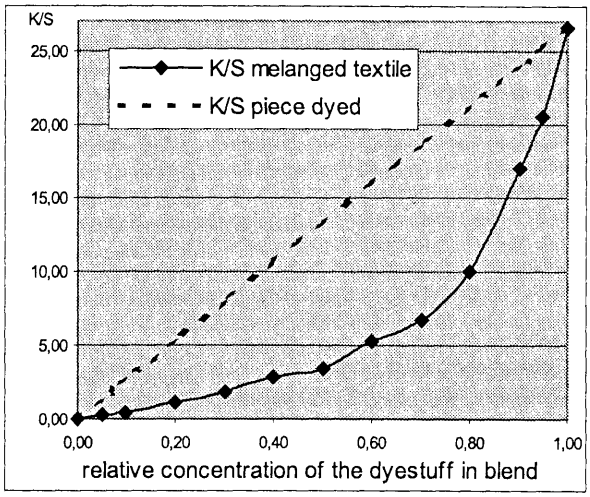

Fig. 1 K/S values as the function of black fibers in blend.

In order to quantify the real trend R and C_B, Stearns and Noechel [4] (already 1944) proposed an additive function of the form:

$$F(R_b) = x_1F(R_1) + x_2F(R_2) \qquad (2)$$

where x_1 and x_2 are the relative weight proportions of fiber components 1 and 2, R_b, R_1, R_2 are the reflectances of the blend and of the components. The F(R) is an empirically derived hyperbolic function of the form

$$F(R) = \frac{(1-R)}{M(R-0{,}01)+0{,}01} \qquad (3)$$

where M is an empirical (Stearns's) constant: e.g. for wool blends M = 0.15, but it is dependent on different fiber physical form and properties. Thus Friele [3] has found values M from 0.09 to 0.18 (felts and loose woll). D. A. Burlone [1] has found for nylon a value of M = 0.11 which varies with the method used to judge best fit. Davidson & Taylor [2] use special form of equation 2

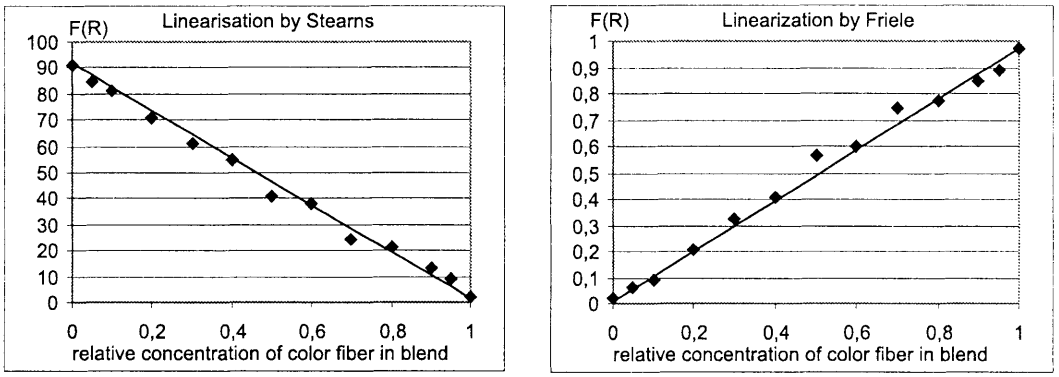

Fig. 2 Linearization of experimental data, vertical axis – F(R) – left Stearns's function (equation 3) – right Friele's function (equation 4)

and have found the best fit to Stearns equation with M = 0.25 for acrylics.

An other empirical equation F(R) in exponential form was proposed by Friele (the symbols have the same meaning as above). F(R) takes the form:

$$f(R) = \left(e^{\frac{-(1-R)^2}{2R}} \right)^s \qquad (4)$$

where s is Friele's parameter

The Friele's equation generally provides good results, but its accuracy decreases if an important amount of a very light color or a fluoroscent color is introduced in the blend.

Each fibre type is assigned a value of the Friele's parameter σ, e.g. wool (circular shape) 0.30, viscose (circular) 0.28, cotton (bean) 0.245, PAN (variable) 0.11, PA6 (trilobal) 0.25, PET (variable) 0.094.

2. EXPERIMENTAL

Fibers used for this study were mass pigmented and colorless cellulose viscose (or polyester) staple fibers. All fibers were matted. The cross-section of all viscose fibers was identical, i.e. lobate – as it is typical for viscose fibers. For the polyester the cross-section is circular. It was prepared 11 blends (from each variant), which differ after 10 or 5 % of color-component.

The blending was carried out by the three times repeated carding on the laboratory cylinder carding machine BEFEMA (180 rpm). It was verified the blend-homogeneity is maximal and the visual and objective chromacity-impression does not further changes. The check-production on the Shirley Miniature Spinning Plant (Sago Nowel, 890 rpm) gave the same results. The samples after carding were mechanical fixed by the bonding technology – known by the nonwoven production and pressed 30 sec. at 150 °C. The reflectance spectral curves of primary colors were measured on the spectrophotometer DATACOLOR (type 3890, measured area 18, screen 18, with lustre, UV 100 %). Each sample was measured in four places – the differences were negligible.

3. RESULTS

Comparation of Stearns's and Friele's model

Comparation of Stearns's and Friele's model was made on the viscose-viscose blends; color component: red, viscose fibers, typical cross-section, dull, fineness 1.4 dtex; colorless component: colorless, typical cross-section, dull, fineness 1.4 dtex

For calculation of Staerns's and Friele's parameters were used experimental remission data of red-colorless blend measured at 540 nm. Calculated parameters were applied to all other lights.

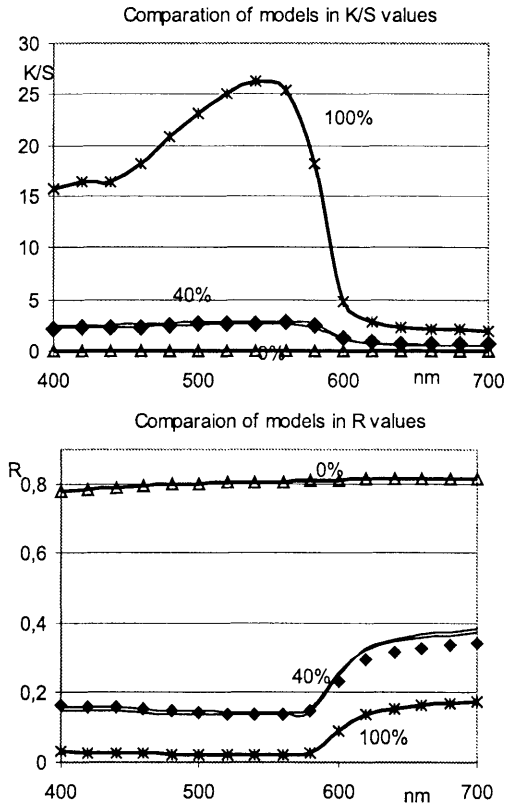

Fig. 3 Compilation of predicted reflectance (R) and Kubelka-Munk (K/S) function with experiments. Tested blend was constructed from 40% of red color part ("100%") and 60% of colorless part ("0%")

From Sterns´s and Friele´s equations is easy to transform the nonlinear function to linear (fig. 2).

The computed and experimental obtained values are demonstrated in figure 3.

Both tested models (Stearns´s and Friele´s) are useful for prediction of optical reflectance of fiber blends. For observed system Stearns´s parameter was 0.10 and Friele´s parameter 0.145.

Influence of fineness of colorless component on color of melange

In all available literature resources we can find an evaluation of melange, which contains colored and colorless components of the same fineness and the same shape of fibers. E.g. colorless component is wool and colored component is the same, but dyed, wool.

In this study color of melanges is evaluated in the case that the same colored component is blended with the colorless components of different finenesses.

The colored component was in all cases viscose, which was mass dyed. The colorless component was polyester fiber with circular cross-section and with different finenesses (1.3–12 dtex). The results can be seen in the Fig. 4.

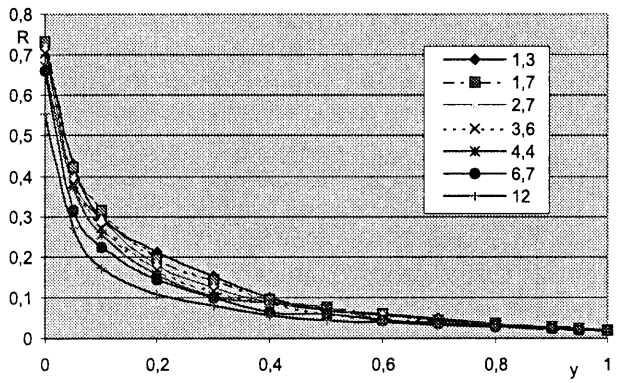

Fig. 4 Color of melanges with different finesses of colorless fibers. R – reflectance, y – mass ratio of colored fibers in the blend; color component: red, viscose fibers, typical cross-section, dull, fineness 1,7 dtex; colorless component: PET, colorless, dull, fineness 1,3 dtex, circular cross-section

By analysis of the dependences of the reflectance on the mass ratio of colored fibers we can calculate Friele´s and Stearn´s parameters for different fineness of the colorless components in the blend with viscose fibers (1.4 dtex). The calculated results are in the figure 5.

The dependences in the figure 5 can be used for prediction of color of melange with a polyester component in wide range of fineness.

A new expression of melange content which eliminate the influence of fineness of the components

The only experimental determination of the Stearns´s and Friele´s parameters on the fineness of the mélange is not enough for the solving of practical problems for melange design.

In this study a new expression of melange content is designed and it depends on these assumptions:

The color of melange will depend on the probability how light waves enter the fibres component of mélange. We can suppose that this probability directly depends on (rather then the weight ratio of fibers y) "a surface" ratio of fibers w. It means how much of the whole surface of the textile go to the follow component of mélange.

For uncircular fibers (e.g. viscose) fibers is possible to use for the calculation a surface of a circular fiber of an equivalent fineness.

For a calculation of "a surface" ratio w of the colored component is possible to use a classical weight ratio y of the colored component:

$$w = \frac{y\rho_2 R_2}{y\rho_2 R_2 + (1-y)\rho_1 R_1} \tag{5}$$

where R – fiber radius, ρ – fiber density

If the density of both fiber components is the same, it is possible to use a simple dependence:

$$w = \frac{yR_2}{yR_2 + (1-y)R_1} \tag{6}$$

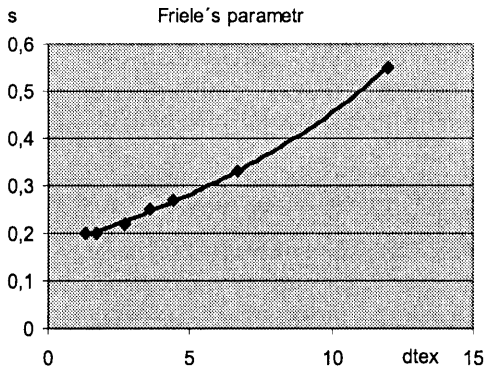

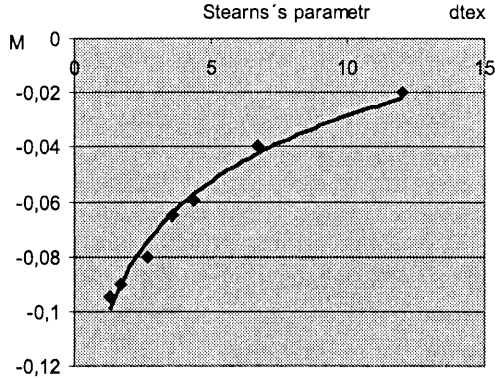

Fig. 5 Dependence of Friele´s a Stearns´s parameter on the finesses of non-colored component in the mixture with red viscose fiber (1.4 dtex)

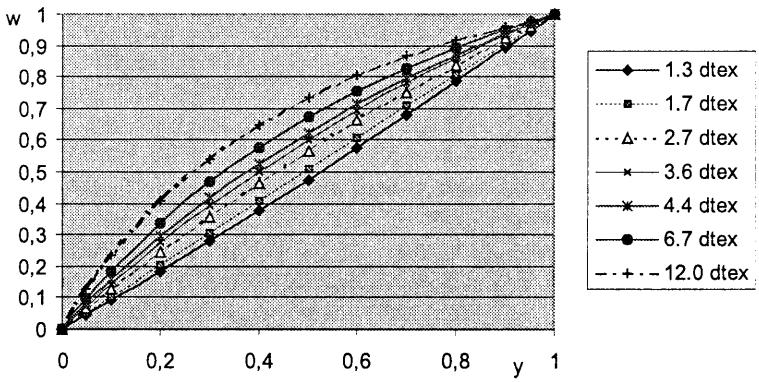

Fig. 6 Dependence of surface ratio **w** of PET fibers (different fineness) on the weight ratio **y** in the blend with viscose fibers with fineness 1.4dtex

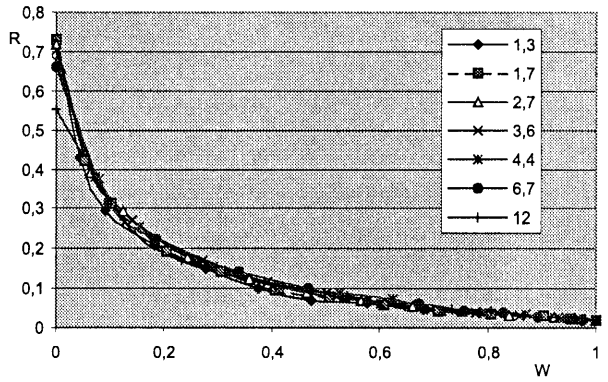

Fig. 7 Color of melanges with different finesses of colorless fibers. R – reflectance, w – surface ratio of colored fibers in the blend; color component: red, viscose fibers, typical cross-section, dull, fineness 1,7 dtex; colorless component: PET, colorless, dull, fineness 1,3 dtex, circular cross-section

The dependence of the surface ratio on the weight ratio of one component is the figure 6.

A novel expression of melange content (i.e. surface ratio of fibers) was used for the data in the figure4. The results are in the figure 7.

All the experimental data are placed one curve – that means, we succeeded in elimination of the influence of the colorless components fineness.

We do expect that all the other melanges will have similar dependences. So the surface fiber ratio in melange causes easier color prediction in melange from fibers of all fineness.

Acknowledgement:
This study was created with the support of "The research project of the Textile Faculty" CEZ:J11/98:244100004

5. REFERENCES

[1] Burlone DA, Effect of fiber translucency on the color of blends of precolored fibers, Text Res J. 1990, 60, 162–167
[2] Davidson HR, Taylor M, Prediction of the color of fiber blends, J Opt Soc Am 1965, 55, 96–100
[3] Friele LFC, The application of color measurement in relation to fiber-blending, J Textile Inst 1952, 43, 604–611
[4] Stearns EI, Noechel F: Spectrofotometric prediction of cotton wool blends, Am Dyest Rep 1944, 33,177–180

NOVÁ METODA PREDIKCE BAREVNOSTI TEXTILNÍ MELANŽE

Translation of Abstract

A novel method of textile melange color prediction

Klasická Kubelka-Munkova funkce nemůže být použita k predikci barevnosti melanží. Pro predikci barevnosti se v tomto případě používá tzv. aditivních funkcí. Nejčastěji používané jsou Frieleho a Stearnsova, které jsou v této práci aplikovány na směs viskóza/viskóza a polyester/viskóza. Oba modely jsou použitelné pro popis barevnosti testovaných vzorků.
Na směsi viskóza/polyester byl studován vliv jemnosti nebarevné polyesterové komponenty na hodnotu Stearnsova a Frieleho parametru.
V práci je navržena původní metoda eliminace změn jemnosti komponent melanže – vyjadřování složení melanže v tzv. povrchových podílech.

MASS IRREGULARITY CHANGES IN SPINNING TECHNOLOGY

Ursíny P.

Technical University of Liberec, Dept. of Mechanical Technologies, Liberec, Czech Republic

The author describe the theory of mass irregularity changes in the spinning technology. Resulting mass irregularity of yarn depends on the several technological stages, but main influence has the finite technological stage – spinning machine.

In the paper is introduced analysis of mass irregularity changes in the ring spinning machine and in the OE – rotor spinning machine

1. INTRODUCTION

In the spinning technology occurs mass irregularity change in consequence with several technological stages applications. For example the preparation of the supply sliver for OE – rotor spinning machines is done at present in a normal way marked by gradual processing of cotton type fibrous raw material in a cotton blow room with continuously arranged system of carding machines. The carded sliver is drawn an doubled in two drafting passages resulting in a sliver suitable for futher processing on OE – rotor spinning machines.

In order to reach the required quality of the rotor spun yarn and to provide for successful course of the spinning process in the rotor spinning unit, certain demands are made on the quality of the supply sliver that must be reliably ensured by the corresponding technological process.

The said production process, hitherto used, creates good technological conditions providing the corresponding quality.

Resulting mass irregularity of yarn depends on the several technological stages, but main influence has the finite technological stage – spinning machine. Analysis of mass irregularity change we achieve not only in the OE – rotor spinning machine but also in the ring spinning machine.

2. THEORETICAL BASIS OF MASS IRREGULARITY CHANGES IN THE SPINNING TECHNOLOGY

Analysis of the change in mass irregularity is performed on the basis of the laws of variation phenomena in random processes. The overall variation in the mass of short lengths of the intermediate product and the end product in yarn manufacture can be regarded as the sum of the variations of the individual components of the mass irregularity. The individual components of the mass irregularity are independent of each other. Their equation is:

$$\delta^2 = \sum_{i=1}^{k} \delta_i^2 \qquad (1)$$

where: δ^2 – the total variation of the mass of short lengths of the sliver, roving of yarn; δ_i^2– the variation of a component i of the mass of short lengths of the sliver, roving or yarn; k – the number of components of mass irregularity.

Applying (1) to the USTER parameter produces the following equation (2):

$$CV^2 = \sum_{i=1}^{k} CV_i^2 \qquad (2)$$

CV is the total square irregularity, and CV_i component i of the square irregularity.

The following CV_i components are also considered [2, 3]:

CV_1 – square threshold irregularity ($CV_1 = CV_{lim}$) determined by the random distribution of the fibre numbers in the sliver or yarn cross – sections.

CV_2 – systematic square mass irregularity due to the incomplete nature of the individual stages of processing before the processing stage under consideration, i.e. before spinning ($CV_2 = CV_s$)

CV_3 – additional square mass irregularity due to the processing stage under consideration, e.g. spinning ($CV_2 = CV_p$)

CV_4 – systematic square mass irregularity which occurs in immeasurable short lengths in drafting ($CV_4 = CV_{VS}$)

3. MASS IRREGULARITY CHANGE IN THE RING SPINNING MACHINE

When the analytical considerations mentioned above are applied to conventional cotton spinning systems, equations (3) and (4) are derived. In conventional spinning, drawframe sliver is the feed material for the speedframe. On the basis of these feed materials the mass irregularity of the yarn is as follows:

For the roving stage the square irregularity of the roving is obtained from equation (3):

$$CV_{VG} = \sqrt{CV^2_{lim.0}P_1 + CV^2_{P1} + CV^2_{VS1} + CV^2_{S,0}} \quad (3)$$

$CV_{lim.0}$ – square threshold irregularity of the feed sliver (a drawframe sliver); $CV_{S,0}$ – systematic square irregularity of the feed sliver; CV_{P1} – additional square irregularity due to the drawing process on the speedframe (P_1 draft applied by the drafting system); CV_{VS1} – resulting systematic square mass irregularity occuring in immeasurable short lenghts at draft P_1.

The square mass irregularity of the yarn is given by equation (4):

$$CV_G = \sqrt{CV^2_{lim.0}P_1P_2 + CV^2_{P1} + CV^2_{P2} + CV^2_{VS1} + CV^2_{VS2} + CV^2_{S,0}} \quad (4)$$

$$CV_G = \sqrt{CV^2_{lim.2} + CV^2_{GP} + CV^2_{GVS} + CV^2_{S,0}} \quad (5)$$

In which

$$CV_{lim,2} = \sqrt{CV^2_{lim.0}P_1P_2}\ ,\ CV_{GP} = \sqrt{CV^2_{P1} + CV^2_{P2}}\ ,$$

$$CV_{GVS} = \sqrt{CV^2_{VS1} + CV^2_{VS2}}$$

In addition there are the following mass irregularity components:

CV_{P2} – additional square mass irregularity due to the drafting process on the ring spinning frame (P_2 draft).

CV_{VS2} – resultant systematic square mass irregularity occurring on immeasurable short lenghts at draft P_2.

It results from equation (5) that the square mass irregularity of the yarn is determined by the square threshold irregularity CV_{lim2} and the systematic square irregularity CV_{S2}, in which CV_{S2} is:

$$CV_{S2} = \sqrt{CV^2_{GP} + CV^2_{GVS} + CV^2_{S,0}}$$

4. MASS IRREGULARITY CHANGE IN THE OE – ROTOR SPINNING SYSTEM

The mass irregularity is ensured in the rotor spinning unit by means of the system of cyclic doubling that takes place in spinning rotor. By previous studies, the said system had been analysed by approaching this system as a dynamic one, characterized by a module of transfer function and the determination of the marginal wavelenghts of the harmonic components of the mass irregularity is an important conclusion for the given set of problems.

To get an idea about the particular marginal wavelenghts we show the results of their calculations for the supply sliver (Table 1).

It results from sufficient range of yarn fineness and diameters of collecting surface shown in the Table 1 that the equalizing system of the cyclic doubling is able to damp down the harmonic components of the mass irregularity with very short wavelenght (max. value= 8,4mm).

Table 1 MARGINAL WAVELENGTHS λ_1, λ_2 OF THE SLIVER MASS IRREGULARITY, T_0 = 3 540 tex

d_3 [mm]	u [mm]	T_4= 25 tex P_c= 141,6	T_4= 29,5 tex P_c=120	T_4= 35,5 tex P_c=99,7
67	210,5	λ_1 = 1,9	2,2	2,6
		λ_2 = 5,9	7,0	8,4
54	169,6	1,5	1,8	2,1
		4,8	5,7	6,8
43	135,1	1,2	1,4	1,7
		3,8	4,5	5,4
32	100,5	0,9	1,0	1,3
		2,8	3,3	3,0

T_0 – sliver fineness, T_4 – yarn fineness, d_3 – diameter of the collecting surface of the rotor, λ_1 [mm] – marginal wavelenght of the sliver ,defining the limits of the interval with high equalizing effect, u – circumference of the collecting surface defining the limits of the interval with high equalizing effect [mm], λ_2 – marginal wavelenght of the sliver mass irregularity definig the lower limit of the interval, as a matter of fact, without any equalizing effect [mm]

It is evident that the supplied sliver must have high mass irregularity even in short terms. Low CV is required (the length of the measured segment on the Tester Uster L = 10 mm) and of course on longer terms even a low CV(L = 1 m) is consequently required.

Further analysis bears on CV [%] i.e. square mass irregularity on the short sections.

Structure of the mass irregularity in the OE – rotor spinning system results from next relations.

Fiber ribbon:

$$CV_p^2 = CV^2_{limp} + CV^2_{sp} \quad (6)$$

CV_p – square mass irregularity of resulting OE yarn (if need be fiber ribbon on the collection surface),

CV_{limp} – square threshold irregularity of OE – yarn

CV^2_{SP} – systematic square irregularity of OE – rotor yarn

$$CV_3^2 = CV^2_{lim3} + CV^2_{S3} \quad (7)$$

$$CV^2_{S3} = CV^2_{S0} + CV^2_{P03} + CV^2_{VS03} \quad (8)$$

CV_3 – square irregularity of fibre flow on the collecting surface

CV_{lim3} – square threshold irregularity of fiber flow

CV_{S3} – systematic square irregularity of fiber flow

CV_{S0} – systematis square irregularity of supplied sliver

CV_{P03} – additional square irregularity induced in the opening process

CV_{VS03} – systematic square irregularity induced trough draft in the opening proces

CV_0 – square irregularity of supplied sliver

$CV_{lim\,0}$ – square threshold irregularity of supplied sliver

P_{03} – draft of the opening system.

$$CV_0^2 = CV^2_{lim0} + CV^2_{S0} \quad (9)$$

We convert the equations (6) ÷ (9) with use of technological patterns of doubling and drawing influence.

$$CV_3^2 = CV_{lim0}^2 . P_{03} + CV_{P03}^2 + CV_{VS03}^2 + CV_{VS03}^2 + CV_{S0}^2 \quad (10)$$

$$CV_P^2 = CV_{lim\,p}^2 + \frac{CV_{S3}^2}{N} \quad (11)$$

$$CV_0^2 = CV_{lim0}^2 + CV_{S0}^2 \quad (12)$$

Machine square irregularity CV_{OE} :

$$CV_{0E}^2 = \left(CV_P^2 + CV_{lim\,P}^2\right) - \left(CV_0^2 + CV_{lim0}^2\right) \quad (13)$$

$$CV_{0E}^2 = \frac{CV_{P03}^2 + CV_{VS03}^2}{N} - CV_{S0}^2 \frac{N-1}{N} \quad (14)$$

N – number of cyclic doubling

Below we explain still the influece of OE yarn fineness on the internal level of opening system draft and number of cyclic doubling.It follows too certein limitation of higher OE yarn fineness.

Total draft of OE rotor spinning system P_c :

$$P_c = P_{03} \frac{1}{N} \eta \quad (15)$$

P_{03} – draft of the opening system, N – number of cyclic doubling, η – take-up coefficient (linear contraction of ribbon in consequence of twist).

Draft of the opening system

$$P_{03} = \frac{P_c N}{\eta} \quad (16)$$

Number of cyclic doubling

$$N = \pi d_3 Z \eta \quad (17)$$

d_3 – diameter of the collecting surface [m], Z – machine twist [m^{-1}].

After substitution in the equation(16) we obtain

$$P_{03} = \frac{T_0}{T} \pi D_3 Z \quad (18)$$

T_0 – fineness of the sliver supplied [tex], T –fineness of the resulting OE – yarn [tex].

By using of the relation for OE – yarn twist as a fineness function with constant twist coefficient we obtain the relations for draft of the opening system P_{03} and number of cyclic doubling in the next form.

$$P_{03} = T_0 \frac{K}{T^{5/3}}, \quad K = \pi d.am.100 \quad (19)$$

where am – twist coefficient.

$$N = \frac{K\eta}{T^{2/3}} \quad (20)$$

The changes of draft P_{03} and number N as a functioon of OE – yarn fineness T(derivation of a function P_{03} and N by course of fineness T as a function of OE – yarn fineness T) are:

$$p(T) = K_1 T_0 \frac{1}{T^{8/3}} \quad (21)$$

$$n(T) = K_2 \frac{1}{T^{5/3}} \quad (22)$$

$p(T)$ – draft change of opening system of relation to unit change of OE – yarn fineness as a function of OE – yarn fineness, $n(T)$ – number change of cyclic doubling in relation to unit change of OE – yarn fineness as a function of OE – yarn fineness, $K_1 = (-5/3)K$, $K_2 = (-2/3)K\eta$.

Ratio $R(T)$:

$$R(T) = \frac{p(T)}{n(T)} \quad (23)$$

Increase in ratio $R(T)$ corresponds with increase of mass irregularity.In the area of higher

fineness of OE – yarns (T = 14,5 ÷ 20 tex) are very high value of ratio R(T) (Table 2).

For this instance we need a higher quality of supplied sliver.

Table 2 Ratio R(T) of draft change of opening system and number change of cyclic doubling system

T[tex]	R(T)	
	T_0 = 3 125 tex	T_0 = 3570 tex
20	411,2	–
22	373,8	–
25	328,9	–
28	293,7	–
29,5	–	318,4
32	–	293,5
34	–	276,3
35,5	–	264,6

T[tex] – fineness of OE – yarn, T_0[tex] – fineness of supplied sliver

5. CONCLUSION

Structure of the mass irregularity of fibre product contains particular components.This is the question of threshold square irregularity determined by the random distribution of the fibre numbers in the sliver, roving or yarns cross – section, systematic square mass irregularity due to the incomplete nature of the individual stages of processing before the processing stage under consideration, i.e. before spinning, additional square mass irregularity due to the processing stage under consideration, e.g. spinning, systematic square mass irregularity which occurs in immeasurable short lenghts in drafting. For a consideration of changes of separate components we determine of mass irregularity change in ring – and OE – rotor spinning system and from this imply requirement on the supplied fibre product (sliver or roving).

Acknowledgement:

The present work is sponsored by the research grant GAČR 106/01/0565.

REFERENCES

[1] URSÍNY, P., MÄGEL, M.: Melliand Textilberichte, 80 (1999), 4, 242–243.

[2] BOWLES, A. H., DAVIES, L.:.The Textile Institut and Industry, (1978), 11, 371–374.

[3] URSÍNY, P.:Textiltechnik, 38, (1988), 2, 71–73.

ZMĚNY HMOTNÉ NESTEJNOMĚRNOSTI V PŘÁDELNICKÉ TECHNOLOGII

Translation of Abstract:

Mass irregularity changes in spinning technology

Autor popisuje teorii změn hmotné nestejnoměrnosti v přádelnické technologii. Výsledná hmotná nestejnoměrnost příze závisí na jednotlivých technologických stupních, ale hlavní vliv má konečný technologický stupeň – dopřádací stroj. V článku je uvedena analýza změn hmotné nestejnoměrnosti u prstencového dopřádacího stroje a u rotorového dopřádacího stroje.

The INFLUENCE OF THE BACK-REST'S BEHAVIOUR ON THE WEAWING PROCESS

Tumajer P.

Technical University of Liberec, The Textile Faculty, Department of Mechanic Technology in Textiles, Hálkova 6, 461 17 Liberec, Czech Republic
e-mail: petr.tumajer@vslib.cz

This contribution deals with experimental measurements of the behaviour of the weaving machine's back-rest and acquaints with the method of the analysis of the effect of this behaviour on the fabric forming. The experimental measurements are realised in Weaving laboratory of Technical University of Liberec on the Air-jet weaving machine. Additional parts of this contribution describe the weaving machine, the used measuring devices and the processing of measured values. The measured values are represented graphically.

1. INTRODUCTION

The back rest on a weaving loom has two main functions. The back-rest roller conducts the warp into the weaving-plane and creates the let of motion's sensor of the force in the warp. Mounting the back-rest roller on sprung two-armed levers provides the sensing of tension force in the warp. The back-rest roller's position changes with the change of the force in the warp. The change of the back-rest roller's position influences the force in the warp's thread in the feedback. The opening of shed, the beat-up process and the change of the back-rest roller position have the influence on the total force in the warp during the weaving cycle. The behaviour of the beck-rest has the negative effect or the positive effect on this force and on the fabric forming.

This contribution deals with experimental measurements of the behaviour of the weaving machine's back-rest and acquaints with the method of the analysis of the effect of this behaviour on the fabric forming. The experimental measurements are realised in weaving laboratory of Technical University of Liberec on the Air-jet weaving machine. Additional parts of this contribution describe the weaving machine, the used measuring devices and the processing of measured values. The measured values are represented graphically.

2 THE WEAVING MACHINE AND THE MEASURING DEVICES

The measurements realised on the Air-jet weaving machine PN-170 FB M2 (see. Fig. 1), with this textile material:

- warp: 25 tex, 730 Z, 67/33 polyester/cotton,
- weft: 18 tex, 600 Z, polyester,
- warp density: 30 threads/1cm,
- weft density: 23 threads/1cm,
- weave: linen.

We used these devices for the measurements:

1) inductive sensors for the measurement of the back-rest position (see Fig 2) and for the measurement of the harness (see Fig 3),
2) force sensors for the measurement of the force in the warp's thread in front of the back- rest (see Fig. 4) and at the back of the back-rest (see. Fig. 5),
3) optoelectronic sensor of the extreme forward position of the reed (see. Fig. 6),
4) data logger (see Fig. 7)

The graphs on the Figure 8 show the dependencies of the measured values on the time during two weaving cycles. The signal of the optoelectronic sensor of the extreme forward position of the reed is displayed in the top part of the every graph.

The third graph on the Figure 8 shows the distance of the point "A" of the back-rest lever S_a. This point "A" is the point, in which the core of the inductive sensor is screw-bolted on the back-rest lever (see Fig. 9).

Further, we will compute the distance of the back-rest roller S: $S = (R2/R1)S_a$. These values are represented graphically on Figure 10 and Figure 11. The Figure 10 shows the graph of the dependence of the distance of the back-rest roller S on the time and the graph of the distance of the reed Sr on the time. The distance of the

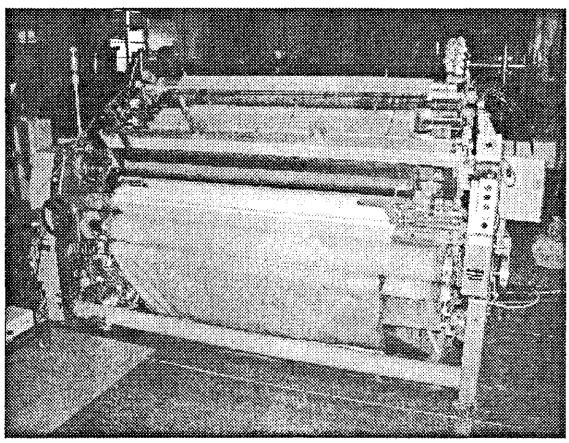

Fig. 1 The weaving machine, revolutions 391 rpm

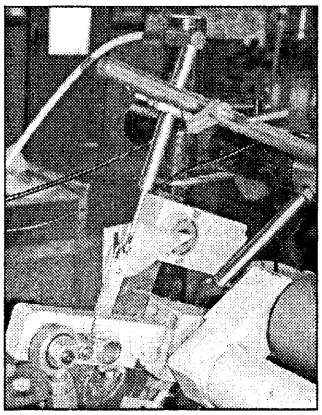

Fig. 2

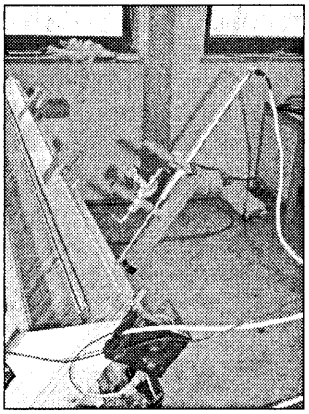

Fig. 3

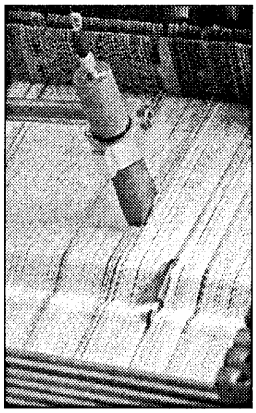

Fig. 4

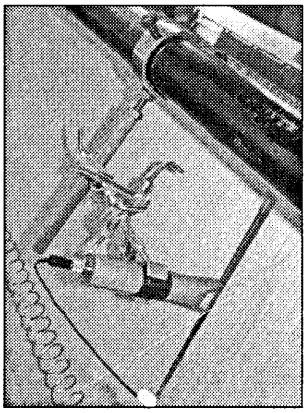

Fig. 5

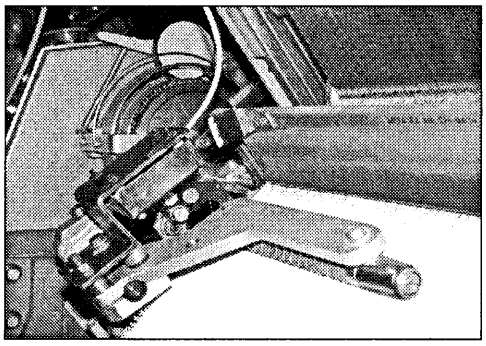

Fig. 6

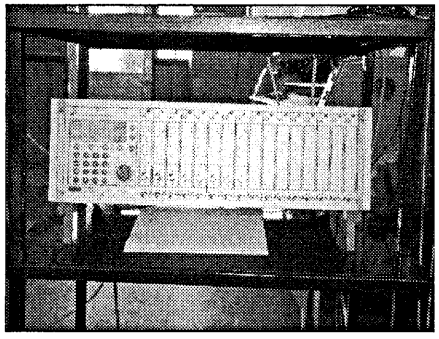

Fig. 7

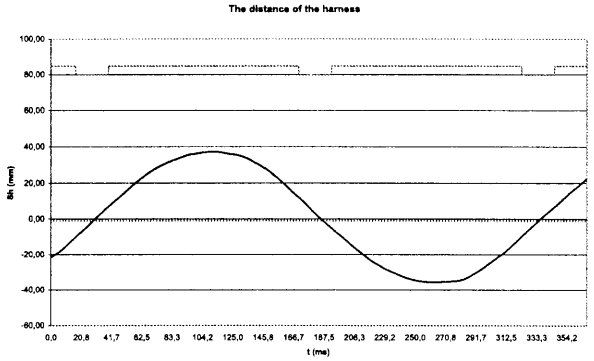

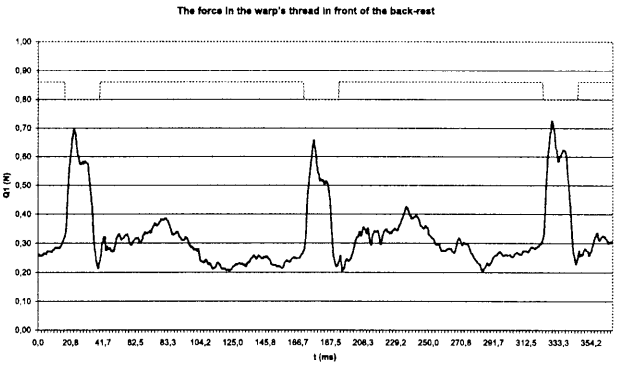

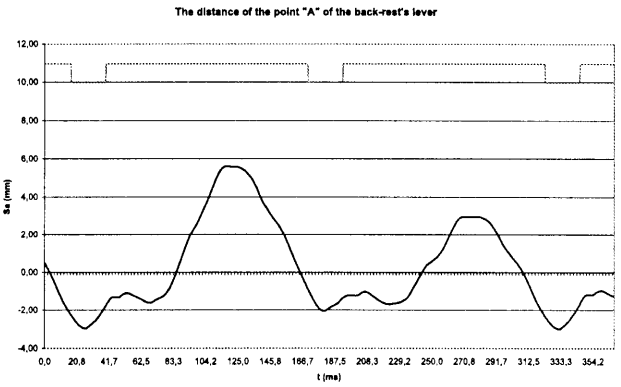

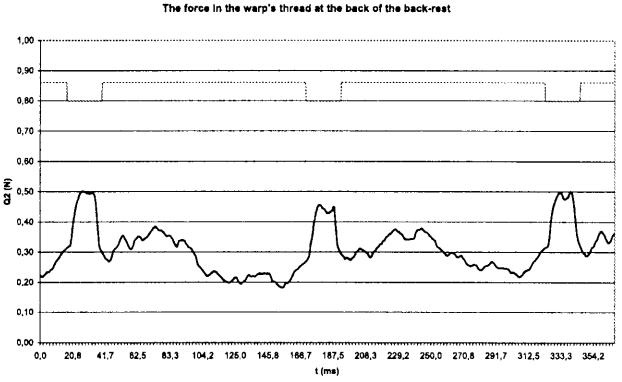

Fig. 8

reed is determined by using the cinematic model of the beat-up mechanism of the weaving machine PN-170 FB M2. The Figure 11 shows the graph of the dependence of the distance of the back-rest roller S on the time and the graph of the distance of the harness S_h on the time.

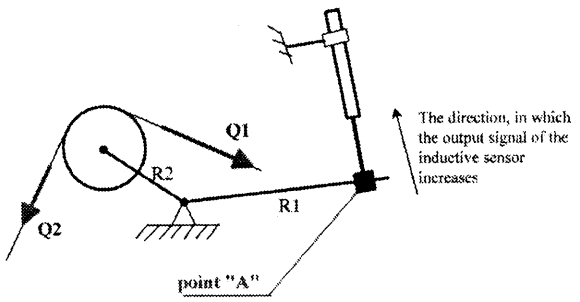

Fig. 9

CONCLUSION

The position of the back-rest roller has an influence on the force in the warp during the weaving cycle. Therefore, we can take advantage of the back-rest's behaviour for the positive interference on the beat-up process and for the compensation of the force in the warp during the opening of the shed.

The positive interference on the beat-up process: If the back-rest roller moves up during the movement of

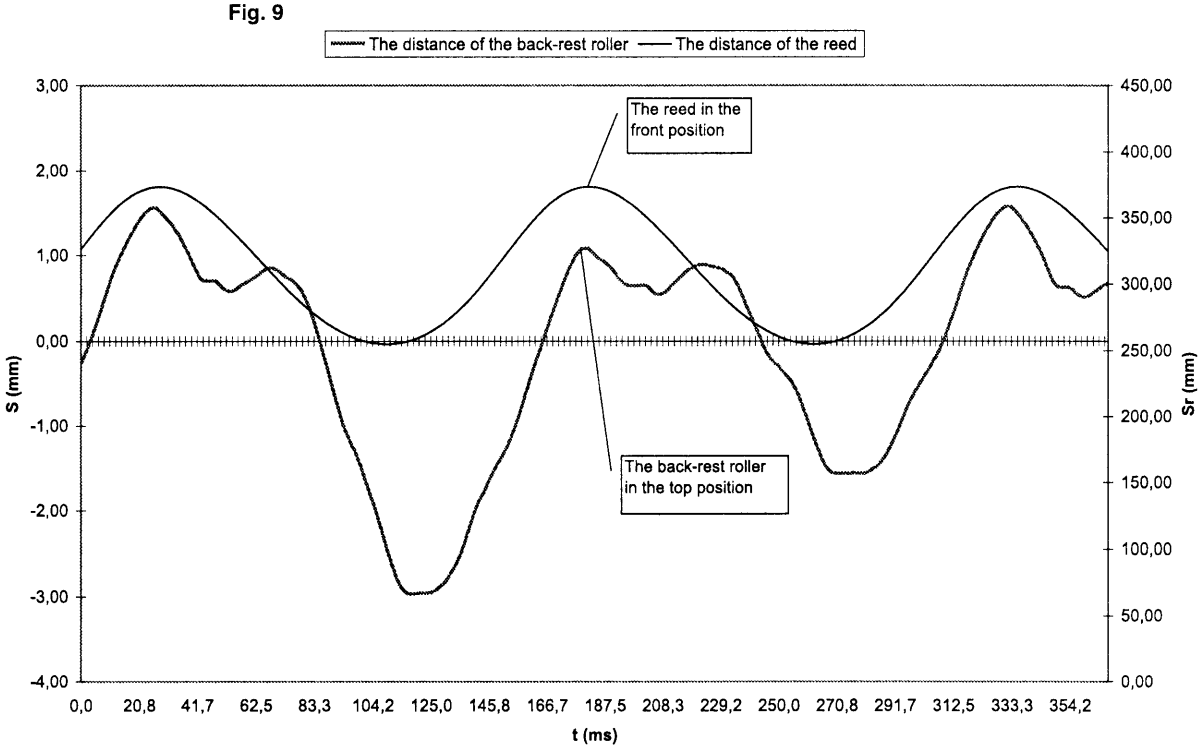

Fig. 10

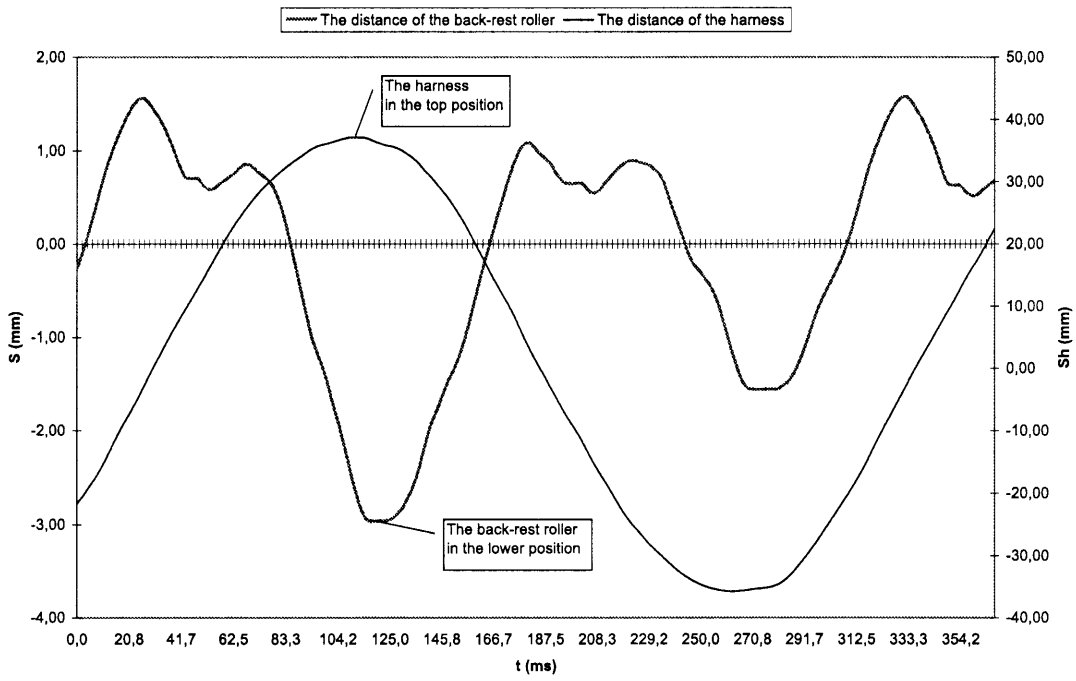

Fig. 10

the reed to the front position, the force in the warp increases, and the fabric shifts counter to the reed during the beat-up process. This behaviour has the positive interference on the weft sliding in to the fabric.

The compensation of the force in the warp during the opening of the shed: The opening of the shed increases the force in the warp. If the back-rest roller moves down during the movement of the harness to the top position, the total force is decreased.

The graphs on the Figure 10 show the mutual coupling of the distance of the beck-rest roller and the distance of the reed: On that case, the beck-rest roller moves up during the movement of the reed to the front position and this behaviour has the positive interference on the beat-up process. The graphs on the Figure 11 show the mutual coupling of the distance of the back-rest roller and the distance of the harness: On that case, the back-rest roller moves down during the movement of the harness to the position and this behaviour has the positive interference on the total force in the warp, too.

This contribution is the part of the project of Grant Agency of the Czech republic with name: "Analysis of possibilities to increase the weft density of the fabrics, which are made on the high-speed weaving loom" (recording number: 101/00D109).

VLIV CHOVÁNÍ OSNOVNÍ SVŮRKY NA TKACÍ PROCES

Translation of Abstract:

The influence of the back-rest's behaviour on the weawing process

Článek se zabývá experimentálním měřením chování osnovní svůrky tkacího stroje a seznamuje se způsobem analýzy vlivu tohoto chování na formování tkaniny. Experimentální měření bylo realizováno v Tkalcovské laboratoři Technické Univerzity Liberec na pneumatickém tkacím stroji. Jednotlivé části článku popisují tkací stroj, použité měřící zařízení a způsob zpracování naměřených hodnot. Naměřené hodnoty jsou prezentovány grafickou formou.

SURFACE QUALITY CONTROL BASED ON IMAGE PROCESSING METHODS

Chrpová E.

Department of „Mechanical Technologies" at the Technical University of Liberec

The surface quality is described by the surface defects. On line testing of the surface defects is done at the factories by the visual testing performed by workers. This way of testing is liable for mistakes produced by human errors and subjectivity. The objective controlling provided by the automatic process gives commercial and safety benefits to the industry. Visual quality testing done by computer vision provides inspection with lower cost. The image processing methods are developed for this purpose.

1. INTRODUCTION

Our research work has focused on the development and application of computer image analysis of dynamic processes. The goal is to affect the quality of the products.

The work was intended to develop a suitable software toolbox, the whole of hardware equipment, measurements and analysis of measurements of production processes of weaving, carding, paper production process and others.

For monitoring and obtaining parameters of analysis, we use three software tools that were developed in house named "Noviscam technique" – fractals, CIE colour space, and statistic measures. There are two distinct requirements for the algorithms. Firstly, they must be flexible enough to enable the best parameters for analysis to be selected and compared with others methods. Secondly, they must be fast enough for on-line controlling. Data can be analysed using various methods. The investigation considered new approach using fractal analysis [1, 2, 3] in comparison with conventional statistical method.

For the analysis a data record from CCD camera was used. Shots were downloaded to a computer as a data record and analysed. Images in a digital form are represented as matrix with values of pixels and the images windows are designed. Average values of pixels in the windows are read. The values are saved, and create time series. These time series are analysed by fractal analysis, CIE colour space and statistical analysis [5].

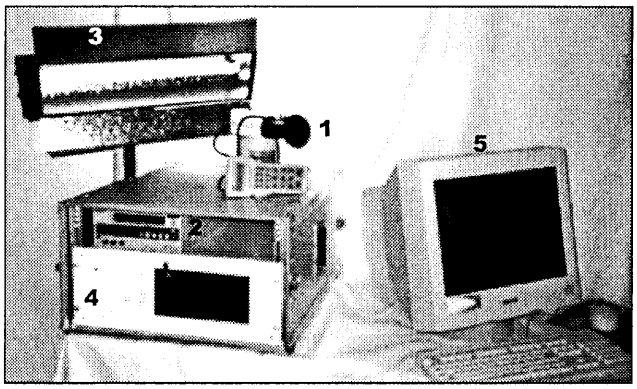

Fig. 1 Modular system "Noviscam" configuration.

Our investigation confirmed that many production processes could use the same principles of analysis in its processes. Our research has shown the possibilities of application of three software tools in various textile processes. Our activity in this problem was supported by the project EU Inco-Copernicus – Noviscam, Erbic 15CT960700 [4, 5].

2. NOVISCAM TECHNIQUE

The entire principle for the monitoring process, the generation of the time series, the estimation of a fractal dimension of the series and for analysis of the fractal dimension we can names as: "NOVISCAM Technique". The technique can be divided into "hardware" and "software" solution.

2.1 Hardware

The technology of the production process is scanned with a high-speed CCD camera, digital CCD camcoder or CCD video camera. Shots are transmitted to a computer as a data record. Results of the analysis are transmitted to a Control Electronic Unit (CEU).

System configuration (Fig.1):

1. 3-CCD colour video camera JVC KY-F55BE with variable focal lens.
2. Digital Video Cassette Recorder DSR-20P.
3. Lightening.
4. Video and graphic system - dpsReality.
5. Monitor.

The heart of the system is the dpsReality card. The dpsReality card provides the means for capturing images in real time. The dpsReality will work with any application that can read or write to any of the file formats supported by Virtual Tape File System, including SGI, BMP, PIC, TIF, IFF, VPB, RAS and RLA. The

dpsReality is simple interface with a trim table, timeline and preview windows designed with the compositor in mind.

The card is on-board SCSI controller, designed to control Ultra Wide SCSI drives means that does not rely on the computer's bus to transfer video to disk. The video data is captured and stored in a 32-bit 4:2:2:4 MJPEG or uncompressed YUV format. The dpsReality card has a single input/output cable, which carries auxiliary, balanced and unbalanced audio, component, composite and S-Video signals in both inputs and outputs. It provides analogue signal processing and character generator support.

2.2 Diagnostic algorithm

The image processing algorithm is realized using Matlab package and image processing toolbox.

The computer shows the data record as single images. The images in digital form are represented as matrices with values of pixels, and windows are created over the images (Fig. 2). The windows are located in important positions of the production process. This means that only some parts of the scanned production process are critical for production process (for quality of process and obtaining a required product). Average values of pixels in the windows are read from the images. The values are saved, and these create a time series in time (signals). The fractal dimension from the time series can be estimated, for example, by using R/S analysis.

The "iso-gray set" can be generated by setting a suitable brightness threshold and making the time at which the brightness of the set average crosses this threshold. The fractal dimension of the points set, so generated, can be estimated using the Box Procedure or another procedure. It appears that this fractal dimension from "iso-gray set" is more sensitive to change than the fractal dimension from the whole time series [4,5].

2.2.1 Rescaled Range Analysis

The Rescaled Range Analysis (R/S) represents the method for estimating fractal dimension [2] of nature self-affined fractals and uses the statistical tools. The Hurst exponent H is computed in the analysis. The fractal dimension of the time series (signal) can then be calculated from the relationship between the Hurst exponent H and the fractal dimension:

$$D_{RS} = 2 - H \quad (1)$$

Where D_{RS} denotes the fractal dimension estimated from the Rescaled Range Analysis. The R/S dimension has a value form 1 up to 2, and the Hurst exponent has a value from 0 up to 1. Fig. 3 shows two different time series (for better demonstration of the same data record, but different position of the windows). The fractal dimension (Hurst exponent) depends on the character of the time series. The rough time series has a higher fractal dimension D_{RS} = 1.70 (lesser Hurst exponent H = 0.30), and smoother time series have lesser fractal dimensions D_{RS} = 1.54 (higher Hurst exponent H = 1.48).

2.2.2 "Iso-gray Set" and Box Dimension

As in Fig. 2 we can elaborate the "iso-gray set" from the time series and estimate a fractal dimension of this set. The "iso-gray set" is generated by setting suitable

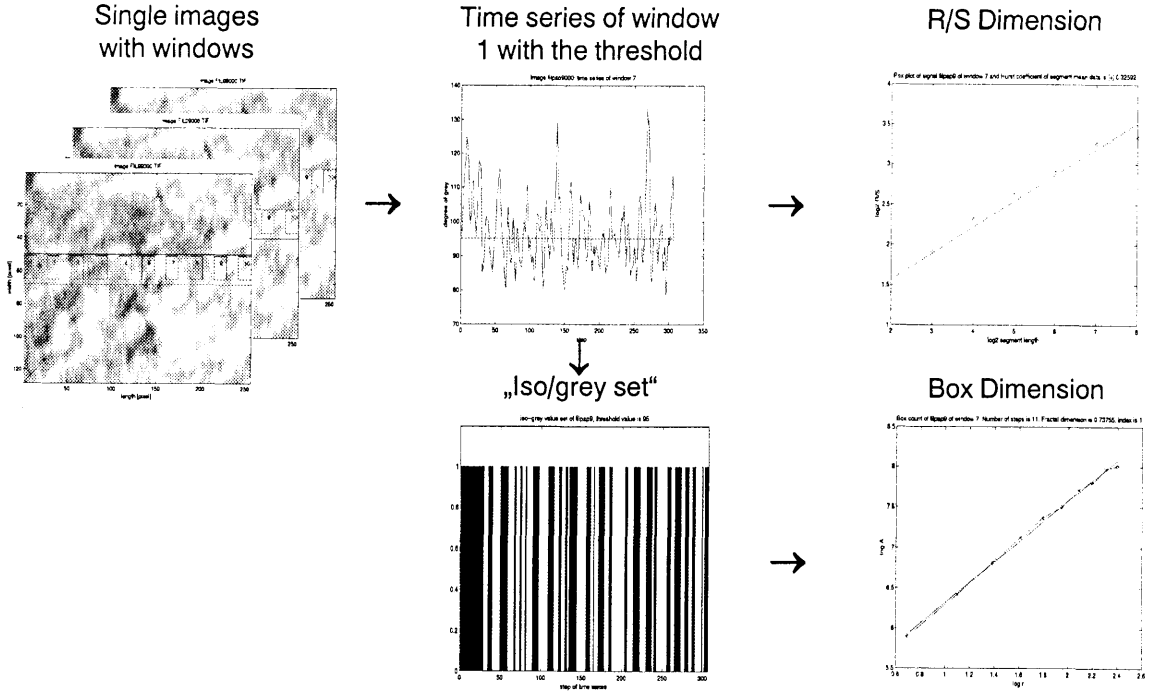

Fig. 2 Elaboration of time series from single images and estimations of the fractal dimension – "software"

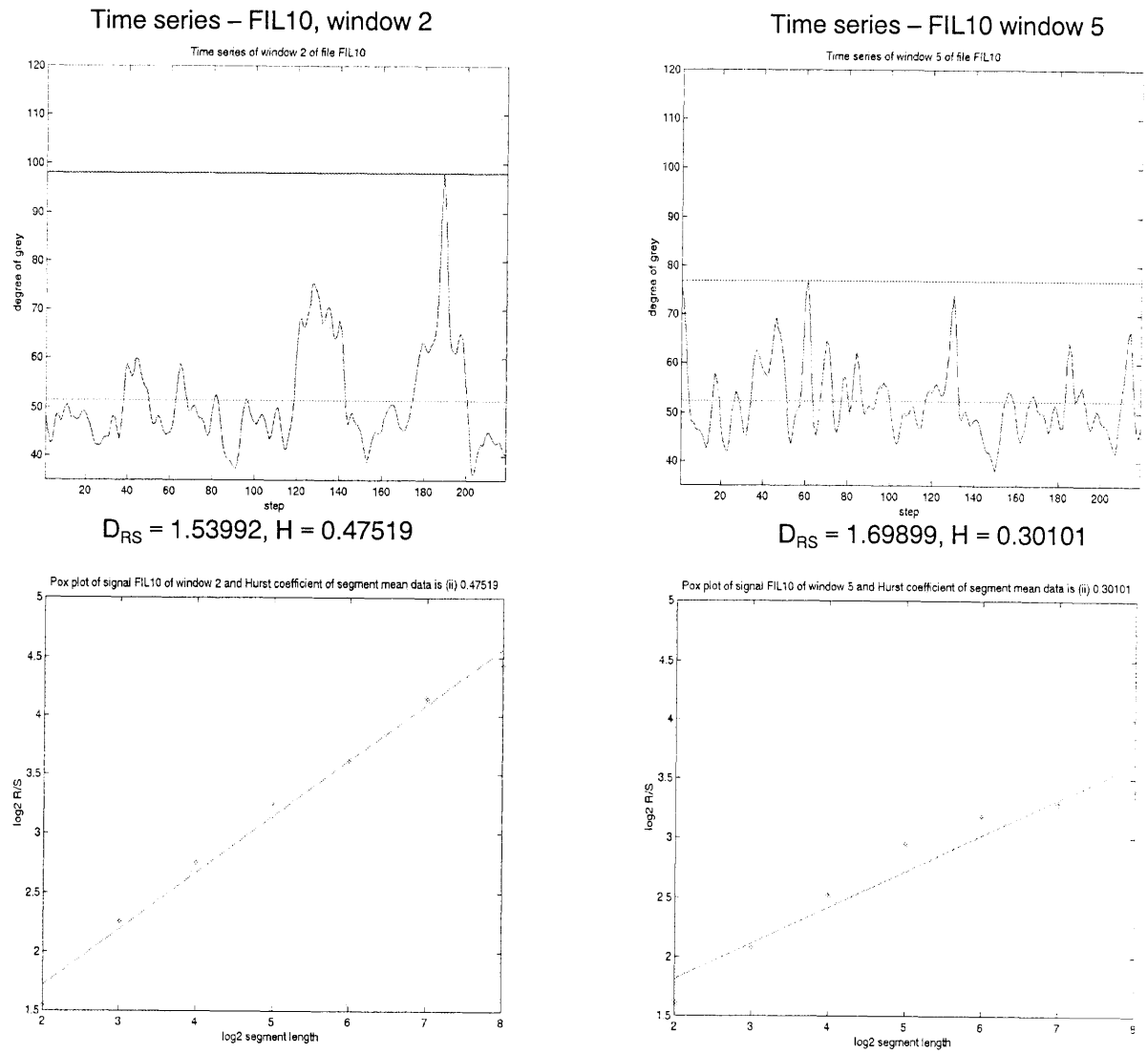

Fig. 3 Comparing of R/S dimension (smoother and rougher time series)

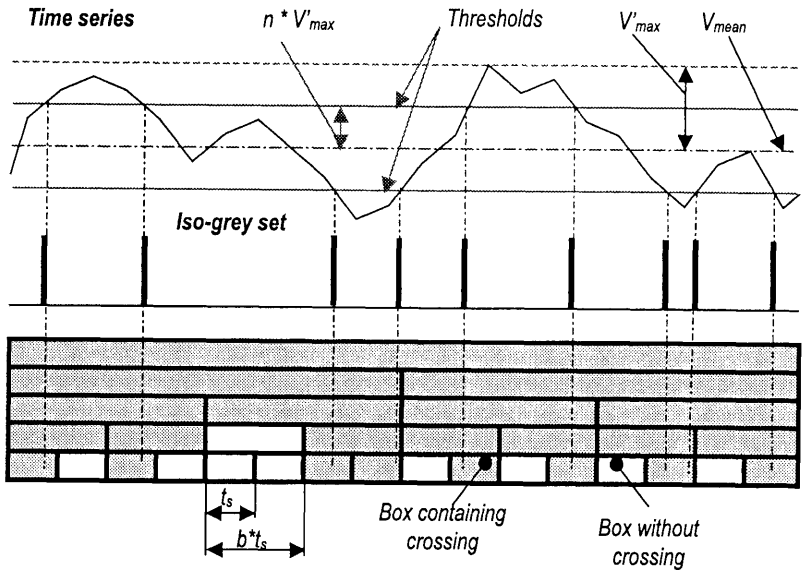

Fig. 4 Construction of iso-gray set – by making each time at which trace crossed chosen threshold values and principle of Box Dimension computing.

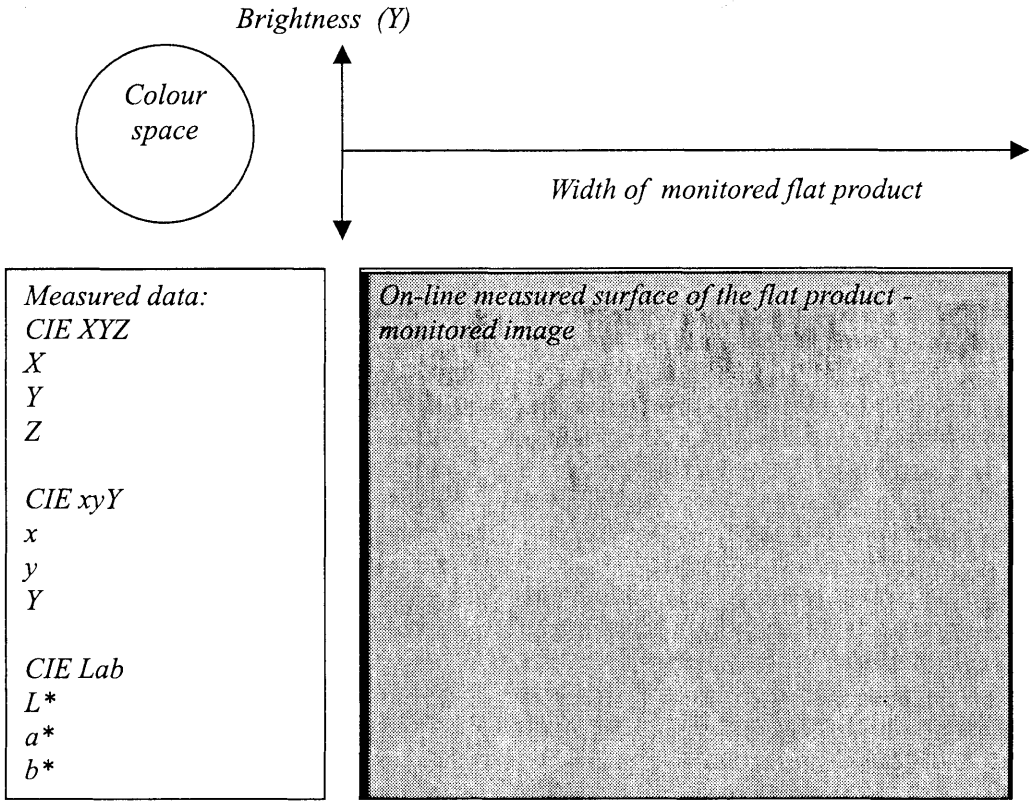

Fig. 5 Monitoring and data analysis by video colorimeter

brightness thresholds and using the time at which the brightness of the pixels average crosses these thresholds (Fig. 4), [4, 5]. The set contains zeros and ones, in which the ones represent the crosses.

The fractal dimension of the "iso-gray set" can be estimated by using the Box Counting Procedure or another procedure. The principle of the box dimension computing is in Fig. 4. Starting from box size t_s (sampling time interval), the number of boxes that contain a crossing is recorded. The box size is then increased by factor b (increasing factor or box division factor) and the procedure continues until the entire time series is contained in one single box. This is illustrated for $b = 2$ in the Fig. 4.

The box-plot is then $\log_2$ of the number of boxes that contain a crossing against the $-\log_2$ [4,5] of the normalised box size (box size divided by sampling time interval t_s).

2.2.3 Analysis by video colorimeter

Video colorimeter expresses the colour of the measured flat object (Fig 5). The image of an original picture is mostly projected through a set of appropriate optical filters and separated to three components of indirect trichromatic reproduction - red, green and blue (RGB). The optical signal generates electrical charge, large proportionality to the light flow, in 2D matrix of sensors of video camera, every element of CCD field behaving as a micro-photometer. The charge is shifted in rows and is sequentially read out and transformed by matrixes from RGB representation to YUV-video devices native colour space. The video signal from camera is fed to an analogue-to-digital converter. The digitised representation, also known as Y Cb Cr according to ITU R.601, is stored in a frame buffer and analysed by software in real time. It is conveyed to the production process control system via TCP/IP network then.

The averaged values of Y,Cb,Cr components are transformed to CIE 1931 trichromatic components XYZ, xyY components, as well as to CIE 1976 Lab components. The lab colour model has been chosen as an optimum in the given application.

Video colorimeter expresses the colour of measured flat object on-line. This is the way, how to compare one colour to the next one with accuracy. This analysis identifies the colour explicitly. That is, it differentiates the colour from all others and assigns it a numeric value. This analysis enable to compare data obtained from the most commonly used spectrophotometers.

3. APPLICATION OF NOVISCAM TECHNIQUE IN TEXTILE INDUSTRY

The application of the "Noviscam Technique" may be used in the entire textile production processes involve typical irregularities – irregularities of the fibre in the fi-

bre web, filaments or yarns in the webs or yarns in woven or knitted fabrics, etc. The improved process and product quality contributes to the increased profitability and customer satisfaction. In textile production exists a significant demand on objective, reliable, time and cost effective evaluation of production processes and their outcomes.

The first experience with "Noviscam Technique" in textile production was obtained in a wet-laying web production. We also tried to use this technique in the web forming processes on the carding machine and in weaving process. The last experience was gained in weaving process. The measurements were made on multiphase weaving machine M 8 300. The measurements were conducted at an inspection frame and a weaving machine. Image data record is currently being analysed. For the scanning we used a high-speed camera, digital camcorder and video colorimeter.

For the analysis of structures and the surface of the textile material we used fractal analysis, statistic analysis and imaging photometry. The segmentation of the scanned surface into pixels and its description with a map of microphotometrical values creates appropriate conditions for the application of means and procedures of more complex and sophisticated evaluation methods such as image analysis, frequency analysis of signals, multidimensional statistical analysis, etc.

4. CONCLUSIONS

The method of visualisation is currently performed by the maximizing of accuracy, hence a greater accuracy than human inspectors may have. The fractal analysis allows "On-line" evaluation with immediate feedback to the process. The fractal dimension is changed according to changes in a scanned production process. The changes are observed between a process conducive to a good-quality product and a process conducive to a poor-quality product. The fractal dimension is suitable for investigation and is used for a process production control.

Results from the carding process, the paper production process and weaving process, show the possibility of using of statistical method applied brightness and colour signals from the video camera. It seams that the use of statistical methods provides an alternative to fractal analysis.

Our investigations open the way for process control, which will reduce the number of defects and will result in high quality of the product.

I can confirm that the "Noviscam Technique" can be used in the textile industry. The possibilities of this technique in the textile industry are still being tested and compared with other methods.

I can state that the fractal dimension is a powerful tool and can be successfully used in chaotic and fast production process.

1. System for monitoring random production processes has been developed.
2. The system is based on video image and suitable signal processing.
3. The system has been applied to textile production processes.

ACKNOWLEDGEMENT

The investigation has been carried out in the framework of EU Inco-Copernicus programme in collaboration with University of Hartfordshire, England, Turboinstitut, Slovenia, CeVis TU Bremen, Germany, BIRAL, England, Filpap and Elmertex, Czech Republic. The author sincerely thanks the kind help from the referees.

REFERENCES

[1] R.W.Conci,A., Proenca, B.C. "A fractal image analysis system for fabric inspection based on a box-counting method", Paper. Federal University, Passo da Pátria 156, 24 210 – 240, Niterói, RJ Brazi,1997.

[2] Peitgen, H.O., Saupe, D.: The Science of Fractal Images, Springer-Verlag, New York, Berlin, Heidelberg (1988).

[3] Tsuji, Y., Honda, K.,Tsunotda,H., Nakamura,I "Fractal aspects of iso-velocity set in turbulent boundary layer", JSME-International Journal, series B, Vol.36, No.1 (1993).

[4] Chrpová, E.: NOvel VIsualisation System for Control And Monitoring. Framework IV (2). The project EU Inco-Copernicus – Noviscam, Erbic 15CT960700, Annual Reports for years 1997-2001 from TU Liberec.

[5] Chrpová,E., Hotař,V. "Application of Fractal Dimension in Textile Production Processes". The Textile Institute, 80th World Conference, Manchester, 2000, ISBN 187037245X, CD, 12 pages.

KONTROLA KVALITY POVRCHU ZALOŽENÁ NA METODÁCH ZPRACOVÁNÍ OBRAZU

Translation of Abstract:

Surface quality control based on image processing methods

Kontrola vzhledu spočívá v popisu vad povrchu. V průmyslových podnicích se hodnocení povrchových vad provádí na prohlížecích strojích kontrolory. Tento způsob hodnocení je ovlivněn chybami způsobenými lidským faktorem a subjektivitou hodnotitele. Objektivní kontrola kvality zajištěná automatickým postupem, kde hodnotitel je nahrazen metodou zpracování obrazu počítačem, je ekonomicky nenáročná a účelná metoda kontroly. V tomto smyslu byl vyvinut modulární systém včetně metod zpracování obrazu.

BENDING RIGIDITY OF TEXTILES

Fridrichová L.

Department of Textile Materials , Technical University of Liberec, Hálkova 6, 460 17 LIBEREC, Czech Republic

This paper presents a simple numerical method to predicting large deformations of fabrics. The bending stiffness is calculation from experimental value of bending angle A good convergence of iteration are produced by the software Mathcad PLUS 6.0.

1. INTRODUCTION

The simple method for measuring the bending rigidity of fabric was proposed by Peirce. Peirce first introduced a linear model of bending behaviour of fabric. The bending rigidity B of the beam is defined as:

$$B = \frac{wL^3 \cos(0.5\Theta)}{8\tan\Theta}$$

This method was developed based on the linear model of bending behaviour but most fabric display a non-linear model of bending behaviour. Several non-linear bending models have been proposed in the literature [1, 2]. The mathematics model presented in this paper is based on the exact geometry non-linear moment-curvature relation [3]. The next model is designed for uneven lap and the last model from this group contains viscoelastic property. All three models obtained input data from experiment. The values of bending stiffness were measured with the tester FLEXOMETR FF 20.

2. MATHEMATIC MODEL

A specimen of the fabrics is pushed over the edge in the point of fixation. Fabrics undergo large deformation to their own weight. The length of the overhang is from 3 to 9 cm with an increase of 1 cm. The bending curve from experiment was digitalised by system Lucia M. and experimental curve was compared with theoretical curve.

2.1 MODEL 1

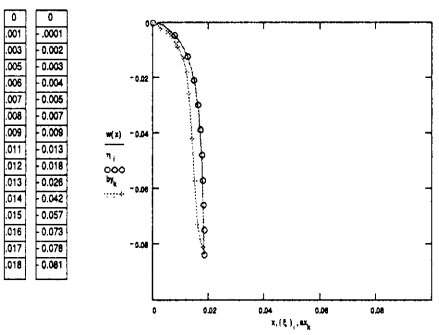

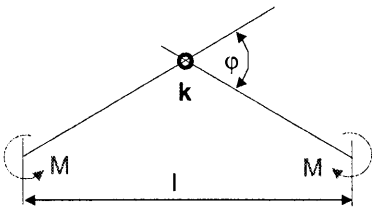

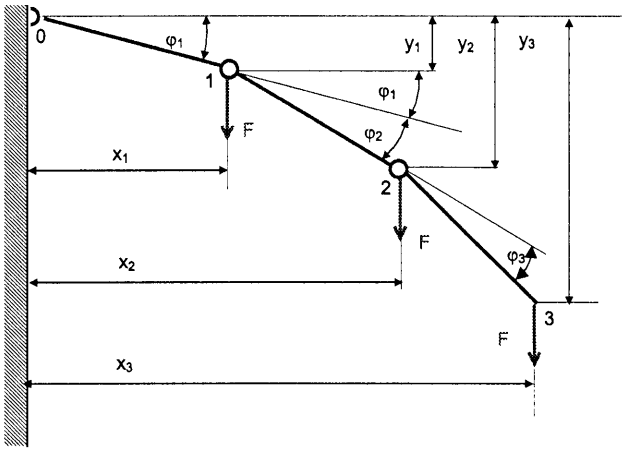

$$\begin{aligned} M_0 &= F.x_1 + F.x_2 + F.x_3 \\ M_1 &= F(x_2 - x_1) + F(x_3 - x_1) \\ M_2 &= F(x_3 - x_2) \end{aligned} \quad (1)$$

$$\begin{aligned} x_1 &= l.\cos\varphi_1,\ x_2 = x_1 + l.\cos(\varphi_1 + \varphi_2), \\ x_3 &= x_2 + l.\cos(\varphi_1 + \varphi_2 + \varphi_3) \end{aligned} \quad (2)$$

$$\begin{aligned} y_1 &= l.\sin\varphi_1,\ y_2 = y_1 + l.\sin(\varphi_1 + \varphi_2), \\ y_3 &= y_2 + l.\sin(\varphi_1 + \varphi_2 + \varphi_3) \end{aligned} \quad (3)$$

$$\begin{aligned} &\Psi\sum_{j=1}^{i}\varphi_j, \quad x_0 = 0, \quad y_0 = 0, \\ &x_i = x_{i-1} + l\cdot\cos\psi_i, \quad y_i = y_{i-1} + l\cdot\sin\psi_i, \\ &M_0 = F\sum_{i=1}^{n} x_i, \quad M_i = F\sum_{j=1}^{n-1}(x_{j+1} - x_i) \\ &\varphi_1 = M_0/2k,\ \varphi_i = M_{i-1}/k,\ \varphi_2 = M_1/k,\ \varphi_3 = M_2/k \end{aligned} \quad (4)$$

2.2 MODEL 2

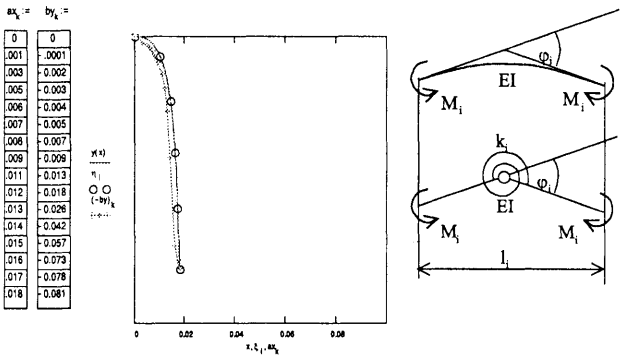

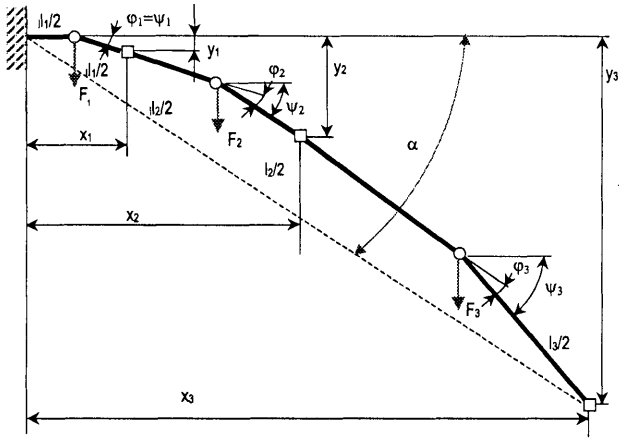

2.3 MODEL 3 (Viscoelastic model of textile specimen)

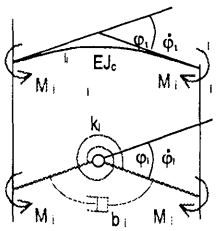

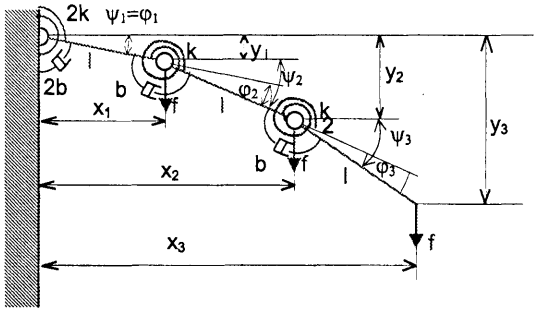

Viscoelastic property concentrated inwards of joint. We suppose, that in the joint takes effect also diskretization tonic loading from own weight about size f = m.g.s.l [N]; g indicate gravitational acceleration. Mathematical description deduces on a simple model with three segments. Results can be generalize for discretionary i-segment, i = 1,2..n, of constant length for chooses numbers of segments.

For the first segment, with joint in fix with double rigidity, hold reaction:

$$M_i = k_i\varphi_i + b_i\dot{\varphi}_i \tag{5}$$

$$\dot{\varphi}_i = (M_i - k_i\varphi_i)/b_i \tag{6}$$

$$\psi_1 = \varphi_1, \quad x_1 = l\cdot\cos\psi_1,\ y_1 = l\cdot\sin\varphi_1 \tag{7}$$

We calculate geometrical parameter of the next segment always from parameter of previous segment:

$$\begin{aligned}\psi_2 &= \psi_1 + \varphi_2,\ x_2 = x_1 + l\cdot\cos\psi_2,\\ y_2 &= y_1 + l\cdot\sin\psi_2\\ \psi_3 &= \psi_2 + \varphi_3,\ x_3 = x_2 + l\cdot\cos\psi_3,\\ y_3 &= y_2 + l\cdot\sin\psi_3\end{aligned} \tag{8}$$

Flexural moments in individual joint, they are:

$$\begin{aligned}M_1 &= f(x_1 + x_2 + x_3)\\ M_2 &= f[(x_2 - x_1) +](x_3 - x_1)\\ M_3 &= f(x_3 - x_2)\end{aligned} \tag{9}$$

Conformable with equation (1) (2) rated angle:

$$\begin{aligned}\dot{\varphi}_1 &= (M_1 - 2k\varphi_1)/2b = (0.5M_1 - k\varphi_1)/b,\\ \dot{\varphi}_2 &= (M_2 - k\varphi_2)/b,\\ \dot{\varphi}_3 &= (M_3 - k\varphi_3)/b\end{aligned} \tag{10}$$

From literature we know that Peirce empirical equation is not so reliable. Values of stiffnes by Peirce are approximate true if bending angle is around 40°. Calculation by our method is correct in whole range of overhang. It is confirmation also comparing with method, which was publication in J. Text. Inst., 1996 [3]; error of our model is under 2%.

3. LITERATURE

[1] Wei, M.: The Theory of the Cantilever Stiffness Test. In: J. Text. Inst., 1989, No.80, p 98–106

[2] Potluri, P., Atkinson, J., Porat, I.: Large Deformation Modelling of Flexible Materials. In: J. Text. Inst., 1996, 87 Part 1. No.1 , p 129–151

[3] Höschl, C.: Pitfalls of finite element modelling In.: Implementation of Nonlinear Continuum Mechanics in Finite Element Codes. Institute of Theermomechanics Prague, 1995

[4] Mevald, J. Fridrichová L.: Bending Rigidity of Fabrics-Large Deformation Modelling, Book of abstracts textile testing and standardisation, Minho Univerzity,.Portugal 1999, ISBN 80-7083-348-3

OHYB TEXTILIÍ

Translation of Abstract:
Bending Rigidity of Textiles

V přednášce je prezentována jednoduchá matematická metoda popisující ohyb textilie pro velké deformace. Ohybová tuhost je vypočtena z úhlů ohybu získaných v experimentu. Výpočet dle matematického modelu a jeho porovnání s experimentem je provedeno softwarem Mathcad PLUS 6.0

PROJECT ON ASSESSMENT METHODS OF CONSTRUCTIONAL ALLOWANCES FOR LOOSENESS OF CLOTHING

Musilová B., Komárková P., Kůs Z.

Department of Clothing, Technical University of Liberec, Czech Republic

In the present study is described assessment method of constructional allowance for looseness to the horizontal dimensions with regards to the looseness of clothing and sequence of the clothing layers. It is suitable for the modification of entrance parameters for automatic construction of clothing by the help of CAD systems. This method is presented for the upper part of the body according to the methodology of the pattern construction JMKO (Unified methodology of the clothing construction).

INTRODUCTION

The assessment of constructional additions for looseness is primarily the matter of subjective opinion and is based on certain empirical experience. The way how to change the attitude to the methods of clothing construction is to substitute these empirical values by those theoretical based with we can apply in automatic construction by the help of CAD systems.

Specific category of allowance for looseness is allowance for the body curve on the bust plane, which have determinant signification by the set of the latitudinal proportional of cloths.

THEORETICAL CONSIDERATION

System of allowance

Graphically displayed list of construction line segment of clothing represents simplified form of the body surface transformed into a sheet. The body surface is transformed into the pattern design by using the system of body measurements in individual construction formula as entrance parameters.

The system of the allowance can be defined as a complex of influences effective in the shape and dimensions constructed clothing. According to way of their application by the construction we divide the allowances as follows:

- Constructional allowances:
  - allowances on looseness of clothing
  - allowances on thickness of material layers
- Technological allowances

Designing line segments

Distances between individual construction points corresponding with somatometrie points delimitate designing line segments $\overline{AB}$, where A and B correspond with certain construction points. The dimension of the designing line segments is the sum of the following components:

$\left(\overline{AB}\right)$ – dimension of the designing line segment without allowances – entrance parameter (part of the body measurement), PV – total value of the looseness allowances, PP – total value of the allowances on the thickness of material layers.

Assessment of the dimension of the designing line segment (without technological allowance):

$$\overline{AB} = \left(\overline{AB}\right) + \sum P \qquad (1.1)$$

$$\sum P = PV + PP \qquad (1.2)$$

where ΣP – resulting value of the additions PV+PP.

Assessment of the dimension of the designing line segment (whit technological allowance)

$$\overline{AB} = \left(\overline{AB}\right) + \sum P^{*} \qquad (1.3)$$

$$\sum P^{*} = \sum P + PT \qquad (1.4)$$

where PT – value of technological allowance [2].

EXPERIMENTAL PART

Experimental assessment of the allowances for looseness of the clothing

Allowances for looseness of the clothing in the bust plane are assessed for clothing with skin- tight silhouette **ladies blouse** (unlined clothes) **ladies polo coat** (lined clothes) **ladies coat** (lined clothes) (Fig.1). They can be assessed in the same way even for the half- skin tight silhouette and loose silhouette. The difference is the assessment of the entrance parameter, which determines looseness of the first layer from the body surface and so determines the particular kind of silhouette.

We must also consider the used clothing material. It is possible to assess it for all the body measurements of such a part of body where can presume the circular section like neck girth, waist girth, hip girth etc.

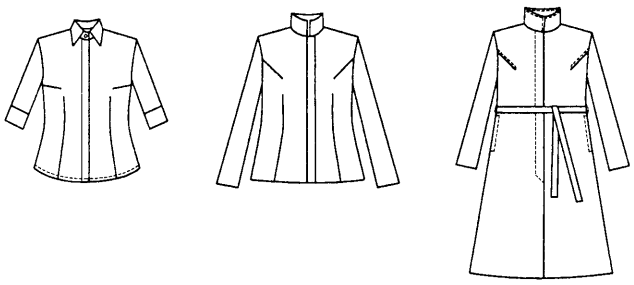

Fig. 1 Drawing of the clothing: ladies blouse, ladies polo coat, ladies coat

Assumptions of the experimental

For the assessment of the looseness allowances is came out from the following assumptions:

1. The humane body can be compared to the geometric figure of the circular section.
2. The entrance parameter is the looseness allowances for the first clothing layer- made subjectively.
3. Between the individual clothing layer is not kept the constant thickness of the air space.

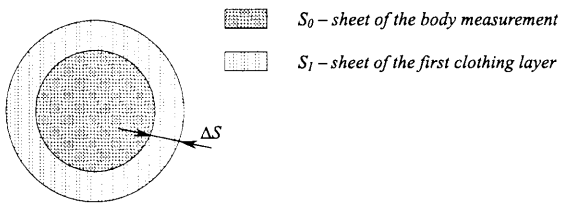

Fig. 2 Drawing of the plane representing the distance of the first clothing layer from the body surface

Principle of the looseness of the clothing assessment

Allowances assessment on looseness for the first layer

The first layer is represented by the blouse. The assessed entrance parameter $\mathbf{PV_1}$ which determines the looseness of the first layer from the body for the body measurement bust girth is given in tab.1. When we know $\mathbf{PV_1}$ we can reckon the girth and area of the plane that creates the distance of the clothing from the body.

$$O_1 = O_0 + PV_1 \text{ [cm]} \quad (1.5)$$

$$r_1 = O_1/(2\pi) \text{ [cm]} \quad (1.6)$$

$$S_1 = \pi r_1^2 \text{ [cm}^2\text{]} \quad (1.7)$$

$$\Delta S_1 = S_1 - S_0 \text{ [cm}^2\text{]} \quad (1.8)$$

The surface that makes the space- gap of the clothing from the body surface i.e. area of the circular ring is the decisive value for allowance assessment of the other layers.

From this value can be assessed the surfaces for the other two layers making the space – gap from the body. Between the body surface and the second layer is plane ΔS enlarged by ΔS/2. The gap between the body surface and the third layer makes plane (ΔS + ΔS/2) enlarged by ΔS/4.

ΔS/2 and ΔS/4 are constant quotients. On the basic of these quotients we can reckon the size of allowances for the following two layers.

Allowances assessment on looseness for the second layer

The second layer of the clothing is represented by the ladies polo coat. The allowances on looseness $\mathbf{PV_2}$ be reckoned on the basis of the quotient ΔS/2. As we don't know the girth and area of this layer we start from the value of the area S_1 and so we can reckon the area for the given layer enlarged by ΔS/2:

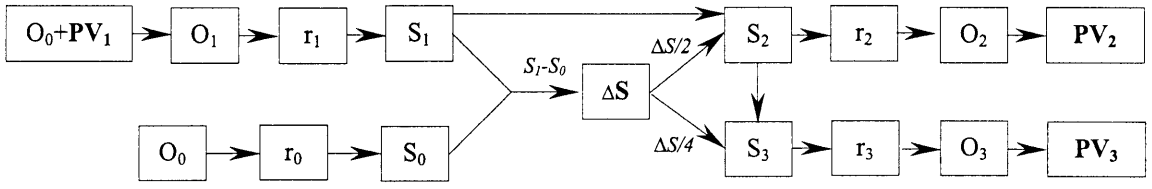

Block scheme on the reckoning of the allowances

Legend:
O_0 – girth gain by measuring (body measurement) [cm]
O_1 – girth of the first layer of clothing [cm]
O_2 – girth of the second layer of clothing [cm]
O_3 – girth of the third layer of clothing [cm]
r_0 – radius of the body measurement [cm]
r_1 – radius of the first layer of clothing [cm]
r_2 – radius of the second layer of clothing [cm]
r_3 – radius of the third layer of clothing [cm]
S_0 – area of the plane to the body measurement [cm^2]
S_1 – area of the plane of the first layer of clothing [cm^2]
S_2 – area of the plane of the second layer of clothing cm^2]
S_3 – area of the plane of the third layer of clothing [cm^2]
PV_1 – allowance on looseness for the first layer of clothing [cm]
PV_2 – allowance on looseness for the second layer of clothing [cm]
PV_3 – allowance on looseness for the third layer of clothing [cm]
ΔS – allowance between the areas of the planes S_1 and S_0 [cm^2]
ΔS/2 and ΔS/4 – quotient from ΔS [cm^2]

$$S_2 = S_1 + \Delta S/2 \ [cm^2] \quad (1.9)$$

than the girt for this layer is:

$$r_2 = (S_2/\pi)^{0,5} \ [cm] \quad (1.10)$$

$$O_2 = 2\pi r_2 \ [cm] \quad (1.11)$$

and the resulting allowances on looseness for the particular body measurement for the second layer is determined by formula:

$$PV_2 = O_2 - O_0 \ [cm] \quad (1.12)$$

Allowances assessment on looseness for the third layer

The third layer is represented by ladies coat. The way of the allowances on looseness $\mathbf{PV_3}$ for this layer is the same as at the previous layer. It is assessed on the basis of the quotient $\Delta S/4$.

$$S_3 = S_2 + \Delta S/4 \ [cm^2] \quad (1.13)$$

$$r_3 = (S_3/\pi)^{0,5} \ [cm] \quad (1.14)$$

$$O_3 = 2\pi r_3 \ [cm] \quad (1.15)$$

$$PV_3 = O_3 - O_0 \ [cm] \quad (1.16)$$

Assessment of the thickness of the air gap

The assessment of the thickness of the air gap between the individual layers is determined on the basis reckoned radiuses $r_0 \ldots r_3$. In the determined value of the thickness of the air gap is contained the clothing material thickness of the layer t_1, t_2, t_3.

The thickness of the of the air layer between the surface of the human body and the first layer is given this way:

$$vm_1 = r_1 - r_0 \ [cm] \quad (1.17)$$

Between the first and second layer is thickness of air gap given:

$$vm_2 = r_2 - r_1 - t_1 \ [cm] \quad (1.18)$$

Between the second and third layer is the thickness of air gap given:

$$vm_3 = r_3 - r_2 - t_2 \ [cm] \quad (1.19)$$

Then is valid $vm_1 > vm_2 > vm_3$.

The result of this is that between the individual layers isn't kept the constant thickness of the air space. Whit the receding layer of the clothing from the body surface the thickness of the air space between individual layers is growing less.

Table1 The result values PV to the body measurement of the bust girth

body measurement		PV – body measurement [cm]			
1/2 bust girth	oh	blouse	3, 0	4, 0	5, 0
		polo coat	4, 5	5, 9	7, 4
		coat	5, 2	6, 9	8, 6

THE RESULT OF THE EXPERIMENT

Entrance parameters for this reckoning are These values:

- body measurement (bust girth)
- addition on looseness to the first layer $\mathbf{PV_1}$

On the basic of these entrance values is made automatic reckoning for the other two layers of clothing.

Additions assessment on looseness to horizontal areas in the plane of the bust perimeter

From the reckoned values PV to the bust girth we can determine how large part from this PV value belongs individual areas this plane. Body angle in the horizontal body plane π *[rad]* can be divided into 3 body angles, which limit **back H1 H3**, **armhole H3 H5** and **front part H5 H7**.

On Fig. 5 can be seen the simplified model representing the bust plane of the human body dissected by the profile plane into 2 halves.

In Tab. 2 are given the half values that determine the size of the allowances for body arc in the bust girth.

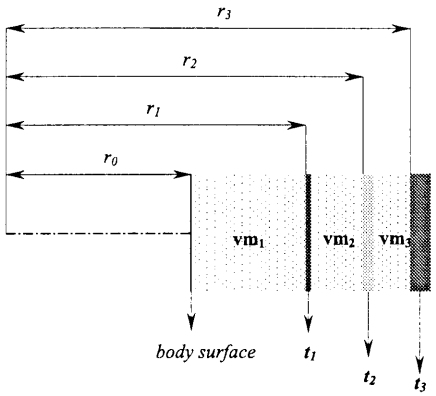

Fig. 3 Air gaps between individual layers

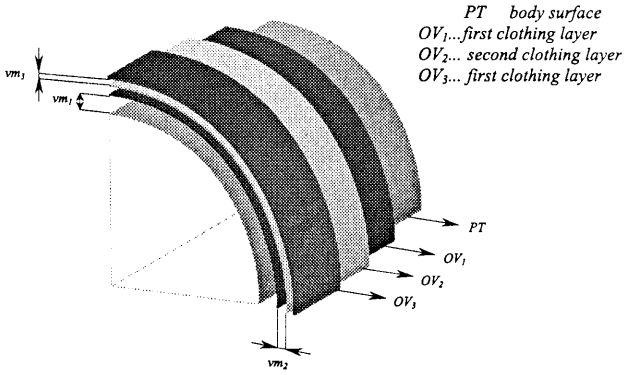

Fig. 4 3D model of the stratification

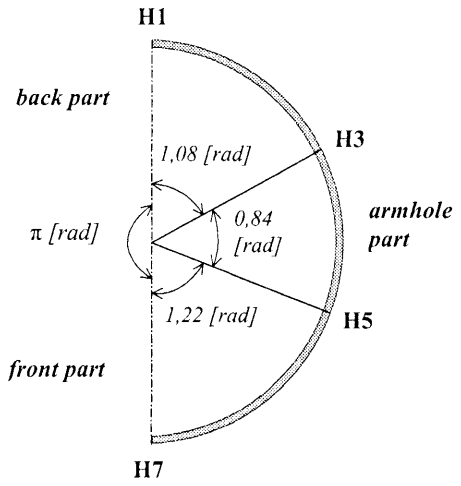

Fig. 5 Drawing of the angles of the horizontal body arc in the bust girth

Conclusion

This article describes the assessment method of the designing allowances on looseness to horizontal construction measurement of the bust girth in regard to the looseness of the clothing and the sequence of the clothing layers. It can be applied even for assessment other

Table 2 PV (1/2 value) to the horizontal body arcs in the plane of the bust girth

		The body arcs in the plane of the bust girth			
		π [rad]	1,08 [rad]	0,84 [rad]	1,22 [rad]
Clothing	PV_{oh} [cm]	H1H7	H1 H3	H3 H5	H5 H7
Blause	4	2	0,69	0,53	0,78
Polo coat	5,9	2,95	1,01	0,79	1,15
Coat	6,9	3,95	1,36	1,06	1,53

PV for neck girth, waist girth, hip girth etc. This simple method is suitable for modification of entrance parameters for an automatic clothes construction by the aid of CAD systems. It is an opening a possibility to use new methods by pattern making on the basic of mathematical modelling [2].

Literature

[1] Svítková, A.Využití programu NERO firmy Parmel s.r.o v konstrukci dámských oděvů pro horní část těla s ohledem na optimalizaci konstrukčních přídavků. [Diplomová práce]. Liberec: TUL, 2002. TU v Liberci, Fakulta textilní.

[2] ZATLOUKAL, L.: Konstrukce oděvů. 1. české. vyd. Praha: SNTL 1989. ISBN:80-04-222969-7

NÁVRH METODY STANOVENÍ KONSTRUKČNÍCH PŘÍDAVKŮ NA VOLNOST ODĚVU

Translation of Abstract:

Project on assessment methods of constructional allowances for looseness of clothing

V práci je popsána metoda stanovení konstrukčních přídavků na volnost k horizontálním konstrukčním rozměrům s ohledem na volnost oděvu a pořadí oděvní vrstvy. Je vhodná k modifikaci vstupních parametrů pro automatickou konstrukci oděvů pomocí CAD systémů. Metoda je prezentována na konstrukci pro horní část těla dle metodiky konstruování střihů oděvů JMKO (Jednotná metodika konstruování oděvů).

TEXTILE PHOTO CHROMIC SENSORS FOR PROTECTIVE TEXTILE

Viková M.

Laboratory Colour and Appearance Measurement, Technical University of Liberec Czech Republic
e-mail: martina.vikova@vslib.cz

Depletion of stratospheric ozone is expected to lead to an increase in the amount of UVB radiation present in sunlight. In addition to its well-known ability to cause skin cancer, UVB radiation has been shown to alter the immune system. The immune system is the body's primary defence mechanism against infectious diseases and protects against the development of certain types of cancer. Any impairment of immune function may jeopardize health by increasing susceptibility to infectious diseases, increasing the severity of infections or delaying recovery from infections. In addition, impaired immune function can increase the incidence of certain cancers, particularly cancers of the skin.

With careful use of protective clothing, skin damage can be reduced drastically. Medical experts frequently recommend the use of clothing for protection from UVR. Not all clothing, however, protects equally or adequately.

The base of solution could be "SMART"textiles with irradiance responsible fibre materials. „SMART" or „INTELIGENT" materials respond to environmental stimuli with particular changes in some variables. For that reason they are often also called responsive or adaptive materials. Depending on changes in some external conditions, adaptive materials change either their properties (mechanical, electrical, appearance), their structure or compositions, or their functions.

Mostly, "SMART" materials are embedded in systems whose inherent properties can be favourably changed to meet performance needs. The primary purpose of the proposed work is development of origin method and device for measurement of adaptive response on UV-VIS and NIR irradiance. This work is widely recognized as establishing the fundamental knowledge base for the creation of variety of new materials as sensors for application to basic textile structures, non-woven, and other related materials and their barrier properties against UV-VIS and NIR irradiance. Our objective is to use the special photo chromic and photo adaptive polymer, which has a response to above-mentioned part of electromagnetic irradiation.

Key words: sensors, photochromic, colour measurement

INTRODUCTION

Reversible colour changing of some substances is well known effect. Name of this effect is chromism and if the effect is reversible colour change depending on temperature, name of this effect is thermo chromic. If is colour change affected on solution name is solvate chromism, light colour change dependence is named photo chromism, etc. This reversible colour change we can use as indicator of different stimulation and true colour measurement method we can quantify by this stimulation.

In present time we have on the market protective clothes, which give good insulation against hazardous substances and radiation. Obviously is on the market measuring systems for measuring dangerous substances and its concentration, respectively excessive intensity of radiation. On the other side we should solve transportation of this measuring systems, stress of acting persons (firemen, solders, etc.) during theirs actions from reason of weight and dimensions of measuring systems. This problem will solve integrated textile sensors, which will be flexible component of protective clothes. Potential possibilities of using textile-based sensors are now intensively studied in Laboratory Colour and Appearance Measurement (LCAM) of Department of Textile Materials of Technical University in Liberec, Czech Republic. In this study are present textile sensors with colour response on UV radiation and we will present studies of dynamic changes, stability of sensitivity these kinds of sensors. Also will be present study of moderating these sensors for different part of UV.

EXPERIMENT

In our experiment we prepared samples from PET fabric that was coated by five different photo chromic agents. In first part of our experiment we measured colour change dependence on the time of stimulation. For measurement was used spectrophotometer SF 300 UV and Microflash 200d fy Datacolor Intenational USA. Modus of measurement was: SCI without UV and with aperture 20 mm and 5 mm. The samples was exposed in Judge box II fy Gretag Magbeth – USA. We used combination of D 65 simulator and UV fluorescent tube. Spectrum of this combination of illumination you can see on the fig.1.

On the following figures 2–6 is shown the response remission curves of studied photo chromic pigments:

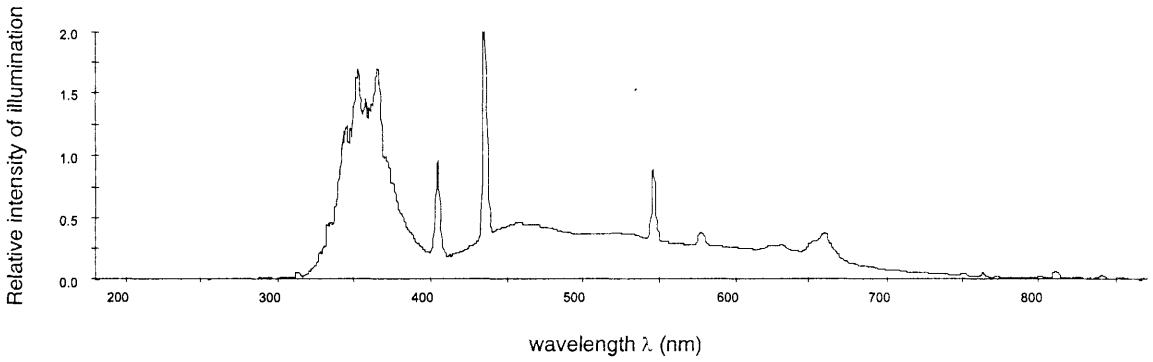

Fig.1

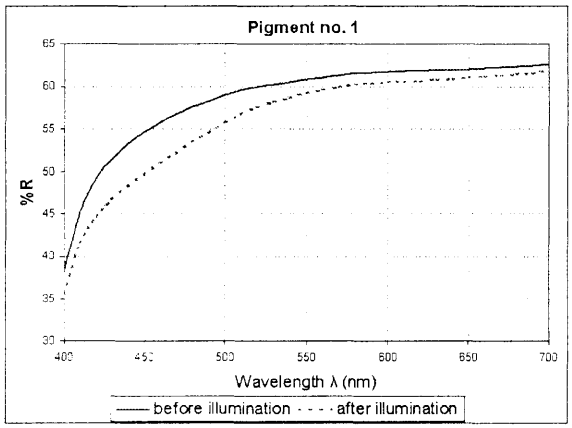

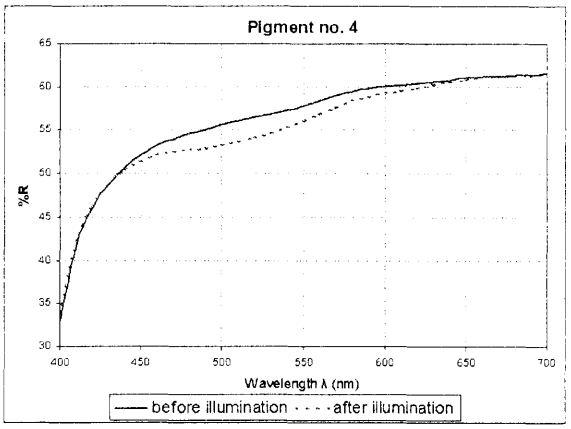

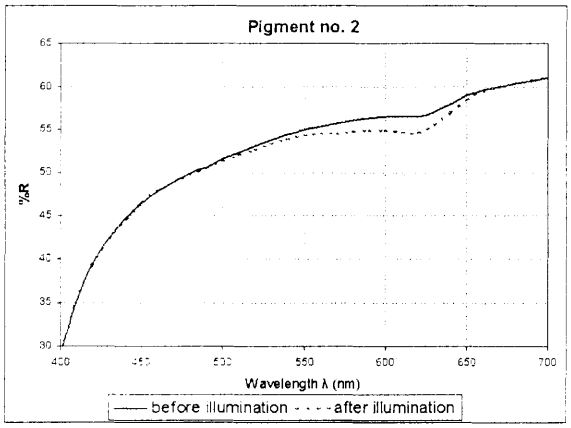

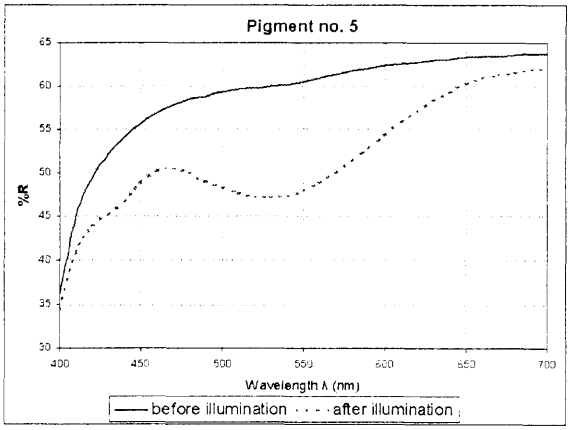

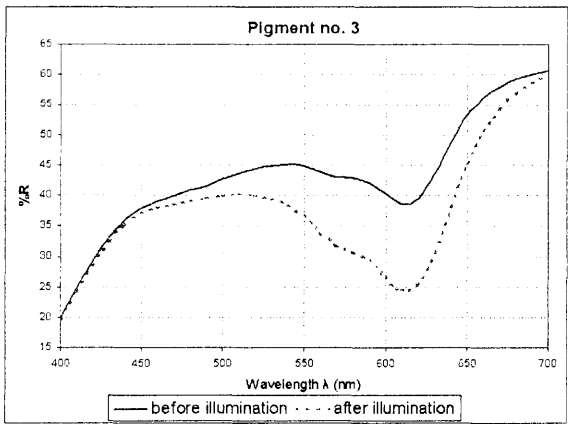

Fig.2–6

We decided, that for our following experiment, to choose the pigments no. 3 and no. 5. Therefore intensity of colour changes for their response on illumination (was approximately 20–25 % R).

In area of intensity of exposition measurement is obviously need to know time and intensity dependency of sensor response. For time dependency study were test samples in following time scale exposed:

Tested photo chromic materials was illumined in following time scale:

Time of illumination [min]	0,5	1,0	1,5	2,0	2,5	3,0	4,0	5,0	10,0

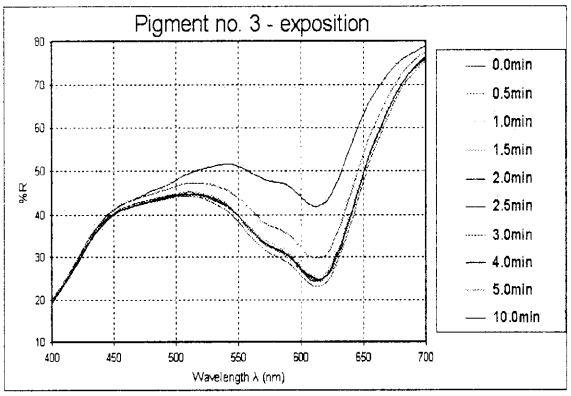

Fig. 7

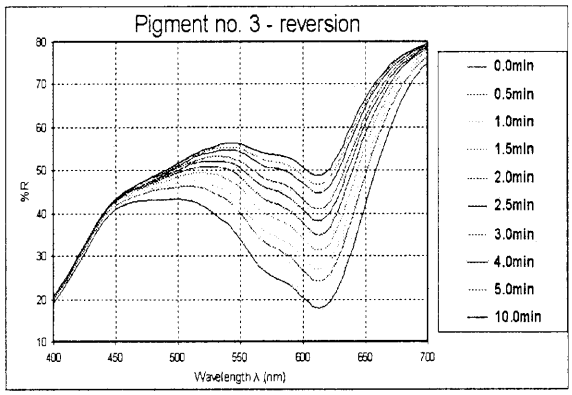

Fig. 8

During the testing of regeneration were samples exposed 15 minutes and following regeneration in some time scale as during exposition:

Time of regeneration [min]	0,5	1,0	1,5	2,0	2,5	3,0	4,0	5,0	10,0

Next figures 7, 8 show the remission curve during exposition and reversion:

There is shown how the minimum is going down with time of exposition and during reversion is going up. Because is relationships between remission and concentration of colorant agent non-linear in colour measurement is obviously used relation between Kubelka-Munk function and concentration, colour change intensity respectively. Colour change intensity that we used was defined as following equation:

$$I = \int_{400}^{700} K / D_{\lambda} d\lambda$$

In our study we prepare new view on the relation ships between intensity and time of exposition, time of relaxation respectively. Name of this new kind of graphs is colour change hysteresis. The colour change speed is higher during of exposition than reversion phase.

On fig. 10 is shown relation between light source distance and intensity of colour change for two exposition

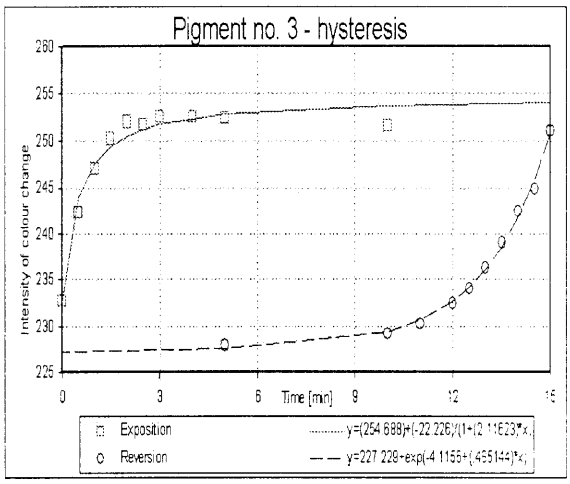

Fig. 9

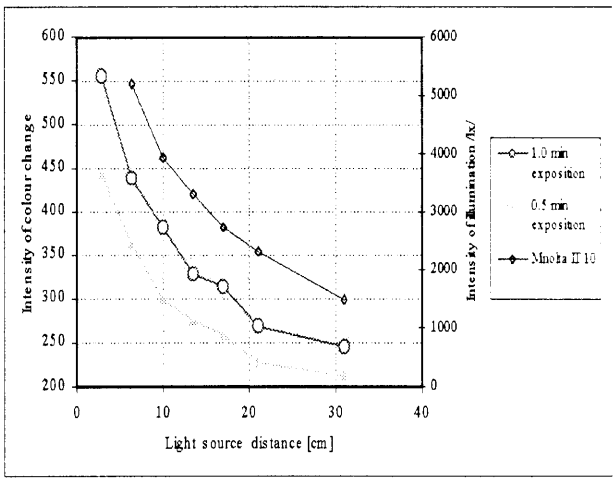

Fig. 10

times and Minolta Illuminance Meter IT10. It stands to reason, that curves for pigment no. 3 are similar to MIM IT 10.

This paper is introducing study of dynamic properties of photo chromic pigments. This study will be followed by experiment with moderating of above mentioned properties by UV absorbents.

REFERENCES

[1] Viková, M.; Vik, M.: Some problems in measurement of UV protective textiles, The 3-rd China International Wool Textile Conference, Xi´an 26-28 September 2002

[2] Viková, M.; Vik, M.: New micro spectrophotometer for measurement of UPF on textile fibre, 6. Dresdner Textiltagung, 19-21.6. 2002 – Dresden, Germany

ACKNOWLEDGEMENTS

This work was supported by the Czech Ministry of Education as research project VCT LN00B090.

FOTOCHROMNÍ TEXTILNÍ SENSORY PRO OCHRANNÉ TEXTILIE

Translation of Abstract:
Textile photo chromic sensors for protective textile

Snižování obsahu ozonu v zemské atmosféře má za následek zvyšování podílu UVB záření v celkovém slunečním záření. To má za následek, jak je obecně známo zvýšení rizika vzniku rakoviny kůže a snižování imunity. Důsledkem těchto procesů je celkové oslabení organizmu a zvýšenou náchylnost k onemocnění.

Jednou z možností ochrany organizmu je použití ochranných textilií, které výrazně snižují riziko vzniku rakoviny kůže. Nošení speciálních ochranných textilií je doporučováno lékaři, na druhou stranu je třeba si uvědomit, že ne všechny textilie chrání před UV zářením stejně.

Základním řešením by mohlo být použití SMART textilií se schopností reakce na UV záření. SMART nebo Inteligentní materiály jsou takové materiály, které reagují změnou určitých vlastností, (elektrické, mechanické, vzhledové) na daný podnět a to i strukturou nebo složením či jejich funkčností.

Často jsou SMART materiály integrovány do standardních systémů, díky čemuž dochází ke zlepšení jejich užitných vlastností. Cílem projektu, který je popsán v tomto článku, je vývoj originální metody měření respektive vývoj speciálních senzorů reagujících na UV VIS a blízkou infračervenou oblast elmg. záření. Tato popsaná práce je zaměřena na výrobu a testování senzorů z tkanin a netkaných textilií za použití fotochromních pigmentů, které jsou aplikovány formou zátěrů nebo barvením ve hmotě. Výsledky ukazují, že vyrobené senzory vykazují citlivost jak na dobu ozařování, tak na intenzitu záření a jejich responzní charakteristika se blíží komerčně dostupným elektronickým luxmetrům.

AIR PERMEABILITY AND A STRUCTURE OF WOVEN FABRICS

Havrdová M.

Technical University of Liberec, Department of textile evaluation, Hálkova 6, Liberec, Czech Republic
E-mail: marie.havrdova@vslib.cz

Main aim of this paper is description of some geometrical models of woven fabric porosity and proposition of a new model. From point of view a relationship between air permeability and a structure of woven fabrics it is not possible to describe fabric only by its porosity. Generally, the porosity indicates how much of air gaps a textile material contains. For a description of airflow through textile materials further details about a configuration of pores in textiles (the pore size, shape, arrangement etc.) are very important. Moreover, a fabric structure changes owing to flowing air and its relation with air permeability is much more complicated. This paper mentions the importance of deformations that can occur in fabric owing to flowing air. It was found that it is necessary to take a type of weave into consideration.
KEYWORDS: porosity, airflow, structure, woven fabrics, deformation, type of weave.

INTRODUCTION

Geometrical characteristics of textile fabrics are very important when evaluating and simulating a lot of fabric properties. One of them is air permeability. A lot of research works concerns on a description of a relationship between air permeability and a structure of a textile fabric. In this case a structure is usually characterized by its porosity.

In some research, a textile woven fabric is compared with a metal woven nets, but metal materials have very different properties. The structure of a metal woven net is unchangeable in airflow (in a range of pressure differences used usually on textile materials). In textiles exposed to airflow some deformations exist and the textile structure is changed. For that reason is relationship between air permeability and structure of textile woven fabric much more complicated.

Deformation of woven fabric caused by airflow is strongly dependent on a degree of interlacing of yarns. Flowing air causes a move of not interlaced parts of yarns (floats) and a "new pores" appear in textiles. It is clear that length of floats is a proportion of the anchor of yarns in fabric. In this paper the influence of interlaced portions on air permeability changes are studied as well.

WOVEN FABRIC POROSITY

In woven fabrics, a distinction among porosity between yarns, inter-yarn porosity, and porosity between fibres inside yarns, intra-yarn porosity should be made. Regarding an air permeability evaluation, intra-yarn porosity is usually neglected [1] and an assumption that air flows only between yarns is accepted. This assumption is questionable for a tightly woven fabric created from staple fibre yarns.

1. CLASSICAL 2-DIMENSIONAL MODEL OF POROSITY

In theory of classical 2-D model, porosity P_S is defined as a complement to the woven fabric cover factor CF. An area of pores is calculated as a perpendicular projection of a woven fabric

$$P_S = 1 - CF = 1 - (d_O D_O + d_U D_U + d_O d_U D_O D_U) \quad (1)$$

where d_O, d_U are diameters of a warp yarn, weft yarn respectively, and D_O, D_U are setts of warp yarns, weft yarns respectively.

This model of porosity completely neglects the third dimension of a fabric and differences of pore forms due to various binding types.

2. MODIFIED 2-DIMENSIONAL MODEL OF POROSITY

This model suggested by Gooijer [1] includes partly a 3-D structure of pores. A various binding type does not show the same relationship between a projected and real effective area opened to a flow. The modified 2-D model of porosity is based on idea that airflow flows around of yarns not only in a perpendicular direction. The influence of the binding was described with four basic unit cells according to Backer [2]. Each type of woven fabrics can be described by four pore types showed on fig 1. Gooijer calculated a projection of a

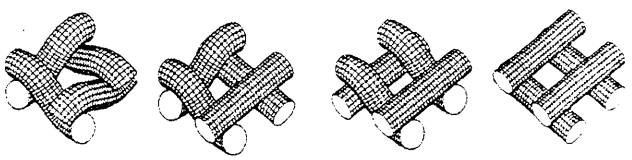

pore type 1 pore type 2 pore type 3 pore type 4

Fig. 1 The unit cells for woven fabric [2]

wetted perimeter at the narrowest cross section of a pore of four yarns creating of a pore into plane of a fabric and derived four equations for a calculation of the effective open areas A_1–A_4 of pore types 1–4.

The final equations have the form

$$A_1 = A_O A_U - \frac{\pi}{4} d_U \left(A_O - \frac{d_O}{2} \right) - \frac{\pi}{4} d_O \left(A_U - \frac{d_U}{2} \right) \quad (2)$$

$$A_2 = A_O A_U - \frac{\pi}{8} d_U \left(A_O - \frac{d_O}{2} \right) - \frac{\pi}{8} d_O \left(A_U - \frac{d_U}{2} \right) - \frac{d_O}{2} A_U \quad (3)$$

$$A_3 = A_O A_U - \frac{d_O}{2} A_U - \frac{\pi}{4} d_U \left(A_O - \frac{d_O}{2} \right) \quad (4)$$

$$A_4 = A_O A_U - A_U d_O \quad (5)$$

Here A_O, A_U are distances between warp and weft yarns (the reciprocal value to sett of yarns D_O, D_U).

It's necessary to note that the equation for the "opened area" of pore type 4 A_4 is not function of the weft yarn diameter d_U. This is one of the important limitation of practical utilization.

3. SIMPLIFIED 3-D MODEL OF POROSITY

The simplified 3-D model of porosity is based on a differentiation of four pore types as fig.1 shows. The intra-yarn porosity is neglected and the yarns are considered to be cylinders of a circular section (compression of the yarns in binding points is neglected).

Each pore cell is created by two segments of warp yarns and by two segments of weft yarns. Such segments can be interlaced or non-interlaced (fig. 2b, c). A volumetric proportion of the interlaced yarn segment in a total volume of a pore cell is higher than a volumetric proportion of the non-interlaced yarn segment. Thus, more interlaced pore cell has higher packing density formed by mass of the yarns (porosity is smaller).

The total volume of one pore cell V_C shown on fig. 2 is described by the

$$V_C = \frac{1}{D_O} \cdot \frac{1}{D_U} \cdot (d_O + d_U) \quad (6)$$

Proposed cell model assumes the same corrugation of the warp and weft yarns (the fabric is balanced). In this case, the fabric thickness is: $t = d_O + d_U$. In the case

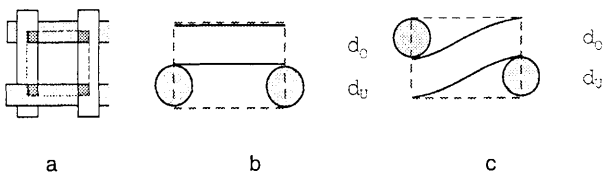

a b c

Fig. 2 Model of total volume of one pore cell; a – upper side, b – edge side (not interlaced segment of yarn); c – edge side (interlaced segment of yarn)

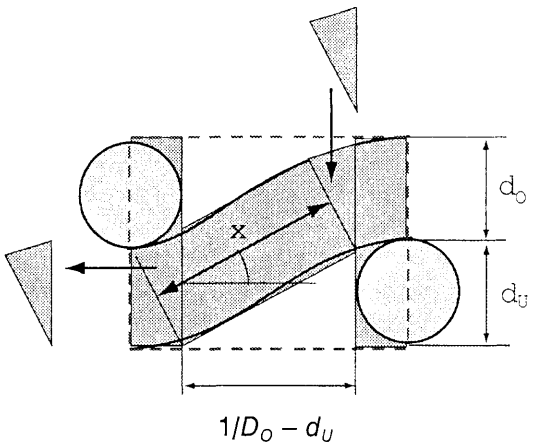

Fig. 3 Simplified 3-D model of porosity

that the warp and weft yarns corrugations are different, the fabric thickness is higher. When evaluating fabric porosity, the model of woven fabric as a plane plate is usually accepted. In reality the surface of a woven fabric has a certain relief. For evaluation of a single pore cell, it seems reasonable to define a vertical dimension by sum of warp and weft yarn diameters in case of not balanced woven fabric too.

As fig. 2 a or 3 show, volume of binding points (the crossing of the warp and weft yarn) is assumed as completely filled by mass of the yarns. This idea is partly similar to the idea of the classical 2-D model of porosity and it's not completely correct.

In the case when the binding point is assumed to be the perpendicular crossing of two cylinders (deformations are neglected), four pore types are in binding points approximately the same. Four pore types are different mainly in connecting segments of binding points. In case of staple yarns it is possible to assume that yarn hairs are denser by arrangement in vicinity of the binding point.

Let the non-interlaced connecting segment of the warp yarn has a cylinder shape. The half of this cylinder volume V_{ZO-} fills the part of the total pore cell volume

$$V_{ZO-} = \frac{\pi d_O^2}{8} \left(\frac{1}{D_U} - d_U \right) \quad (7)$$

The interlaced connecting segment of warp yarn is possible to replace approximately by cylinder with the base diameter d_O and with the height x_O (fig. 3). The half of this cylinder volume V_{ZO+} fills the part of the total pore cell volume

$$V_{ZO+} = \frac{\pi d_O^2}{8} \frac{\left(\frac{1}{D_U} - d_U \right)}{\cos \phi_O} \quad (8)$$

Here ϕ_O is the angle of the warp yarn interlacing. For calculating of volume V_{ZU-} and V_{ZU+} it is necessary to change subscripts O ↔ U in equations (7, 8). By using

of these equations it is possible to determine the packing density volume or the porosity for all kind of the pore cells.

The *pore type 1* is symmetrical and is formed by two interlaced connecting segments of the warp yarn and by two interlaced connecting segments of the weft yarn.

The *pore type 2* is symmetrical too and is formed by one interlaced connecting segment of the warp yarn, one non-interlaced connecting segment of the warp yarn, one interlaced connecting segment of the weft yarn and one not-interlaced connecting segment of the weft yarn.

The *pore type 3* is not symmetrical. It is necessary to take into account its orientation in a fabric. Pore of the type 3A is formed by two non-interlaced connecting segments of the warp yarn and by two interlaced connecting segments of the weft yarn. The pore of the type 3B is formed by two interlaced connecting segments of the warp yarn and by two non-interlaced connecting segments of the weft yarn.

The *pore type 4* is symmetrical and is formed by two non-interlaced connecting segments of the warp yarn and by two non-interlaced segments of the weft yarn.

The "empty volumes" of all pore types are given by equations

$$V_1 = V_C - \left[d_O d_U (d_O + d_U) + 2V_{ZO+} + 2V_{ZU+} \right] \quad (9)$$

$$V_2 = V_C - \left[d_O d_U (d_O + d_U) + V_{ZO+} + V_{ZO-} + V_{ZU+} + V_{ZU-} \right] \quad (10)$$

$$V_{3A} = V_C - \left[d_O d_U (d_O + d_U) + 2V_{ZO-} + 2V_{ZU+} \right] \quad (11)$$

$$V_{3B} = V_C - \left[d_O d_U (d_O + d_U) + 2V_{ZO+} + 2V_{ZU-} \right] \quad (12)$$

$$V_4 = V_C - \left[d_O d_U (d_O + d_U) + 2V_{ZO-} + 2V_{ZU-} \right] \quad (13)$$

Porosity of a woven fabric with any binding type is calculated as

$$P_H = \frac{n_1 V_1 + n_2 V_2 + n_{3A} V_{3A} + n_{3B} V_{3B} + n_4 V_4}{V_C s_O s_U} \quad (14)$$

where n_1, n_2, n_{3A}, n_{3B} a n_4 are the numbers of pore types in pattern repeat and s_O, s_U are numbers of a binding points in pattern repeat in a warp direction and in a weft direction respectively.

For a comparison of models of porosity the set of 26 shirting woven fabrics (15 with plain weave and 11 with another weave) was used. For all fabrics the basic parameters mentioned above: D_O, D_U [1/cm], d_O, d_U [μm] (according to methodology described in [4]), ϕ_O, ϕ_U (using image analysis system LUCIA), n_1–n_4 and s_O, s_U were quantified. For all fabrics air permeability AP (m/s) were measured. The porosity according to classical 2-D model (P_S), modified 2-D model (P_G) and simplified 3-D model (P_H) of porosity were calculated. Fig. 4 shows

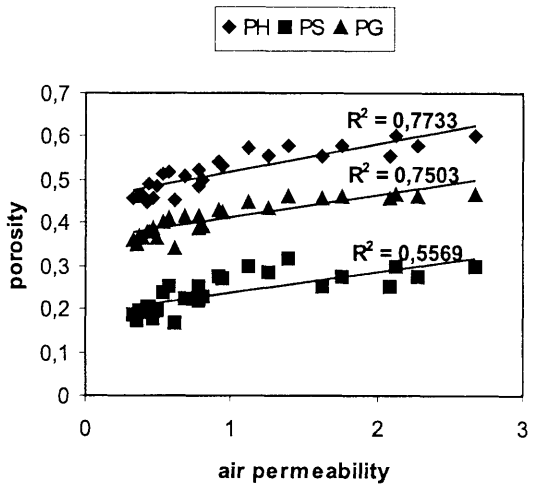

Fig. 4 Comparison of porosity and air permeability

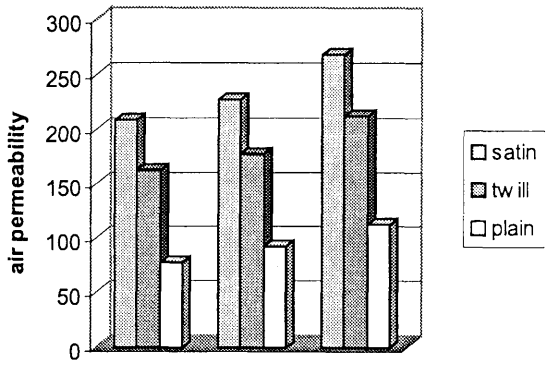

Fig 5 Air permeability of woven fabrics with plain, seven-binding twill and seven-binding satin weave

a correlation between air permeability and porosities of woven fabrics. New model of porosity gives slightly better results with model proposed by Gooijer.

DEFORMATIONS OF WOVEN FABRIC CAUSED BY AIRFLOW

A correlation between a porosity of fabric and air permeability is very complicated because a structure of textiles changes by influence of airflow. A deformation of a fabric caused by stream air has the following main reason:

1. A bagging of a circular sample clamped in the instrument (in direction of flowing air). This phenomenon leads to enlarge the sample area and to open pores. This deformation is classified as a *horizontal increase of the porosity*. An importance of this phenomenon is very individual according to mechanical properties of a fabric (the flexural rigidity, the extensibility etc.). A horizontal increase of porosity can result in a considerable increase of an air permeability value. This phenomenon is especially important in the evaluation of an air permeability of

knitted fabrics. Some measuring instruments have support of the sample avoided this type of deformation.

2. Moving of free yarn sections. Yarns in plain fabrics are interlaced very closely and the introduced phenomenon does not start. In twill or satin weaves relative moving of yarns causes an increase of its porosity predominantly in a vertical direct. This deformation is classified as a *vertical increase of the porosity.*
3. Flowing air pushes aside outside layers of staple yarns. Some fibres in an area of hairiness are pressed to a relatively compact yarn core. Some fibres float in the airflow and increase an flow resistance of a fabric.

DEGREE OF YARNS INTERLACING IN WOVEN FABRIC

A degree of interlacing of yarns in a woven fabric influences a lot of fabric properties. A modified 2-D model of porosity takes a shape difference of four types into account, but is based on an idea of an isolated pore. This idea is not acceptable for finer evaluation of air permeability.

A degree of interlacing of yarns in a woven fabric f [3] describes the relative passage of weft yarns between the right side and underside. f can be calculated as

$$f = \frac{1}{n_U / s_O} \tag{15}$$

Here n_U is a number of passages of one weft yarn between the right side and the underside and s_O is a number of warp yarns in a pattern repeat. For plain weaves is $f = 1$. For other weaves is $f > 1$. If the number of weft yarn passages is not the same for every weft yarns in a pattern repeat, a degree of interlacing can be calculated as

$$f = \frac{1}{\frac{\frac{1}{s_O}\sum_{i=1}^{s_U} n_{Ui}}{s_U}} = \frac{s_U}{\frac{1}{s_O}\sum_{i=1}^{s_U} n_{Ui}} \tag{16}$$

Here s_U is a number of weft yarns in a pattern repeat.

From projection of the woven fabric it is possible to identify the arrangement of four pore types in a pattern repeat (fig. 6). It is evident that seven-binding twill and a seven-binding satin have the same number of floats. The lengths of floats are the same too. A degree of interlacing f is the same. The arrangement and a number of four pore types is different. Fig. 5 shows air permeability values of tree woven fabrics. There are one plain weave, one seven-binding twill and one seven-binding satin. Construction parameters of fabrics are the same (D_O, D_U, d_O, d_U). It is evident that the air permeability of twill and satin woven fabric is different.

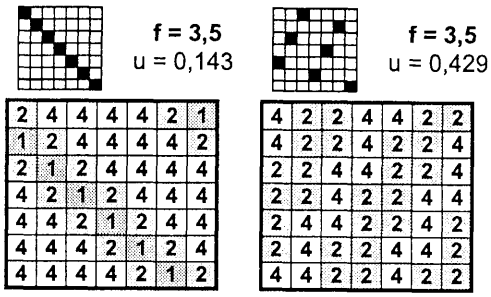

Fig. 6

This discrepancy can be explained for example by assumption that the move floats in the twill weave have developed a "pocket". Neighbouring new pores caused by the vertical increase of porosity cover up each other. They are shifted only about one binding point. The shift of neighbouring weft yarns passages in the satin weave is larger and then airflow is more intensive (sea fig. 7 and 8).

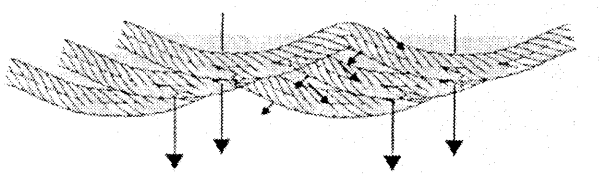

Fig. 7 Air flowing in twill weave

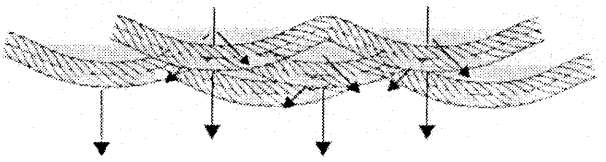

Fig. 8 Air flowing in satin weave

THE SHIFT OF NEIGHBOURING WEFT YARNS

In basic twill and satin weaves there is in a pattern repeat only one warp binding point (in case of weft-binding) or one weft binding point (in case of warp-binding). The shift of interlacing of two neighbouring weft yarns is the same in all pattern repeat (fig. 6). In the best simplifying cases the shift of neighbouring weft yarns can be described as:

u = shift of interlacing of neighbouring weft yarns/s_O (17)

For further evaluation the selected fabrics were used. Some fabrics had a more complicated type of binding and shift of interlacing of neighbouring weft yarns was not simple to determine. Experimental data for set of remaining 22 fabrics (plain weave, seven-binding twill and seven-binding satin, four-binding reinforced twill) were tested by regression analysis. The characterization of structure S was introduced

$$S = Pf^u \tag{18}$$

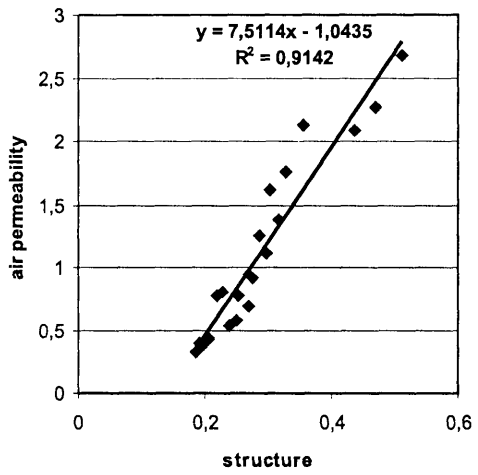

Fig. 9 Comparison of air pereability and overall parameter of structure

Where P is porosity determined as P_S, P_G or P_H, f is degree of interlacing of yarns in fabric and u is the shift of neighbouring weft yarns. Fig. 9 shows a correlation between air permeability and overall parameter of structure S (where $P = P_S$ was used).

CONCLUSION

The main aim of this contribution was to show that deeper description of the textile structure is necessary for finding of relationship between fabric structure and air permeability. A standard evaluation of static porosity is insufficient. The introduction of four basic types of pore is very rational, but the quantitative expression of their representation in a pattern repeat is insufficient. Very important is arrangement four pore types. New model of woven fabric porosity includes a 3-D structure of pores and their different shape. This model gives comparable results as model proposed by Gooijer. It seems suitable for any type of binding, but it not takes arrangement of four pore types into account. The overall parameter of woven fabric structure that gives better correlation with a value of air permeability was proposed. This overall parameter is suitable only for some basic type of binding.

REFERENCES

[1] Gooijer, H.: Flow resistance of textile materials, PhD Thesis, 1998
[2] Backer, S.: The relationship between the Structural Geometry of a Textile Fabric and Its Physical Properties, Part IV: Interstice Geometry and Air Permeability, Text. Res. Journal, 21, 1951.
[3] Nosek, S.: Struktura a geometrie tkanin, Výzkumný ústav bavlnářský 1974
[4] Havrdová, M., Drašarová, J.: Prediction of woven fabric permeability basic on geometrical model of porosity. 6th conf. of Faculty of Engineering and Marketing of Textiles. Lodz. March 2003.

ACKNOWLEDGEMENT
This work was supported by the research project of Czech Ministry of Education Textile Research Center LN 00B090.

PRODYŠNOST A STRUKTURA TKANIN

Translation of Abstract:
Air permeability and a structure of woven fabrics

Hlavním cílem tohoto příspěvku je popsat vybrané modely porosity tkaniny a navrhnout model nový. Z hlediska vzájemného vztahu mezi prodyšností a strukturou tkaniny není možné popisovat tkaninu pouze její porositou. Obecně porosita udává, kolik vzduchu je v textilii obsaženo. Pro popis proudění vzduchu přes textilní materiály jsou velmi důležité další detaily o uspořádání pórů v textilii (velikost pórů, jejich tvar, vzájemné uspořádání a pod.). Navíc se struktura textilie účinkem proudícího vzduchu mění a její vztah s prodyšností je proto komplikovanější. Tento příspěvek zmiňuje také význam deformací, ke kterým v tkanině vlivem proudícího vzduchu dochází. Bylo zjištěno, že při popisu struktury je nezbytné vedle porosity uvažovat také typ vazby tkaniny.

LONG TERM CYCLIC DEFORMATION OF FABRICS WITH IMPROVED ELASTICITY

Militký J., Bajzík V

Textile Faculty, Technical University of Liberec 461 17 Liberec, Czech Republic
e-mail : jiri.militky@vslib.cz

The aim of this contribution is description of simple simulation study based on the long-term cyclic tensile deformation of fabric to the selected stress levels combined with one-day recovery. This simulation has been realized on the Tiratest machine for tensile testing. From the experimental results the relative portion of plastic deformation; elastic recovery and change of rigidity were computed. The fabrics with special improved elasticity were evaluated.
KEY WORDS: cyclic tensile deformation, elastic recovery, mixing with Lycra

1. INTRODUCTION

The low stress level cyclic deformation combined with long-term relaxation occurs frequently during the wearing of textile products. The small portion of permanent deformation and small shape instability (good stiffness) due to cyclic deformation are required for clothing purposes.

For improving of there characteristics the small amount of elastomeric fibers are added to fabric. The main aim of this contribution is proposal of methodology for evaluation the textiles response to the cyclic deformation combined with long term relaxation. The parameters characterized recovery; permanent deformation and stiffness change are computed.

2. CYCLIC DEFORMATION OF TEXTILES

Typically, the deformation of textiles is due to cyclic straining to the very small level of stress. The simple deformation cycle consists of phase of straining and strain release (see fig. 1a). The area bounded by the curves from *A* to *B*, from *B* to *C* and from *C* to *A* is proportional to the total deformation energy W_D. Energy of recovered work W_Z is proportional to the surface area bounded by the curves from *D* to *B*, from *B* to *C* and from *C* to *D*. The plastic energy imposed to the textile is then equal

$$W_P = W_D - W_Z \tag{1}$$

The so called work *r* recovery is defined by the simple relation

$$r = W_Z / W_D \tag{2}$$

The quantity *(1 – r)* is proportional to the energy dissipated as heat. Plastic deformation energy can by expressed by the form

$$W_P = W_D(1-r) \tag{3}$$

After *N* deformation cycles is the stored energy ΣW_{Pi} equal to the total work to break *W* and rupture occurs. The work to break is defined by relation

$$W = \int_0^{\varepsilon_P} \sigma(\varepsilon)d\varepsilon \tag{4}$$

where ε_P is strain to break (tenacity). Number of cycles N_P to the break is then equal

$$\sum_{i=1}^{N_P}(1-r_i)W_{Di} = W \tag{5}$$

where r_i and W_{Di} are recovery work and total deformation energy for the *i*-th cycle. For the simple case of $r_i = r$, $W_{Di} = W_D$ the following relation can be obtained

$$N_P = \frac{W}{(1-r)W_D} \tag{6}$$

Fig. 1a

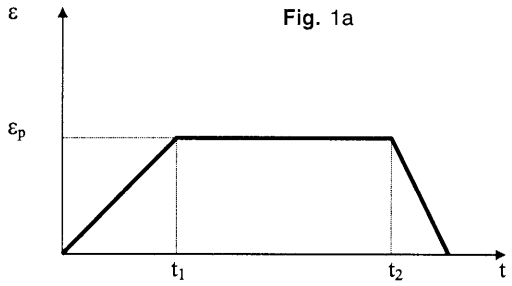

Fig. 1b

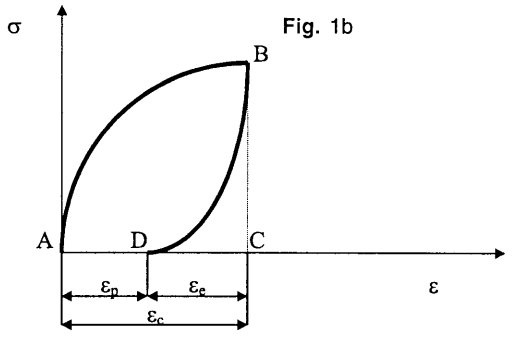

Fig. 1 Typical deformation cycle

Long-term stability after cyclic deformation requires:

I. Fibers with great work to break
II. Fibers with good recovery
III. The small energies W_D (low applied stress and stiff fabric)

There exist a lot of various methods of cyclic deformation. For simulation of cyclical action during wearing the variant consists of loading to the required degree ε_c with subsequent relaxation and releasing has been selected. The one cycle of deformation consists of the:

a) Loading up to required level of deformation ε_C at time t_1
b) Stress relaxation in the interval t_2–t_1
c) Recovery (stress releasing).

This cycle for time dependent deformation is shown on the fig. 1b. Plastic deformation after this cycle is equal to

$$\varepsilon_P = \frac{l_{A-B}}{l_0} \qquad (7)$$

where l_0 is initial length of sample and l_{A-B} is increment of sample length after finishing the one cycle.

For the long-term deformation and recovery combination the following procedure using this deformation cycle have been applied:

1. 20 times repeating on cycle up to ε_C (one run)
2. One day recovery
3. 20 times repeating of cycle up to ε_C
4. One day recovery
5. 20 times repeating of cycle up to ε_C
6. One day recovery.

For quantifying of this long-term cyclical deformation the following parameters has been selected:

- Maximum load in the first cycle F_{1C}.
- Maximum load in the 20th cycle F_{20C}.
- Plastic deformation after whole procedure ε_P

These parameters can be used for the evaluation of fabric response to this complex procedure

3. EXPERIMENTAL PART

Four types of fabrics containing elastometric fibers have been used for evaluation of portion of plastic deformation and changes of stiffness after above described complex cyclic deformation.

The experiments are realized for the

- Standard fabrics (abbreviation S)
- Washed fabrics (abbreviation W)

Basic information about tested fabrics are summarized in the Table 1.

For characterization of mechanical behavior of individual fabrics the load to break and deformation to break were measured under standard conditions (sample width 5 cm). Results are summarized in the table 3a and 3b.

For characterization of mechanical behavior of individual fabrics the load to break (tenacity) and deformation to break were measured under standard conditions (sample width 5 cm). Results are summarized in the table 3a and 3b.

Cyclic deformation was realized up to the deformations selected according the deformation to break (see table 2).

Experiments were realized on the tensile testing device TIRATEST under these conditions (see fig. 1b)

- Rate of deformation 0.15 min^{-1}
- Relaxation time 5 min
- Number of cycles in one run 20
- Time between runs 24 hours
- Number of runs 3

For individual ε_C the loads F_{1C} and F_{20C} and plastic deformation after whole procedure ε_P were measured.

In these tables CV denotes coefficient of variation. Confidence intervals are computed after normality proving [2].

Table 1 Basic Parameters of Fabrics

Fabric No	Content	Pattern	Areal weight [g/m^2]	Width [cm]
502	98%cotton, 2% Lycra	Combined	300	130
687	98% cotton, 2% Lycra	Twill (Z)	400	150
700	73% TENCEL, 24% cotton, 3% Lycra	Twill (S)	310	130
549	64% PAD, 32% cotton, 4% Lycra	Twill (Z)	286	140

Table 2 Selected deformations degrees

Fabric No	Deformation degree ε_C
502	5, 7, 10, 12, 15
687	8, 12, 15, 18, 21, 24
700	5, 7, 10, 12, 15
549	15, 19, 23, 27, 31, 35

4. CYCLIC DEFORMATION CHARACTERISTICS

From the measured parameters of fabrics some characteristics of total recovery, degree of plastic deformation and change of stiffness were computed. For characterization of the fabrics recovery the total recovery Z_C [%] has been computed

$$Z_C = 100\frac{\varepsilon_C - \varepsilon_P}{\varepsilon_C} \qquad (8)$$

where ε_C is maximum deformation and ε_P is plastic deformation after finishing of whole deformation procedure (3 days).Portion of plastic deformation has been characterized by the cumulative extension after whole procedure

$$E_P = 100\ln(\varepsilon_P + 1) \qquad (9)$$

Higher E_P is indication of the higher plastic deformation during wearing.

Degree of plastic deformation is equal to

Table 3a Tenacity – warp

Fabric No	Before washing Mean [N]	Confidence interval [N]	Standard deviation [N]	CV [%]	After washing Mean [N]	Confidence interval [N]	Standard deviation [N]	CV [%]
502	1100	1070–1129	9,4	0,9	954	879 –1029	20,3	2,1
687	1429	1377–1481	27,6	1,9	1544,5	1383–1706	80,8	5,2
700	1174	931–1417	88,8	7,6	1238,5	1149–1328	39,3	3,2
549	763	679–847	28,5	3,7	703,5	593–814	39,6	5,6

Table 3b Tenacity – weft

Fabric No	Before washing Mean [N]	Confidence interval [N]	Standard deviation [N]	CV [%]	After washing Mean [N]	Confidence interval [N]	Standard deviation [N]	CV [%]
502	565,5	538–593	22,7	4	467	455–479	7,9	1,7
687	647,5	566–729	32,7	5,1	548	530–567	19	3,5
700	529	449–609	21,6	4,1	447	422–472	12,2	2,8
549	870	852–888	26,5	3,1	592	571–613	7	1,2

Table 3c Deformation at break – warp

Fabric No	Before washing Mean [%]	Confidence interval [%]	Standard deviation [%]	CV [%]	After washing Mean [%]	Confidence interval [%]	Standard deviation [%]	CV [%]
502	15,21	14,68–15,73	0,67	4,38	16,93	16,05–17,81	0,29	1,68
687	32,69	31,49–33,89	1,57	4,81	27,42	26,84–28	0,48	1,75
700	12,67	10,98–14,35	0,46	3,76	15,91	15,41–16,42	0,48	3,03
549	61,31	56,21–66,42	1,78	2,91	40,9	38,46–43,33	1,44	3,54

Table 3d Deformacion at break – weft

Fabric No	Before washing Mean [%]	Confidence interval [%]	Standard deviation [%]	CV [%]	After washing Mean [%]	Confidence interval [%]	Standard deviation [%]	CV [%]
502	18,69	17,89–19,5	0,25	1,4	19,48	14,92–24,03	2,93	15,02
687	18,22	17,79–18,7	0,41	2,2	23,81	22,61–25,01	1,01	4,23
700	17,42	16,14–18,7	0,74	4,3	13,72	13,03–14,41	0,2	1,48
549	54,87	51,13–58,6	1,28	2,3	58,44	53,66–63,21	1,65	2,82

$$Z_P = \frac{E_P}{E_C} 100 \qquad (10)$$

where $$E_C = 100 \ln(\varepsilon_C + 1) \qquad (11)$$

As the characteristic of stiffness the secant modulus

$$y_C = \frac{F_{1C}}{\varepsilon_C} \qquad (12)$$

has been selected. Stiffness after 20 times repeating of cycle is

$$y_K = \frac{F_{20C}}{\varepsilon_C} \qquad (13)$$

Relative stiffness change Z_T is defined by the relation

$$Z_r = \frac{y_C - y_K}{y_C} 100 \qquad (14)$$

Higher Z_T shows higher influence of long-term cyclic deformation to the stiffness change. For the case ε_C = 15 % are above-mentioned characteristics shown on the fig. 2, 3, 4.

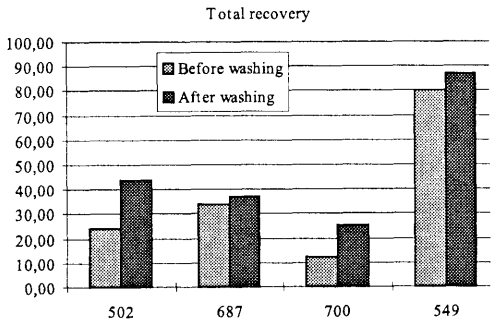

Fig. 1 Total recovery before and after washing

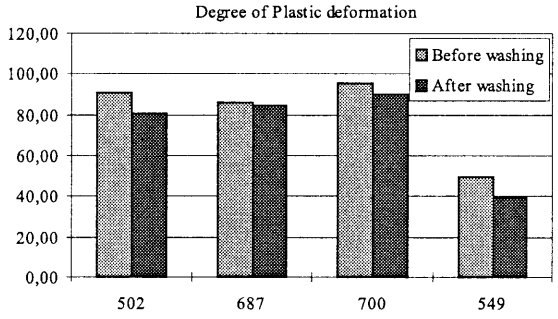

Fig. 2 Plastic deformation before and after washing

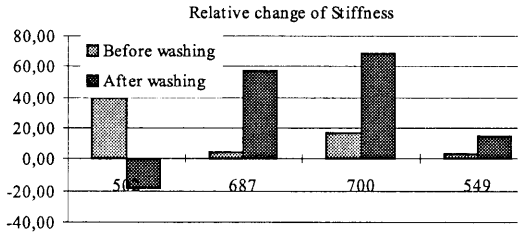

Fig. 3 Stiffness before and after washing

5. RESULTS AND DISCUSSION

The characteristics Z_C, Z_P and Z_T are graphically represented on the figs 2, 3, 4. Based on the previous finding the values Z_C of total deformation recovery at low ε_C are for shape retaining materials above 85–90%. Only the fabric No 549 composed from PAD/cotton/Lycra blend satisfies to this criterion. For other materials is Z_C under 50% and therefore the stability of shape after long-term cyclic deformation will be not on the required level.

Interesting results were obtained by comparison of washed and no washed samples. At low ε_C have fabrics after washing:

a) The better recovery Z_C for all tested samples
b) Lower plastic deformation degree for all samples excluding the No 502
c) Markedly lower degree of stiffness for all samples excluding the No 687.

These results show that the behavior of fabrics under long-term cyclic deformation is very complex and can be significantly changed by the washing. The influence of elastometric fibers could be improved by structure and pattern of fabric.

Acceptable low permanent plastic deformation can be obtained for materials hawing good elastic properties as well (see fabric No 549).

6. CONCLUSION

The proposed procedure for evaluation of the response of fabrics to the cyclic deformation with relaxation a recovery is very simple but can be applied for prediction of shape stability during wear. Influence of washing is important especially for fabric containing cotton

ACKNOWLEDGEMENTS:

The Czech Ministry of Education Grant LN B090 supported this work.

REFERENCES

[1] Hearle, J.W.S., Morton, W.E.: Physical Properties of Textile Fibers, TI 1993
[2] Meloun M. Militký J. and Forina M. Chemometrics in Analytical Chemistry vol. I, Ellis Horwood, Chichester (1994)

DLOUHODOBÉ CYKLICKÉ NAMÁHÁNÍ TKANIN SE ZLEPŠENOU ELASTICITOU

Translation of Abstract:

Long term cyclic deformation of fabrics with improved elasticity

Cílem této práce je popis simulační studie zaměřené na dlouhodobé cyklické tahové namáhání při vybraných úrovních zatížení kombinované s jednodenním zotavením. Tento speciální experiment byl simulován na trhacím přístroji TIRATEST. Na základě experimentu byl určen podíl plastické deformace, elastické zotavení a změna tuhosti. Experiment byl prováděn na speciálních tkaninách s přídavkem elastomerních vláken.

CHARACTERIZATION OF PILLS SIZE DISTRIBUTION

Militký J, Kovačič V., Kašparová A.

Textile Faculty, Technical University of Liberec 461 17 Liberec, Czech Republic
e-mail : jiri.militky@vslib.cz

Pilling is unwanted phenomena having negative influence on the appearance of textile fabrics. Classical pilling characteristics are based on the computation of number of pills after defined abrasion on special devices. This contribution describes the characterization of pilling by using of image analysis. Results of image analysis are the number of pills and the size of pills. Main aim of this contribution is description of the distribution of pills size after selected times of abrasion.
KEY WORDS: pilling tendency, distribution of pills size, image analysis, abrasion of surface

1. INTRODUCTION

Pilling is a long-standing problem in relation to staple-fiber fabrics and fabric containing synthetic fibers. It is well known that when two fabric surfaces are rubbed together under a light pressure, those fibers where ands are protruding on the surface are gradually pulled out. As they emerge, these fibers are rubbed into small balls or pills, which remain on the surface anchored by one or more fibers, which are still partly within the fabric. These unsightly pills are formed on weaves of knitted garments during wear.

The main aim of this work is description of pills size distribution and changes of parameters of this distribution during the prolongation of pilling (mechanical action). The pills size is characterized by the area S [mm^2] of perpendicularly projected pills to the plane of image.

2. PILLING MECHANISM

Previous investigations have shown that the mechanism of pilling involves three distinct stages [1]

i) Fibers are drawn to the fabric surface as a result of some mechanical action and there form *fuzz*,
ii) The fuzz entangles into *pills*,

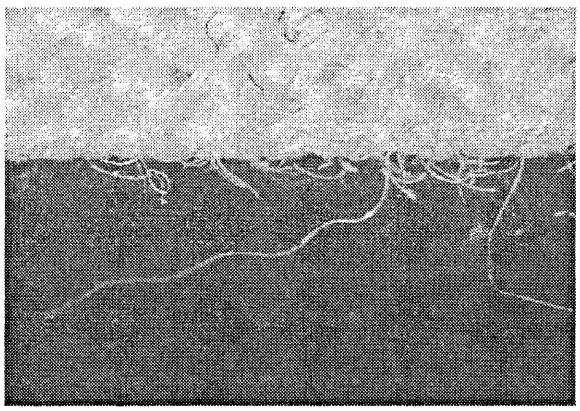

Fig. 1 Fuzziness on the surface of fabric

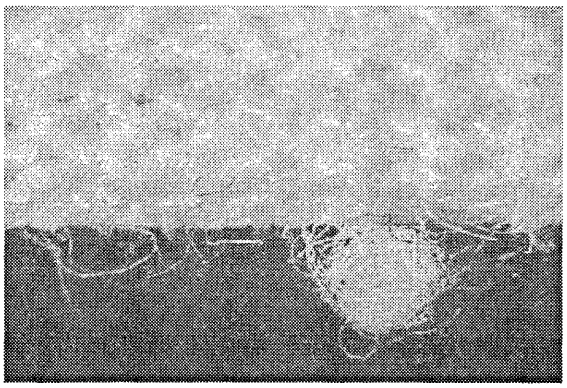

Fig. 2 Pill on the surface of fabric

iii) The pills wear off under continued mechanical action.

Creation of fuzz on the surface of fabric is shown on the fig. 1. The pill formation is shown on the fig. 2.

Several techniques have been developed to investigate these three stages of pill formation independently [2].

The most usual manner of characterizing the pilling behavior of fabric is by the so called *pill-curve*. The *pill-curve* is dependence of numbers of pills measured on standard area [3] or the degree of pilling [4] against the duration of mechanical action (pilling).

A complex mathematical model of pilling was proposed by Brand and Bohmfalk [2]. Simplified model based on the assumption that rates of pills formation and wear-off remain constant was described by Conti and Tassinari [5].

In the another paper of Conti and Tassinari [6] the numerical distribution of fibers in pills were derived. It has been shown that distribution of the numbers of fibers in pills is the sum of binomial distribution.

3. CHARACTERIZATION OF PILLING

The characterization of pilling is closely connected with the device used for testing. The WIRA (Martindale)

abrasion machine uses as the specimen the 6×6 cm fabric square. Assessment is by cutting the pills of this square and weighting them or by visual comparison.

The ATLAS pilling tester (random tumble pilling tester) use the fabric specimen 12×12 cm and number of pills are evaluated subjectively or classified using five ratings.

Richards [7] has found close correlation between these devices. Approximately 20 hours in the random tumble pilling tester is equivalent to 2 000 rubs on the WIRA (i.e. 40 min rubbing time). For description of pilling the various combinations of mean pill number N_m and mean pill mass M_m were proposed [8]. The Product N_m M_m is equivalent to the total pill weight.

Naik and Lopez-Amo [9] have suggested a correlation between N_m M_m and random tumble pilling test subjective rating.

In some cases, the product $N_m^2 M_m$ was proposed for description of pilling behavior or construction of „pill curve". By using of kinetic model of pill curve the amount of pill able fuzz portion of fiber removed that formed pills and mass of worn-off pills can be computed [8].

From point of view of fabric appearance the size of pills is predominant and pilling can be characterized by the total size of all pills. In some standards the rating of pills according to their size is proposed.

In ČSN 80 0839 (Czech Standard) are three categories:

a) Maximum diameter of pills up to 0.5 mm (area of equivalent circle is 0.196 mm^2),
b) Maximum diameter of pills up to 2 mm (area of equivalent circle is 3.14 mm^2),
c) Maximum diameter of pills over 2 mm.

From point of view of fabric appearance the case a) is the best one.

4. STATISTICAL ANALYSIS OF PILLS SIZE

On the base of large number of samples it has been proved that distribution of pills size S [mm^2] (projected area) is unimodal and positively skewed to the right and can be well approximated by the lognormal distribution [11].

$$F(S) = \int_{-\infty}^{S} \frac{(x - S_0)^2}{2\pi A^2} \exp\left(-\frac{(\ln(x - S_0) - C)^2}{2A^2} \right) dx \quad (1)$$

Here $F(S)$ is distribution function (cumulative frequency), S_0 is threshold (minimal) pill size, A and C are scale and shape parameters. In sequel the sample containing N experimentally measured independent pills sizes (S_i) i = 1, ...N is analyzed. The estimation of these parameters can be realized by using of sample values of pills size S_i by maximum likelihood method.

For measured independent pills size S_i having probability density $f(S_i)$ the log of likelihood function has the form [11]

$$\ln(L) = \sum_i \ln(f(S_i)) \quad (2)$$

By maximizing of $\ln(L)$ the maximum likelihood estimates can be computed. For above selected distribution the maximization of $\ln(L)$ leads to three nonlinear equations from which the parameters S_0, A, C can be iteratively refined.

4. EXPERIMENTAL PART

The 100 % polyester plain weave having high tendency to pilling has been used. Selected characteristics of this weave are given in Table 1.

The experiments were realized on random tumble pilling tester of Czech provenience (ŽMOLTEX – Partex). Test specimens were caused to tumble freely in a cylindrical chamber (diameter 146 mm and length 152 mm) by the action of two 120 mm long impellers equally spaced on a horizontal shaft located at the axis of the cylinder and rotating at a speed 1200 r.p.m.

The inside wall of each cylinder was covered with a removable cork sheet (thickness 1.5 mm). Test specimens were 110 mm squared pieces cut at 45° bias from the fabric. Sewing stabilized each edge of specimens. Three fabrics specimen and 25 mg of cotton sliver cut to 5 mm length pieces were placed to the test chambers.

The specimens were removed at selected times 30, 60, 90 and 120 min. After measurements of pills numbers and size the process was continued with the same specimens.

For measurements of numbers and size of pills the imager analysis system LUCIA-M has been used. The specimens were clamped to special rotational holder enabling realization of perpendicular projection of pills to plane of CCD Camera (image plane). In this projection the size of pills were characterized by the surface

Table 1 Selected Fabric Properties

Property	Units	Value
sett warp	[m^{-1}]	1760
sett weft	[m^{-1}]	1520
areal weight	[g m^{-2}]	198.5
thickness	[mm]	0.52
friction resistance *)	[mN]	158.49
roughness *)	[mN]	90.58

*) see work [12]

Table 2 Parameter estimates of lognormal distribution

Time [min]	30	60	90	120
Threshold S_0 [mm^2]	0.12775	0.17774	0.061903	0.23087
Mean C [mm^2]	−1.3741	−1.7030	−1.1283	−1.7954
Standard deviation A [mm^2]	0.99116	1.2057	0.84716	1.3878
Number of pills	48	88	48	21

Table 3 Characteristics of pills size

Time [min]	S_M [mm^2]	S_{Med} [mm^2]	S_C [mm^2]
30	0.095	0.25	30.0
60	0.043	0.18	79.2
90	0.016	0.32	53.2
120	0.024	0.17	19.6

area S [mm^2]. Details about realization of image analysis and extraction of individual pills from image are described in work [13]. Numbers of pills are in Table 2 and total pills area S_C [mm^2] is given in Table 3.

4. RESULTS AND DISCUSSION

The estimation of parameters of lognormal distribution was realized by the maximum likelihood methods. Results are summarized in the Table 2.

For characterization of mean size of pills the mode S_M and median S_{Med} were computed. The mode is defined by the relation

$$S = \exp(C - A^2)$$

and median by the relation

$$S = \exp(C)$$

These characteristics are given in the Table 3.

The computation of confidence intervals for S_{Med} leads to conclusion that median of pills size is not significantly dependent on the time of pilling.

The total pills area S_C can be assumed to be close to total mass of pills. The corresponding „pill curve" has typical shape (see [5]) and can be described by the simplified kinetic model.

The knowledge of pills size distribution can be used for estimation of pills portion with size below or above special limit. In the table 4 are portions of pills sizes P_1, P_2 and P_3 corresponding to Czech standard (see chap. 2) computed from relations

$P_1 = 100 \times \text{Prob}(S < 0.196)$

$P_2 = 100 \times \text{Prob}(0.196 < S < 3.14)$

$P_3 = 100 \times \text{Prob}(S > 3.14)$

Here Prob(.) denotes probability and correspond to values of cumulative density of lognormal distribution with parameters from table 2.

It is clear that according to Czech standard the most of pills have moderate size (see value P_2) and portion of very large pills is very small (see value P_3).

By this way is possible to characterize the pilling as portion of pills in selected size limits. These limits will be suitable to estimate pilling tendency based on the appearance of pilled fabrics.

Table 4 Portion of pills below a above specified limits

Time [min]	30	60	90	120
P_1 [%]	9.6	3.3	26.4	0
P_2 [%]	89.8	95.6	73.2	98.06
P_3 [%]	0.6	1.1	0.4	1.94

5. CONCLUSION

The image analysis can be used for objective characterization of pilling. The size of pills distribution can be described by the lognormal distribution. It is interesting that the modal size of pills is statistically independent on the time of mechanical action (abrasion).

ACKNOWLEDGEMENTS:

The Czech Ministry of Education Grant LN B090 supported this work

6. REFERENCES

[1] Gintis D., Mead E. J.: Text. Res. J. **29**, 578 (1959)
[2] Brand R. H., Bohmfalk B. M.: Text. Res. J. **37**, 467 (1967)
[3] Albrecht W.: Chemiefasern **20**, 387 (1970)
[4] Thimm J. K.: Melliand Textilberichte **51**, 177 (1970)
[5] Conti W., Tassiari E. A.: J. Text. Inst. **65**, 119 (1974)
[6] Conti W., Tassiari E. A.: J. Text. Inst. **66**, 73 (1975)
[7] Richards N.: J. Text. Inst. **53**, 357 (1962)
[8] Williams V. A.: Tex. Res. J. **55**, 312 (1985)
[9] Naik A., Lopez-Amo F.: Melliand Textilberichte **63**, 416 (1982)
[10] Weibull W.: J. Appl. Mech. **18**, 293 (1951)
[11] Meloun M., Militký J., Forina M.: Chemometrics for Analytical Chemistry, vol I, Ellis Horwood, Chichester, 1992
[12] Militký J., Bajzík V.: Int. J. of Clothing Science and Technology Vol. 6, No 2-3, p. 32 (1994)
[13] Kašparová A.: Diploma thesis, TU Liberec 1997

CHARAKTERIZACE ROZDĚLENÍ VELIKOSTI ŽMOLKŮ

Translation of Abstract:
Characterization of pills size distribution

Žmolkovitost je jev, který silně negativně ovlivňuje vzhled textilií. Klasické charakteristiky žmolkovitosti jsou založeny na stanovení počtu žmolků po definované době odírání ve speciálních přístrojích. V tomto příspěvku je popsán způsob charakterizace žmolkovitosti založený na obrazové analýze, která umožňuje určení také velikosti žmolků. Pro stanovení rozdělení žmolků po různých dobách oděru je použito metod průzkumové analýzy dat.

INSTRUCTIONS FOR AUTHORS

The journal "Vlákna a textil" is the scientific and professional journal with a view to technology of fibres and textiles, with emphasis to chemical and natural fibres, processes of fibre finishing and dyeing, to fibrous and textile engineering and oriented polymer films. The original contributions and works of background researchs, new physico-analytical methods and papers concerning the development of fibres, textiles and the marketing of these materials as well as review papers will be published in the journal.

Manuscript

The original research papers are required to be written in English language (10 type-written pages maximum) with summary (abstract – maximum 10 lines). Text of contribution from Slovak and Czech Republic have to be in Slovak a Czech language as well. The other parts of the journal will be published in Slovak language, the advertisements will be published in a language according to the mutual agreement.

The first page of the manuscript has to contain :

- The title of the article.
- The initials of the first name (s) and also surname (s) of all authors.
- The complete address (es) of the working place of the authors, (e-mail if it is possible).

The manuscript has to be type-written at the size A4 in standard form, 30 lines with 65 beates, at a page. The total number of figures and tables would have been less than 10.

All figures, tables, schemes and photos have to have their own number and title.

The figures would have been drawn at the tracing paper or Bristol, drawn round by black ink, numbered by Arabic numerals and titled beneath the figure.

The tables would have been written at an individual piece of paper with number and title above them.

Photos and schemes have to be sufficiently contrastive at a photographic paper or to be drawn at a white paper.

Equations and schemes are stated right in the text.

Numbers of the figures and tables shall be stated in the text at the left margin.

Physical and technical properties have to be quantified in SI units, names and abbreviations of the chemical materials have to be stated according to the IUPAC standards.

References in the text have to be in square brackets and literature cited at the end of the text has to respect the international conventions.

The manuscript together with the tables and figures are demanded original copy.

Authors are kindly requested to deliver all papers to be published on PC disks 3,5" in WINWORD

Address of the Editor Office:

"Vlákna a textil"
Doc. Ing. Michal Krištofič, Ph.D.
STU-FCHPT
Radlinského 9
812 37 Bratislava
Slovak Republic
e-mail : mikristo@chelin.chtf.stuba.sk